Whole Brain Profile of Connector Hub Alteration Patterns in Focal Epilepsy When Compared to Healthy Controls

Arielle Dascal

A Thesis

In the Department of

Physics

Presented in Partial Fulfillment of the Requirements

For the Degree of

Master of Science, Physics

at Concordia University

Montreal, Quebec, Canada

August 2023

CONCORDIA UNIVERSITY
School of Graduate Studies

This is to certify that the thesis prepared

By: Arielle Dascal

Entitled: Whole Brain Profile of Connector Hub Alteration Patterns in Focal Epilepsy When Compared to Healthy Controls

and submitted in partial fulfillment of the requirements for the degree of

Master of Science (Physics)

complies with the regulations of the University and meets the accepted standards with respect to originality and quality.

Signed by the final examining committee:

Dr. Claudine Gauthier Examiner

Dr. Jean-Paul Soucy Examiner

Dr. Christophe Grova Thesis Supervisor(s)

Approved by: Dr. Pablo Bianucci
Graduate Program Director

Dr. Pascale Sicotte
Dean of the Faculty of Arts and Science

Abstract

Whole Brain Profile of Hub Alteration Patterns in Focal Epilepsy When Compared to Healthy Controls

Arielle Dascal

Using resting-state functional Magnetic Resonance Imaging (rs-fMRI), we can non-invasively measure functional connectivity (FC) between brain regions using the blood-oxygen-level-dependent (BOLD) signal which characterizes slow fluctuations of hemodynamic processes. Through various FC analysis techniques, we can extract the resting state networks (RSNs) of the brain, and identify highly connected regions called hubs, which are important for long-range and efficient communication within the brain. In this thesis, we applied, adapted, and carefully investigated the method entitled SParsity-based Analysis of Reliable *k*-hubness (SPARK), introduced by our group, to identify and quantify in a reliable manner the reorganization of connector hubs for patients with frontal lobe epilepsy (FLE) and temporal lobe epilepsy (TLE), when compared to healthy controls (HC). In this work, we used several metrics to characterize reorganization of connector hubs, aiming at generating whole-brain fingerprint models to characterize patients with epilepsy. We considered the following metrics, estimated on different parcellations of the brain in either nineteen anatomical regions or eleven functional networks: the hub disruption index (HDI), the hub emergence index (HEI), the hierarchical segregation index (HSI) and regional *k*-hubness. Our results are suggesting that we found more significant reorganization of hubness assessed using HDI and HEI when considering a segmentation in functional networks, as opposed to a segmentation in anatomical regions. We also reported significant decreases in regional *k* in epilepsy patients when compared to controls. In addition, we reported a significant decrease in HSI between epilepsy and controls as well. These preliminary results should be confirmed when applied on larger epilepsy cohorts, where we can use our proposed methodology and metrics combined with other non-invasive imaging modalities to discover potential biomarkers that could predict the postsurgical outcome of these patients.

Acknowledgements

I would like to start off by thanking my supervisor, Dr. Christophe Grova. Thank you for accepting me into your lab, even though I had little to no experience in epilepsy, coding, and MRI. You have opened your lab to me, opened your home and family to me, shared your passions with me and have shared your enthusiasm and passion for your work with me. Your guidance and encouragement these past two years has been instrumental in this process, and I am honored to be continuing with you for PhD. Thank you.

I would also like to show appreciation for my committee members, Dr. Claudine Gauthier, and Dr. Jean-Paul Soucy for taking their time to review this document and provide invaluable feedback which will make me a better researcher in the years to come.

To all my colleagues: Édouard Delaire, Jawata Afnan, Tamir Avigdor, Dr. Chifaou Abdallah, Yimeng Wang, Helia Mirabi, Shahla Bakian-Dogaheh, Dr. Hassan Khajehpour, Dr. Mathilde Reyt, Dr. Makoto Uji, Dr. Zhengchen Cai, Mahdi Mobark Abad, Guilia Rocco, Aude Jeou and Léa Larreur – thank you all for making these past two years such a positive and meaningful experience for me and offering me help, guidance, and fun when needed.

To my parents and brother: Deborah, Howard, and Joshua, I can never express how much your love, support and guidance throughout the years has meant to me. I am beyond grateful for every opportunity you have given me, and all the unwavering support you have shown. You have all be instrumental in my growth as a person. I would not be where I am today if you all weren't by myside. Thank you, I love you all.

To my grandparents: Natalie and Fred Wiseman and the late Clarita and Levi Dascal, you have all helped shaped me into who I am today. I would not be where I am today without all your love and support throughout the years. I love you and thank you for always believing in me.

To my partner: Dan Kazakov, I could not have gone through this experience without you. I cannot express how thankful I am that you were able to be physically by my side throughout this entire journey. You have been my rock, my biggest hype man, and a shoulder to cry on. I love you and thank you for everything you have done for me. I am lucky to have you in my life.

To my closest and dearest friends: Kaela O'Connor, Barbara Stuart, Hailey Pelland and Lauren Foreman; you have all been an instrumental part in this journey. I am so grateful that I have such a supportive friend group in my life.

To my extended family: my aunts, uncles, and many cousins, thank you for your support and encouragement throughout my journey.

Contribution of Authors

All the work presented in this thesis was done in close collaboration with my supervisor **Dr. Christophe Grova**. The contribution of all the co-authors other than my supervisor and I are summarized below.

Chapter 4: Whole Brain Profile of Hub Alteration Patterns in Focal Epilepsy When Compared to Healthy Controls

Dascal, Arielle[1] , Wang, Yimeng[1] , Delaire, Édouard[1] ; Lee, Kangjoo[2] ; Royer, Jessica[3] , Rodríguez-Cruces, Raúl[3] , Frauscher, Birgit[4] , Bernhardt, Boris[3] , Grova, Christophe[1]

- Yimeng Wang performed further preprocessing, launched SPARK, provided the initial code for hub reorganization metrics and collaborated on the manual identification of noisy atoms.
- Édouard Delaire provided invaluable help in optimizing code.
- Dr. Kangjoo Lee gave valuable input on the hub disruption index and hub emergence index metrices and helped with the configuration of SPARK.
- Dr. Jessica Royer and Dr. Raúl Rodríguez-Cruces performed the data acquisition and performed the fMRI preprocessing using MICApipe toolbox developed in Dr. Bernhardt's lab.
- Dr. Birgit Frauscher and Dr. Boris Bernhardt led patient screening and recruitment and provided overall guidance, design and suggestions throughout the project.

[1]Multimodal Functional Imaging Lab, Physics Department / PERFORM Centre, Concordia University,

[2]Division of Neurocognition, Neurocomputation and Neurogenetics, Department of Psychiatry, Yale University School of Medicine

[3]Multimodal Imaging and Connectome Analysis Lab, Montreal Neurological Institute Department of Neurology and Neurosurgery, McGill University,

[4] Analytical Neurophysiology Lab, Montreal Neurological Institute, Department of Neurology and Neurosurgery, McGill University

[5]Multimodal Functional Imaging Lab, Biomedical Engineering Department, McGill University, Montréal, Québec, H3A 2B4, Canada

Funding: Dr. Christophe Grova is funded by the Natural Sciences and Engineering Research Council (NSERC) of Canada Discovery grants, Canadian Institutes of Health Research (CIHR) (PJT-159948and MOP-133619). Top Concordian Graduate Entrance Scholarship, Lorraine Gosselin Graduate Entrance Award: Research and Academic Excellence from Concordia University; Yvonne and Andrew Koenig Scholarship from Jewish Community Foundation for Arielle Dascal.

Table of Contents

List of Figures

List of Tables

Chapter 1 – Introduction

Resting state (RS) functional magnetic resonance imaging (fMRI) was first introduced in (Biswal et al., 1995) where using the blood-oxygen-level-dependent (BOLD) signal, he demonstrated that there were spontaneous fluctuations of hemodynamic activity occurring when the subject was at rest, which resulted in spatial maps which were nearly identical to spatial maps produced through task-activation studies. Investigations further validating this work started appearing, such as in (Binder et al., 1999; Cordes et al., 2000; Lowe et al., 1998) who all published on discovering various resting state networks (RSNs) using seed-based functional connectivity applied on resting state fMRI data. Today, many studies are designed within the framework of a resting-state study, and numerous ways of studying functional connectivity have been developed. First, the aforementioned studies used seed based cross correlational analysis which uses the time course originating from a 'seed region' and cross correlates this time course with every other voxel in the brain through the use of Pearson correlation (McKeown & Sejnowski, 1998). Independent component analysis (ICA) works under the assumption that spatial temporal data can be decomposed in a set of statistically spatially independent maps (or networks), each of them being associated with a specific time course, within a linear mixing model (Zhao et al., 2004). Graph theory classifies the brain as a series of modules, nodes and edges and measures functional connectivity through the statistical dependencies of resting state functional topology of brain networks (Sporns, 2018; Van Den Heuvel & Hulshoff Pol, 2010). Graph theory allowed us to classify the functional connectivity of the human brain as having both the connectivity of *small-world* and *rich-club* networks, therefore allowing rapid and efficient communication through the network through locally connected modules rapidly accessible using few long distance connections (Bassett & Bullmore, 2017; Kim & Min, 2020). Finally, through graph theory, the concepts of *connector hubs* and *provincial hubs* have been proposed (Royer, Bernhardt, et al., 2022), which are nodes which have a higher number of connections with other nodes within the brain network (Power et al., 2013).

In the context of this Master thesis, we investigated a new functional connectivity method which was proposed by our group in (Lee et al., 2016) named SParsity-based Analysis of Reliable *k*-hubness (SPARK). The method extracts the spatial resting state network maps and identifies connector hubs to form a *k*-hubness map of the brain. In these maps, the value of *k*-hubness is defined for each voxel in our image, which is the discrete number of overlapping resting state networks in the voxel (usually $k < 10$ networks). Furthermore, we also considered the metrics of *hub disruption index (HDI), hub emergence index (HEI)* (Lee et al., 2018) and *hierarchical segregation index (HSI)* (Lee & Wang, n.d.) to quantify the changes in functional connectivity which occur between our healthy population and our patient groups.

In this manuscript, we proposed to study the reorganization of functional connectivity, and more specifically the reorganization of the distribution of connector hubs occurring in frontal lobe epilepsy (FLE) and temporal lobe epilepsy (TLE), in comparison with a healthy control group (HC). Epilepsy is a neurological disease which affects around 50 million people worldwide

(Kramer & Cash, 2012). Those who are diagnosed with epilepsy experience seizures, which are associated with a pattern of abnormal neuronal activity, and rapid firing of neurons (Blumenfeld, 2014). Many studies have already shown that there are measurable changes in functional connectivity for those diagnosed with the disease (Bettus et al., 2010; He et al., 2015; Narasimhan et al., 2022; Pittau et al., 2012; Royer, Bernhardt, et al., 2022; Waites et al., 2006; Wills et al., 2021; Woodward et al., 2014; X. Zhang et al., 2011). Furthermore, SPARK has been previously used to study changes in functional connectivity in temporal lobe epilepsy in the mesial temporal structures, where our group reported that hub disruption was occurring (Lee et al., 2018).

Therefore, in this thesis, we will be using the SPARK methodology to study the populations of temporal lobe epilepsy patients and frontal lobe epilepsy patients while using a group of healthy controls as a baseline. There were two main analyses which were performed at a group level with our patient groups. First, we studied the group level comparison of connector hub reorganization using resting state fMRI data by calculating the hub disruption index and the hub emergence index. To perform this analysis, we segmented the brain two ways (i) through an anatomical segmentation with 19 regions of interest; (ii) through a functional network segmentation with 11 functional networks of interest. We further introduced a new validation scheme for the indices, using a nonparametric permutation test to assess whether the hub disruption and emergence indices which we obtained may be deemed significant or not. The aim of this analysis is to build a fingerprint model characterizing for the first time the reorganization of connector hubs within the whole brain for two patient populations, assessing what are the key regions exhibiting reorganization of connector hubs close to the presumed focus, but also in distant regions.

This thesis is organized in the following manner: **Chapter 2** will introduce the imaging modality of functional magnetic resonance imaging (fMRI) in further details, describing the physics behind the method, describe the acquisition and analysis of resting-state fMRI data and how impactful its contribution was to neuroscience field. We will then describe the evolution of some of the most common functional connectivity measures, describing both their advantages and disadvantages. **Chapter 3** will further present the field of epilepsy, we will introduce the cohorts of frontal lobe and temporal lobe epilepsy patients, describing the typical seizures occurring for each group. We will then present some of the work which has been published describing changes in FC in epilepsy. Lastly, we will introduce the concept of epilepsy surgery and how it may be considered the only cure for patients and introduce the notion of a fingerprint model in epilepsy, and how they may be used in practice, and how it may relate to the work presented in this thesis. Finally, **Chapter 4** will present our main study, entitled *Whole brain profile of hub alteration patterns in focal epilepsy when compared to healthy controls.* **Chapter 5** will present our overall discussion and conclusions of the thesis and introduce future developments which can improve the SPARK methodology and the proposed metrics to assess hub reorganization.

Chapter 2 - Functional Magnetic Resonance Imaging

2.1 – Magnetic Resonance Imaging

Functional magnetic resonance imaging (fMRI) is the imaging modality used throughout the project presented in this thesis. The uniqueness of this modality cannot be understated; due to its reliance on oxygen consumption, which occurs naturally in the body, fMRI is a non-invasive way to study the human brain (Ogawa et al., 1990). Furthermore, this imaging technique benefits from a high spatial resolution, is widely available, and can be considered to perform longitudinal studies on patients without any adverse effects on their health (Logothetis, 2008; Logothetis & Wandell, 2004). Importantly, fMRI is a powerful tool which is used to study the functional connections in the brain, allowing us to investigate the architecture and the interaction within and between brain networks in physiological conditions (Hampson et al., 2002). In this chapter, there will be a brief introduction on the physics behind an fMRI acquisition, a description of the blood-oxygen-level-dependent (BOLD) response, which is the signal being measured during a scan, and the two types of fMRI scans we can perform, resting state fMRI (rs-fMRI) and tasked based fMRI. Finally, we will review the different functional connectivity (FC) analysis methods which exist to study the results from these fMRI acquisitions.

2.1.1 – Physics Principles of Magnetic Resonance Imaging

A Magnetic resonance imaging (MRI) scanner is a versatile non-invasive imaging modality which can provide a wide range of images. Using MRI, we can obtain anatomical images from a T1w sequence, generate a contrast image which will boost the signal from moving blood to further highlight anatomical malformations in the body's vasculature and assess lesions using a T2w or FLAIR sequence, model the flow of water molecules through the white matter tracts in the brain using diffusion weighted imaging and much more. Most relevant to this thesis, is the sequence known as functional MRI, which allows us to study brain activation and the hemodynamic response occurring in the brain in either task or resting conditions. Several steps are required during data acquisition to get usable results. The acquisition of an MRI image will be discussed in this section.

MRI relies on the concept of nuclear magnetic resonance, mainly applied to hydrogen atoms due to their magnetic susceptibility and the significant amount of these atoms found in the body (Maier et al., 2018). These atoms have a spin, which is an intrinsic property of angular momentum (Levitt, 2008). Once the subject is lying inside of the scanner, there is a large static uniform magnetic field $\mathbf{B_0}$, generated by a superconducting coil inside the MRI scanner, which aligns the spin of the hydrogen nuclei in the body either parallel or antiparallel to the direction of $\mathbf{B_0}$. At this point, the spins of the hydrogen atoms precess around $\mathbf{B_0}$ at a frequency ω, named the Larmor frequency. This frequency is expressed by the following formula:

$$\omega = \gamma \mathbf{B_0}$$

where γ is the gyromagnetic ratio (in MHz/T) which is the field strength dependent ratio for a given nucleus and $\mathbf{B_0}$ is the strength of the static magnetic field (in T) (Maier et al., 2018). Since

there are more hydrogen atoms which align themselves in a direction parallel to $\mathbf{B_0}$ than antiparallel, a net magnetization **M** is then generated in the direction of $\mathbf{B_0}$. The principle of nuclear magnetic resonance is then used to generate tissue specific signals of interest for imaging. To do so, a radiofrequency pulse (RF-pulse) sends radiofrequency waves into the body through an antenna. The RF-pulse consists in applying a second magnetic field $\mathbf{B_1}$, which is orthogonal to of $\mathbf{B_0}$, rotating specifically at the Larmor frequency. Applying $\mathbf{B_1}$ will result in resonance and therefore tips **M** away from the direction of $\mathbf{B_0}$ into the transverse plane by using the same amount of energy as the Larmor frequency ω. Once the RF-pulse is turned off, **M** precesses around the transverse plane until it reorients itself along $\mathbf{B_0}$. Here, the resulting magnetization will decrease within the transverse plane and will increase along $\mathbf{B_0}$, generating an observable nuclear magnetic resonance signal, called the free induction decay, in the transverse plane that can be measured with the same antenna.

The chosen contrast of a magnetic resonance image will depend on the desired outcome for medical diagnosis. There are three major contrasts: proton density, T1w, and T2w. Proton density is highly susceptible to the density of water, where the change in water density across body allows for the differentiation between tissues (Maier et al., 2018). We may specify a particular pulse sequence which in turn will generate the desired image contrast by exploiting the relaxation parameter of said contrast, where relaxation is the change in net magnetization over time. Therefore, when we have an image which is T1w, a pulse sequence is chosen which exploits the longitudinal relaxation time, which is the amount of time it takes for the net magnetization **M** to reorient itself with $\mathbf{B_0}$ and return to its original energy state after excitation. Longitudinal relaxation, also called the spin-spin relaxation, is the recovery of **M** in the longitudinal direction while the spins of the nuclei return to a parallel to $\mathbf{B_0}$. The amount of time it takes for the recovery to take place is denoted by T1. When we wish to acquire a T2w image, a pulse sequence is chosen which exploits the transverse relaxation time of the tissue. The transverse relaxation time, also known as the spin-lattice relaxation, is time is the amount it times it takes for **M** to decay solely in the transverse plane due to the loss of coherence in phase between the spins of the nuclei. The time constant for the transverse relaxation time is denoted by T2 (Huettel et al., 2008). Due to the length

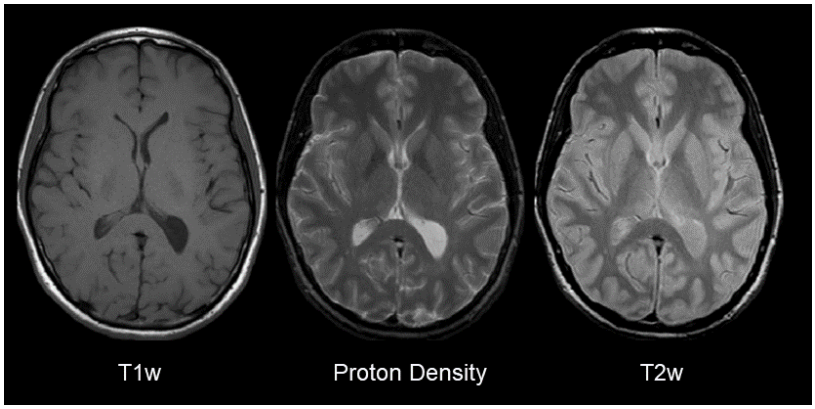

Figure 2-1 Results of applying the different pulse sequences in the brain. Adapted figure from *Elnakib, 2013*.

of the relaxation time, different structures of the brain are highlighted in T1w and T2w images. In a T1w image, the white matter (WM) is the brightest, grey matter (GM) is the next brightest and cerebrospinal fluid (CSF) is the darkest element in the image. In contrast, in a T2w image, the CSF is the brightest structure, followed by GM and finally WM is the darkest element in the image (Filler, 2009; Logothetis & Wandell, 2004). The differences between the different contrasts can be seen in **Figure 2-1**.

2.1.2 - Blood-Oxygen-Level-Dependent Response and functional MRI

The blood-oxygen-level-dependent (BOLD) signal arises due to the local changes of the concentration of oxygenated (Hb) and deoxygenated hemoglobin (dHb) in the brain, following the response to neuronal stimuli (Hillman, 2014). The BOLD response is obtained through a T2* weighted contrast, which has a very similar pulse sequence to a T2 weighted contrast. The difference between the two sequences is that T2* takes field inhomogeneity into account (Logothetis & Wandell, 2004), which is when there is a deviation in the strength of the static magnetic field due to either the main magnet, the antenna or the subject themselves (Manson et al., 2022). Oxygenated hemoglobin is a diamagnetic substance, whereas deoxygenated hemoglobin is paramagnetic, which has a strong magnetic susceptibility. The change that we see in the MR signal in a T2* contrast image is due to the hemodynamic response function which can be described in four phases: (1) Upon an increase of neuronal activity, local changes in blood flow are not seen until 1 to 2 seconds following stimuli, but when it does occur, an initial dip is observed. This initial decrease in BOLD signal is up to two seconds long and occurs due to the local increase of deoxygenated hemoglobin, mainly driven by the local increase of oxygen consumption. (2) Following this initial dip, (which is usually difficult to measure in practice), the neurovascular

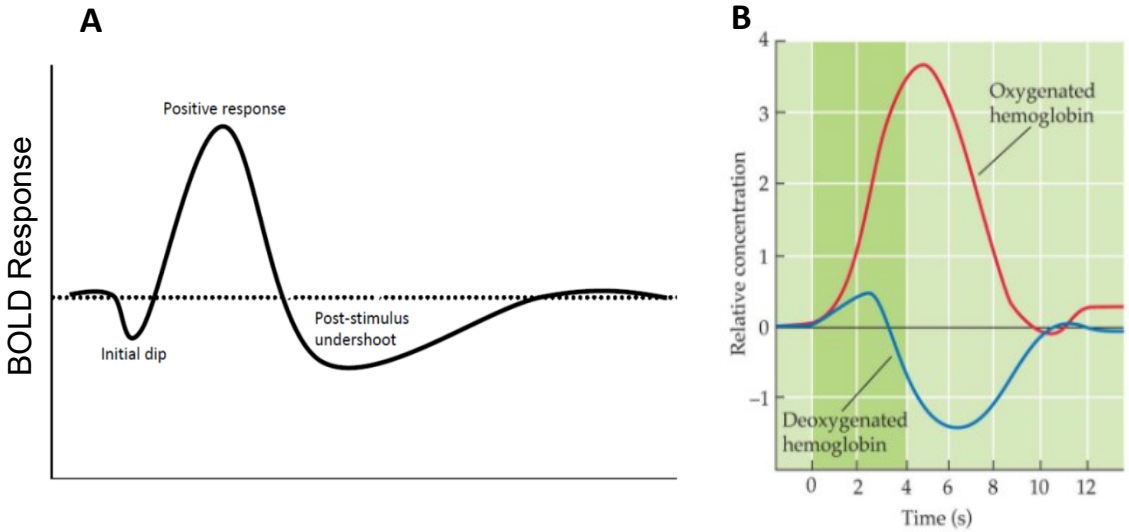

Figure 2-2 The hemodynamic response function. (A) The blood-oxygen-level-dependent signal after stimulation. Adapted figure from *Hu and Yacoub, 2012.* **(B)** The change in relative concentration of deoxygenated hemoglobin (dHb) and oxygenated hemoglobin (Hb). *Source: Huettel et al., 2008*

coupling process is characterized by a large local increase in cerebral blood flow due to vessel vasodilation, which will wash out local deoxyhemoglobin content by dilution and bring fresh oxygenated blood to the region (Hoge et al., 1999). This results in a large increase in BOLD signal, peaking around five seconds after the initial neuronal stimuli. The large decrease in the amount of paramagnetic deoxygenated hemoglobin results in less distortion of the magnetic field and therefore a large positive BOLD response. An uptick of oxygenated hemoglobin results in a relative decrease in diamagnetic deoxygenated hemoglobin reducing the magnetic resonance signal. If the stimulus lasts for a long period of time, this peak turns into a plateau, with a constant stream of oxygenated hemoglobin being supplied to the area. (3) Once the neuronal activity has terminated, the hemodynamic response function returns to a level below the baseline, which is denoted as the undershoot. (4) Finally, the BOLD hemodynamic response function returns to the local baseline level (Huettel et al., 2008).

Functional magnetic resonance imaging (fMRI) is a neuroimaging technique which was used to gain insight on how the brain processes information regarding sensory input, movement and cognitive abilities (Logothetis, 2008). The modality was first invented by Dr. Ogawa and Dr. Kwong in the 1990's and was tested on animals, where they discovered the BOLD contrast can be used to monitor the blood oxygenation in stimulated brain regions (Ogawa et al., 1990). After this discovery, researchers started using the BOLD contrast to study how brain regions responded to different stimuli using different types of tasks (such as finger tapping for motor tasks, sounds for auditory tasks, or pictures for visual tasks). These task-based activation studies used either a block design, where the subject is performing a task for a set period of time and then is in a resting-state for an equivalent amount of time, or an event-related design, where discrete random events are occurring during the experiment (Huettel et al., 2008). Experiments are performed in this manner to observe how the stimuli are associated with a hemodynamic response in the region of interest when compared to the baseline BOLD signals (Kannurpatti et al., 2012). In 1992, Dr. Kwong published a paper which used task-based fMRI to map the functional activation of the visual and motor cortices.

2.1.3 – Functional connectivity using fMRI

The notion of resting state functional connectivity using fMRI started with the seminal work of (Biswal et al., 1995). In his study, Dr. Biswal discovered that when they were scanning a subject in the absence of a task, there were low frequency fluctuations occurring (<0.1Hz) in the resting brain, and those resting state BOLD signals were spatially correlating (seed based connectivity) within similar brain regions involved during a bilateral finger tapping task in the primary sensorimotor cortex (Biswal et al., 1995). This was the beginning of studying resting state fMRI (rs-fMRI) functional connectivity, exhibiting the so-called sensorimotor resting state network (**Figure 2-3**). Nowadays, rs-fMRI studies are performed continuously during several minutes, where participants are instructed to keep their eyes closed or open (fixed on a cross), while lying still and refrain from thinking of any specific thoughts and from falling asleep. (Fox & Raichle, 2007).

The earliest resting state functional connectivity studies consisted of a seed based functional connectivity analysis. These studies extracted the BOLD signal from a region of interest and correlated it with the BOLD time course of all other voxels in the brain. The results were resting state functional connectivity maps associated with this specific seed (Binder et al., 1999; Biswal et al., 1995; Cordes et al., 2000; Lowe et al., 1998).

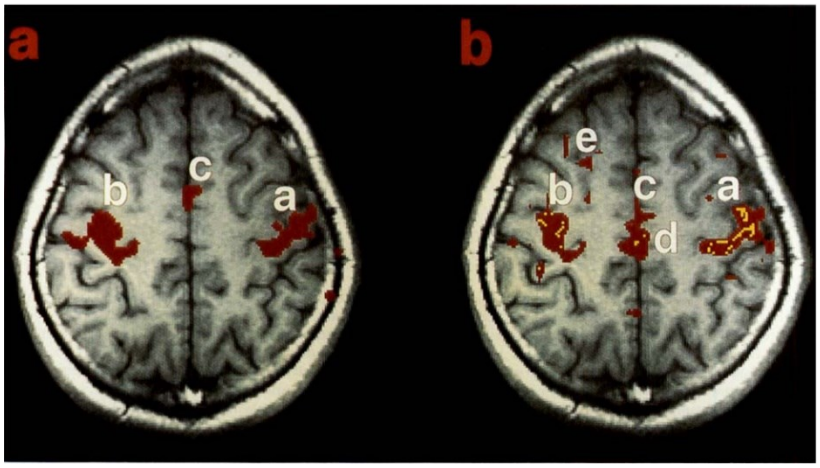

Figure 2-3 Task activation map and the corresponding resting state network. (A) The activation seen after a bilateral finger tapping task. **(B)** The resting state network found in the corresponding region. *Source: Biswal et al., 1995*.

2.1.4 – Resting State Networks

Resting state networks (RSNs) are an ensemble of brain regions which demonstrate synchronous functional connectivity without exposing the brain to any external stimuli (Seitzman et al., 2019), and can be visualized by mapping them spatially on the brain. As previously stated, the study performed by (Biswal et al., 1995) was the first time participants were studied while resting in the scanner. In this study, Biswal and his colleagues uncovered what we now know as the sensorimotor network, which was found to exhibit resting state low frequency fluctuations in the motor cortex, sharing a similar activation pattern as the BOLD response elicited by a bilateral finger tapping task. These results were replicated in (Lowe et al., 1998), confirming the existence of resting state networks. In (Cordes et al., 2000), resting state connectivity was further explored when they compared seed regions in functional connectivity maps to the activation maps which arose from a finger tapping task, an auditory task, and a visual task, further confirming the existence of the sensorimotor network, but also discovering what we now know as the auditory and lateral visual resting state networks. In (Binder et al., 1999), it was found that when a subject was awake but at rest, the brain enters a 'default state' of brain activity, which deactivates when the brain becomes engaged with a task to allocate the necessary resources to other brain regions. This network is now known as the default mode network. (Raichle et al., 2001) further confirmed the existence of this network. As time progressed, many more studies further supported our knowledge of resting state networks of the brain, as in (Hampson et al., 2002) who reported a language network and (Mazoyer et al., 2001) who reported the frontal-parietal network which was emotion driven. Today, the mapping of resting state networks is used to describe the functional connections of the brain, with

the most known networks being the somatomotor network, vision network, auditory network, default mode network, dorsal attention network, ventral attention network, language network, frontoparietal network, cinguloopercular network, salience network, parietal memory network, medial temporal lobe network, and the parietooccipital network (Seitzman et al., 2019).

2.2 – Statistical Approaches to Study Resting State Functional Connectivity

Measures of functional connectivity have been used in both task-based and resting-state studies. This section will describe the evolution of studying functional connectivity in the brain.

2.2.1 – Seed Based Cross Correlational Analysis

Seed based cross correlational analysis is a univariate technique which takes the time course of a given region of interest ('seed region') and cross correlates this time course with every other voxel in the brain through the use of the Pearson correlation (McKeown & Sejnowski, 1998). This means that the seed region must be carefully chosen, as the size, and location of it will have an impact on the resulting spatial map (Ma et al., 2007). This approach of functional connectivity analysis is designed to test a specific hypothesis, due to the *a priori* knowledge required for the selection of the seed region (Beckmann et al., 2005). Furthermore, there are some disadvantages which arise when working with the cross correlational analysis technique. Firstly, it is imperative that the seed region chosen is not near any large blood vessels or veins, as they will contaminate the time course of the voxel with noise, resulting in poor spatial maps full of noise. Second, for each spatial map being studied, a new seed region will need to be defined, meaning this method can only be applied considering one seed region BOLD time course at a time. (Ma et al., 2007). When performing fMRI connectivity studies, it is important to remove signals not related to the BOLD response, such as head motion, cardiac, respiratory, and vascular noise. Head motion is critical to correct since we are studying the correlation between voxels in a particular anatomical region over time, while the physiological signals will mix with the low frequency signal of <0.1Hz of the resting state networks. To remove these confounds to prevent potential aliasing and bias in the results, motion correction and a regression of physiological signals occurs during the preprocessing of the fMRI data (Soares et al., 2016).

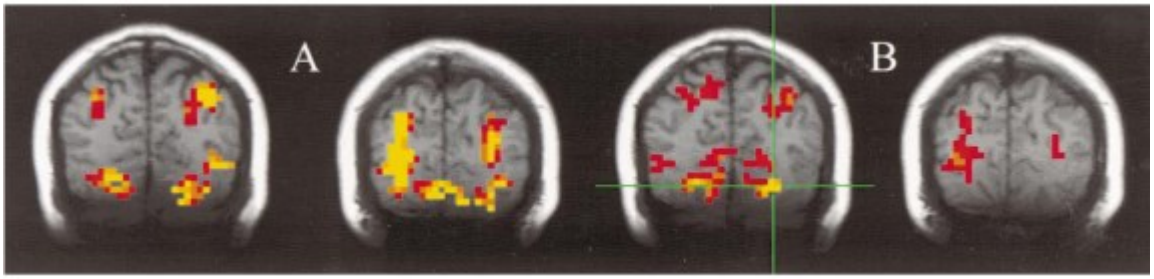

Figure 2-4 A seed-based cross correlational connectivity analysis map. (A) The results after a CCA analysis performed on a subject exposed to a visual paradigm. **(B)** The results after selecting a seed region (where the cross hairs are located) and performing a cross correlational analysis on the low frequency fluctuations, uncovering a visual resting state network. *Source: Cordes et al., 2000*.

2.2.2 – Independent Component Analysis

Independent Component Analysis (ICA) is a commonly used and robust multivariate analysis technique when performing BOLD-fMRI studies, which can generate multiple statistically independent spatial maps describing the underlying spatio-temporal structure of the data (Ma et al., 2007). Considering either temporal or spatial ICA, ICA aims at decomposing spatio-temporal data into a reduced set of N 'sources' or components, consisting either in N statistically independent time courses (and associated spatial maps) or N statistically independent spatial maps (and associated time courses), within a linear mixing model. For fMRI analysis, spatial ICA is usually considered. Once ICA has been applied to resting state fMRI data, the output results in individual statistically independent spatial maps, each of them associated with their own unique, characteristic time courses and yields easy to manipulate outputs due to linearity (Zhao et al., 2004). The algorithm was formally proposed for use in fMRI studies in (Mckeown et al., 1998), but was originally proposed in (Bell & Sejnowski, 1995). Although ICA is a reliable methodology when compared to cross correlational analysis since it does not require any *a priori* knowledge, such as selecting the seed location of interest, (Ma et al., 2007), an important assumption of the model relies on the fact that data can be linearly decomposed in a sum of spatially independent maps and corresponding time courses (McKeown & Sejnowski, 1998; Zhao et al., 2004). Furthermore, when being compared to cross correlational analysis, ICA analysis is usually more efficient when dealing with noise, since the underlying spatial structure of noisy components (motion, respiration, and cardiac fluctuations) are fulfilling the hypothesis of statistical independence with the maps of interest (Ma et al., 2007). One of the main limitations of ICA is

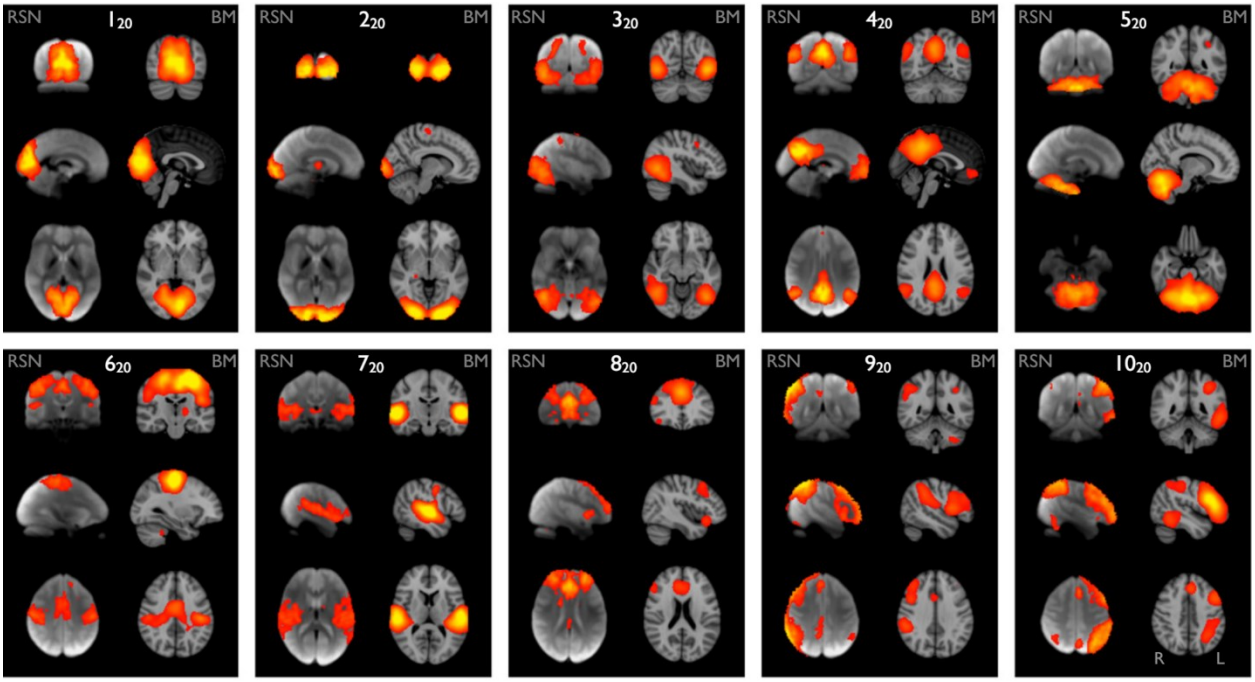

Figure 2-5 An example of the resting state networks extracted using ICA. An adapted figure from *Smith et al., 2009.*The resting state networks are as follows: I_{20}, 2_{20}, 3_{20} are the visual networks (medial, occipital, lateral), 4_{20} is the default mode network, 5_{20} is the cerebellum network, 6_{20} is the sensorimotor networks, 7_{20} is the auditory network, 8_{20} is the executive control network, 9_{20}, 10_{20} are the frontoparietal network.

that the total number of ICA components to be extracted should be set *a priori.* If the number of components is too low, many spatial maps will be mixed into others, whereas if this number is too high, those same spatial maps would end up being separated into multiple, smaller networks. (Ma et al., 2007; D. Zhang & Raichle, 2010). In (Smith et al., 2009), an ICA decomposition was performed with 20 components, and the resulting spatial maps were compared to known 'behavioral domains', which were the known task-activation maps. This allowed the team to associate each resulting RSN with a particular behavior, allowing them to report a significant cognitive role for every RSN. The results from this study are shown in **Figure 2-5**.

2.2.3 – Graph Theory and Hubs

Graph theory is a functional connectivity analysis tool aiming at describing statistical dependencies of resting state functional topology of brain networks in the form of a connectivity graph composed of edges and nodes (Sporns, 2018; Van Den Heuvel & Hulshoff Pol, 2010). Starting from a connectome matrix reporting pairwise Pearson correlations between brain regions or voxels, a connectivity graph is extracted, where the nodes represent a different anatomical brain regions (such as brain regions defined through a template or fMRI voxels), and the edges representing the functional connections (i.e.: correlation values) between each of the nodes. Within such a graph model, the so called resting state networks usually appear as modules, which are a group of predefined nodes (Van Den Heuvel & Hulshoff Pol, 2010). The modules are typically defined through brain atlases, which segment the brain into either functional networks (Thomas Yeo et al., 2011; Urchs et al., 2017) or anatomical parcels (Rolls et al., 2020). Graph theory allows for studying functional connectivity properties both at the local nodal scale and at the global brain network scale (Sporns, 2018). Several key metrics have been proposed to characterize brain networks, for instance:

- The degree of a node represents the total number of connections to a given node, and plays a key role in identifying highly connected hubs (Royer, Bernhardt, et al., 2022; Van Den Heuvel & Hulshoff Pol, 2010). These hubs will be later discussed.
- The clustering coefficient, which is a value ranging between zero and one, is a ratio between degree of a node *i* and the number of connections of the neighbors of node *i*. When the clustering coefficient is close to one, it means that the number of connections between the neighbors of node *i* is similar to the degree of node *i* (Achard et al., 2006; Van Den Heuvel & Hulshoff Pol, 2010).
- The path length of a node *i* estimates the minimum number of edges required to connect two nodes in the graph, without repeats, providing information regarding the efficiency and the transfer of information within the network (Achard et al., 2006; Sporns, 2018; Van Den Heuvel & Hulshoff Pol, 2010).
- The centrality of a node is the number of shortest pathlengths of the network which go through node *i*, and is a vital measure in finding the hubs of the network, which are vital for overall network efficiency (Sporns, 2018; Van Den Heuvel & Hulshoff Pol, 2010).

- The modularity is when the whole brain network can successfully be divided into distinct, nonoverlapping modules (Newman, 2006; Rubinov & Sporns, 2010). The number of connections which are found within each module is much larger than the connections which occur between modules. The nodes which connect the different modules are denoted as connector hubs (Kim & Min, 2020), which will be further discussed later.

By using graph theory in neuroscience, the behavior of brain networks can be expressed as both *small-world* and *rich-club* networks using these metrics, which are typical properties characterizing several network architectures, including brain networks. When a network is classified as *small-world*, the brain network has a large average clustering coefficient, meaning the nodes are more highly interconnected with each other inside a cluster or module, while exhibiting few long distance connections between modules, through the rich club hubs (Achard et al., 2006; Watts & Strogatz, 1998). Indeed, a *small-world* networks are also characterized by short pathlengths, allowing for rapid and efficient long distance communication through and between networks (Bassett & Bullmore, 2017; Kim & Min, 2020). In addition, the human brain has also been deemed a *rich-club*, which is where the highly connected nodes (i.e. the hubs) are more interconnected with each other than with non-hub nodes of the network (Kim & Min, 2020) therefore ensuring within and between network (or modular) communication. In the first *rich-club* study (Van Den Heuvel & Sporns, 2011), it was found through the use of diffusion tensor imaging (DTI) data that the *rich-club* interconnections are found in the bilateral superior parietal lobe, precuneus, superior frontal cortex, putamen, hippocampus, and thalamus, making them important regions of interest for hub studies.

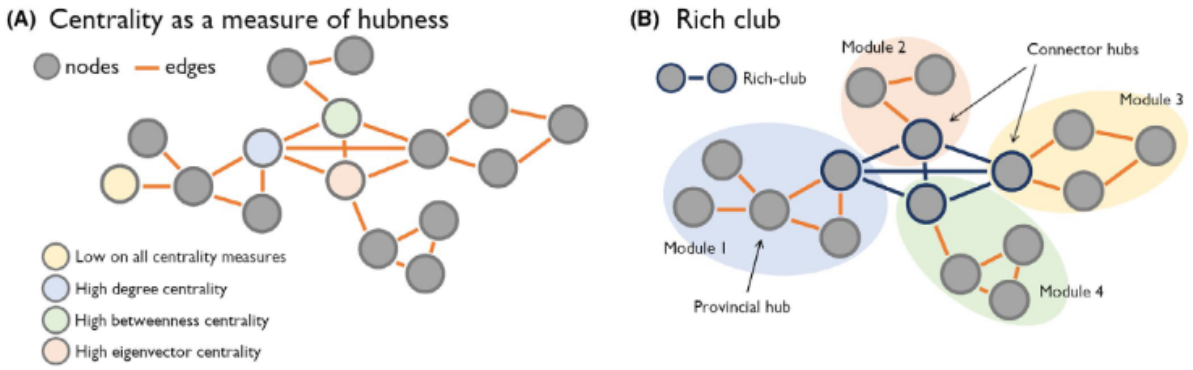

Figure 2-6 Visual representation of Graph theory and the identification of connector hubs. (A) Nodes are connected by edges, and the number of edges connected to the node can result in centrality measures for the node, determining if it is a hub or no. **(B)** Modules are connected by connector hubs, allowing for a 'rich club' organization to take place. Within each module, there are provincial hubs which connect the other nodes within the module. *Source: Royer et al., 2022.*

Hubs are important regions of the brain as they are instrumental to its overall function and efficiency. Hubs are nodes which have many connections with other nodes in the brain network (Power et al., 2013), and based on the participation of a node within their own module, or their

connection to any other modules, the node can be either deemed as a *connector hub* or a *provincial hub* (Royer, Bernhardt, et al., 2022). The participation coefficient is a measure of the connectivity of the node to the rest of the graph; if a node is completely restricted to its own module, it has a participation coefficient of zero. When a node is only connected to other networks, the participation coefficient is one (Power et al., 2013). Therefore, nodes which have a high degree of intra-modular connections and a low participation coefficient are provincial hubs, whereas nodes which have a high participation coefficient are connector hubs, which facilitate inter-module communication (Rubinov & Sporns, 2010).

2.2.4 – SParsity-based Analysis of Reliable k-hubness (SPARK)

SParsity-based Analysis of Reliable k-hubness (SPARK) is a sparse coding methodology developed by our collaborator Dr. Kangjoo Lee, former PhD student of our laboratory, now postdoctoral fellow at Yale University. SPARK was designed to specifically assess spatial overlaps between resting state network structures, whereas the notion of spatial overlap between resting state networks is not considered by other standard approaches such as ICA (Mckeown et al., 1998) or hierarchical clustering (Bellec et al., 2010). Within the SPARK framework, we define *hubness*, which is the property of a voxel to exhibit connections with multiple resting state networks. Therefore, we may define *k*-hubness for each voxel in our image, where *k* is the discrete number of overlapping resting state networks in the voxel. If there is a voxel with $k = 1$, we know that the voxel is associated with only one resting state network, whereas if a voxel has $k > 1$, the voxel is associated with multiple resting state networks and is denoted as a connector hub. Importantly, SPARK is providing a sparse decomposition of the signal of each voxel, therefore providing a unique realistic description of what are the few discrete networks connected within a specific voxel ($k < 10$ networks)(Lee et al., 2016), as opposed to a metric such as degree centrality which is counting the very large number of regions or voxels connected to a specific voxel (or region) after thresholding the connectome.

SPARK is built upon the sparse coding algorithm K-SVD to solve a general linear model by decomposing fMRI time series into multiple sparse atoms, i.e. specific time courses that would have been learnt from the data using a dictionary learning approach. Then, each atom was found to be associated with a spatial network. The original sparse GLM method developed in (Lee, 2011) employed a sparse dictionary learning algorithm called K-SVD (Aharon et al., 2006), where SVD stands for Singular Value Decomposition and K indicates a sparsity assumption (*k*) applied for the algorithm. Note that the sparsity assumption means that the inter-network connection is sparse (in general $k<10$ networks). In order to ensure reproducibility of the atoms, our team then proposed to launch K-SVD several times after generating several bootstrap samples of the data, using a modified version of circular bootstrap resampling as suggested in (Bellec et al., 2010). To find a spatially reproducible set of resting state networks across the $B = 100$ resampled datasets, we then applied nearest neighbor spatial clustering across to the collection of all $B \times N$ spatial maps to identify *N* stable and reliable clusters. The spatial maps were then spatially averaged within each

cluster, therefore only retaining most the most reproducible results at the individual level (*N* final spatial maps).

SPARK is unique as it removes some of the issues which have been proposed regarding graph theory. In graph theory, many studies have solely focused on studying non-overlapping modules, therefore assuming that the brain is functionally segregated, which is unlikely due to the existence of connector hubs. Graph theory also introduces the issue of multicollinearity, which is alleviated by SPARK. To further define, if we have A correlated with B, and B correlated with C, A and C can exhibit signs of correlation, even if they do not belong to the same functional network (Lee et al., 2016). Furthermore, SPARK has the advantage of not assuming independence such as in ICA and encourages the assumption of the existence of overlapping networks when compared to ICA. SPARK is the methodology used in this thesis for fMRI analysis. The method will be further elaborated in **Chapter 4**.

In conclusion, in **Chapter 2**, we introduced the main physics principles of MRI acquisitions and the most popular acquisition sequences which are used with the modality. Furthermore, we have introduced the concept of fMRI and different statistical functional connectivity analyses which can be applied on the data. In the following chapter, we will study how functional connectivity changes due to frontal lobe and temporal lobe epilepsy.

Chapter 3 - Epilepsy

3.1 – The Epilepsy Disease

Epilepsy is a neurological disease which affects around 50 million people worldwide (Kramer & Cash, 2012). In 2014, the International League Against Epilepsy (ILAE) refined the definition of the disease to include any of the following conditions: "1- At least two unprovoked seizures occurring > 24 hours apart; 2- One unprovoked seizure and the probability of further seizures similar to the general recurrence risk (at least 60%) after two unprovoked seizures occurring over the next 10 years; 3- Diagnosis of an epilepsy syndrome" (Fisher et al., 2014). A seizure is a manifestation of abnormal neuronal activity, caused by the rapid firing of neurons (Blumenfeld, 2014). Individuals who are diagnosed with the disease tend to display signs of cognitive impairment, as well as increased cases of depression and anxiety when compared to healthy cohorts (Theodore et al., 2006). Due to the all-encompassing nature of the disease, it is important that research continues forward to enable those diagnosed to return to a healthy and productive lifestyle.

Around 30% of all epilepsy cases are drug-resistant, meaning the seizures cannot be controlled through the use of medication (Kalilani et al., 2018). Standard surgical intervention in these cases consist of a resection which targets the epileptic focus, the brain region where seizures are initiated, however the reoccurring pattern of long-term and post-operative failures which occur in 25% to 50% of patients leads to questioning whether the best possible treatment is being offered (Krucoff et al., 2017; Spencer & Huh, 2008; Tellez-Zenteno et al., 2007). Patients who are considered as candidates for surgery will undergo a wide range of presurgical evaluations, namely using video-electroencephalography, psychological testing, anatomical MRI, positron emission tomography (PET) and single proton emission tomography (SPECT) (Sala-Padro et al., 2021). It has been suggested that resting state functional connectivity can play a role in the presurgical workup for a patient, as abnormalities in the rs-FC can aid in identifying the epilepsy network and the epileptic focus, and in surgery outcome prediction (Tracy & Doucet, 2015).

In the following sections, we will discuss two common types of epilepsy, frontal lobe epilepsy (FLE) and temporal lobe epilepsy (TLE), and how functional connectivity, which was discussed in **Chapter 2**, is altered in those conditions. Furthermore, we will then discuss how surgery may be the only solution to becoming seizure free in the case of drug-resistant epilepsy. Finally, we will discuss the emerging field of fingerprinting, as a new tool which can help with the prediction of post-surgical outcome.

3.1.1 – Frontal Lobe Epilepsy and Temporal Lobe Epilepsy

Frontal Lobe Epilepsy and Temporal Lobe Epilepsy are both forms of focal epilepsy, characterized by the fact that the seizures originate from a specific focal region of the brain, meaning they have either frontal or temporal lobe origins. With focal epilepsy, the seizures may or may not propagate throughout the brain, and there are specific symptoms which can occur depending on where the focus is located (Kramer & Cash, 2012).

In this thesis, we will be focusing our analysis on patients with drug-resistant Frontal Lobe Epilepsy (FLE) and Temporal Lobe Epilepsy (TLE), who were all scanned as a part of their presurgical investigation. For those with FLE, the epileptic focus (EF) is located somewhere in the frontal lobe of the brain. Of all drug-resistant focal epilepsy cases, 25% of those diagnosed are FLE (Beleza & Pinho, 2011). These patients are often reported to have poor executive functions and behavioral problems (Culhane-Shelburne et al., 2002). Those diagnosed with FLE may experience either unilateral clonic seizures (unvoluntary twitching or jerking of muscle groups on one side of the body), tonic asymmetric seizures with preserved consciousness (sustained muscle contractions on a random side of the body, with preference for a specific side while remaining conscious), and hyperkinetic seizures (pedaling, thrusting, thrashing movements). Surgery for FLE patients accounts for less than 50% of all surgical cases, but for those who undergo surgery, they have a 55.7% probability of being seizure free at one year, with the chances of being seizure free after 5 years down to 30.1% (Beleza & Pinho, 2011; Blume et al., 2002). In the case of TLE, the EF is localized within the temporal lobe structures of the brain, and account for nearly 66% of all diagnosed focal epilepsy cases (Abarrategui et al., 2021). Those who are diagnosed with TLE tend to lack adaptive skills (Culhane-Shelburne et al., 2002), and often experience focal seizures without loss of consciousness, and experience an aura, which can range from a feeling of familiarity, to fear and panic, and altered senses (Blumenfeld, 2014). Furthermore, impaired consciousness is also reported in temporal lobe seizures (Englot et al., 2010). In TLE, the seizures often originate from the hippocampus and propagate outwards throughout the brain (Morgan et al., 2021). Of all TLE patients, up to 71% are drug-resistant and may be considered for surgery (Abarrategui et al., 2021).

3.1.2 - Functional Connectivity in Epilepsy

Using only a few minutes of resting state fMRI recordings, often without the simultaneous recording of EEG, many studies have demonstrated that the epileptic brain is characterized by reorganization of functional connectivity patterns. Particularly, many studies have focused on the changes in functional connectivity within the mesial temporal lobe and the subcortical regions for patients. In TLE studies, it has been found that there are volume decreases in the subcortical structures of the caudate (X. Zhang et al., 2011) and the thalamus (Wills et al., 2021). This anatomical modification of the underlying structures could be at the origin of changes in the strength of the functional connections. When studying the thalamus, (He et al., 2015) used cross correlational analysis and thalamic segmentations to study the functional connectivity between the different regions of the thalamus and the cortical surface, which have been shown to have a strong functional connectivity in healthy controls (Behrens et al., 2003; D. Zhang et al., 2008). In the results of (He et al., 2015), they report that although FC was preserved between these regions in TLE patients, the strength of FC had decreased. As the hippocampus is the main seizure generator in TLE, it is an important ROI that has been considered as a seed for FC studies, reporting mainly decreases in FC with contralateral mesio-temporal structures as well as with the default mode network (Bettus et al., 2010; Pittau et al., 2012). In addition, (Waites et al., 2006) used seed-based functional connectivity analysis where they reported a decrease in FC between the different

language areas of the brain in TLE when compared to healthy controls. In a study involving both FLE and TLE patients using graph theory, (Výtvarová et al., 2017) reported: (i) for TLE patients, a decrease in functional connectivity of the nodes of the mesial temporal structure and the temporal and frontal lateral cortices, insula and the cingulate cortex; (ii) for FLE patients, there was a significant decrease of FC between the nodes in the frontal lobe when compared to controls, and reported that there were slight changes not reaching the significance threshold between the nodes for a within-region analysis of temporal and posterior regions of the brain. In another study investigating FLE patients, (Woodward et al., 2014) using seed-based analysis suggested a decrease of functional connectivity between the two hemispheres of the sensorimotor network, decreased connectivity in the memory networks, and showed that the frontal lobe became less connected with other brain regions.

There is a theory that, to make up for the decrease in functional connectivity experienced on the ipsilateral side, the epileptic brain creates compensatory mechanisms in the contralateral side to the seizure onset zone. For example, (Bettus et al., 2009) studied the epileptogenic zone (EZ) of mesial TLE patients using seed based analysis, and found that there was a decrease in functional connectivity in the EZ relative to healthy subjects, and an increased connectivity on the contralateral region to the EZ.

It is of interest to study the changes in functional connectivity of connector hubs in epilepsy. Using a complex network analysis to estimate hubs from resting state fMRI, (Výtvarová et al., 2017), found that the connector hubs were exhibiting a decrease of functional connections in the subcortical regions of the putamen, caudate and pallidum when compared to healthy controls. In their review (Royer, Bernhardt, et al., 2022) discussed how changes in hubness at the global (i.e: entire brain network) and regional (RSNs) levels in TLE may directly impact the efficiency of the entire network, affecting signal transmission throughout the brain. Finally, in a study performed by our group using SPARK, (Lee et al., 2018), reported specific reorganization patterns of connector hubs involved in mesial temporal structures in left and right TLE patients. They reported overall hub disruption (i.e.: a loss of hubness) in the mesial temporal regions and the default mode network.

3.1.3 – The Need for Epilepsy Surgery due to Drug Resistance

Drug resistant epilepsy occurs when the disease is not adequately controlled through the use of anti-epileptic drugs, and occurs in nearly a third of all of those diagnosed (Löscher et al., 2020). In these cases, epilepsy surgery in the form of a resection, ablation or neurostimulation (Narasimhan et al., 2022) of the epileptic focus (EF) is the final opportunity for the patient to become seizure free. Therefore, in the hopes of having a positive surgical outcome, localization of the seizure focus is needed (Bettus et al., 2010; Wills et al., 2021). In the work of (Negishi et al., 2011), is was proposed that studying rs-fMRI functional connectivity analysis around the EF region can provide us further information regarding the postsurgical outcome. Although epilepsy surgery may be an effective treatment course for some, there is a pattern of long-term post operative failures which occur in 25% to 50% of patients, leading to questioning if the most

optimal treatment is being recommended (Krucoff et al., 2017; Spencer & Huh, 2008; Tellez-Zenteno et al., 2007).

3.1.4 – Fingerprinting in Epilepsy

When developing a fingerprint, one is searching for unique identifying features belonging to a population which can be used as an identifier for the research question they wish to address. Recently, there have been an emerging number of studies which are considering fingerprinting for the automatic prediction of the epileptogenic zone (Grinenko et al., 2018; Woolfe et al., 2019), generating presurgical prediction tools (Morgan et al., 2022; Sala-Padro et al., 2021), and even for the diagnosis of the disease (Liao et al., 2018).

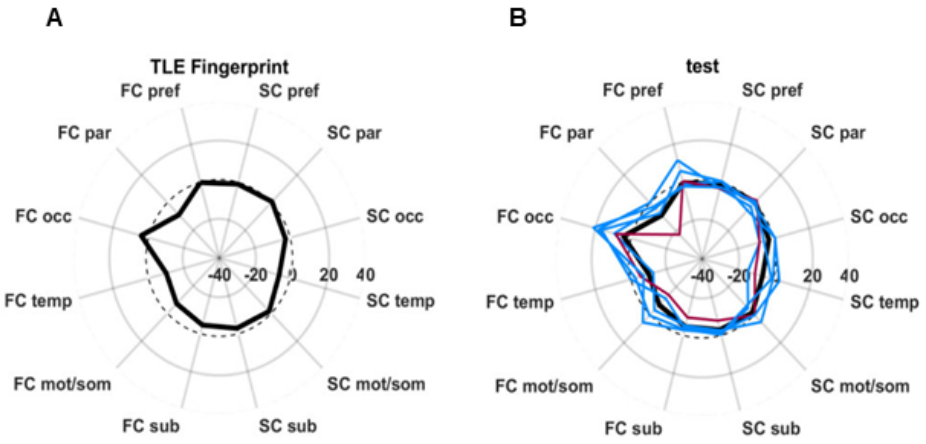

Figure 3-1 Sample of a fingerprint developed as a surgical prediction model. FC is a measurement of functional connectivity and SC is a measurement of structural connectivity. The regions of interest are: pref = prefrontal lobe; par = parietal lobe; occ = occipital lobe; temp = temporal lobe; mot/com = motor and sensorimotor lobe; sub = subcortical structures. **(A)** The functional and structural connectivity profile of the TLE fingerprint. **(B)** The connectivity profiles of five patients. *Adapted Figure from Morgan et al., 2022.*

In **Figure 3-1**, we are reporting results from (Morgan et al., 2022), presenting an example of a fingerprint model which uses whole brain functional and structural connectivity to characterize emerging patterns that can predict postsurgical outcome. The fingerprint, shown in **Figure 3-1A**, was proposed for TLE patients using both functional and structural connectivity patterns in different regions. It is a specific connectivity profile which was generated using connectivity data from seizure free TLE patients and is therefore a model representing a seizure-free outcome after surgery. The goal is to use the fingerprint on presurgical connectivity data on test groups, to assess if it could accurately predict the surgery outcome. In **Figure 3-1B**, we see the connectivity profiles of few test subjects showing Engel IA outcome (seizure-freedom) in blue, Engel III (non-seizure free) in red and the fingerprint in black. In this thesis, we propose to build a similar approach using reliable measurements of hubness provided by SPARK.

In conclusion, in **Chapter 3**, we introduced the epilepsy disease. We provided examples of the types of seizures experienced by frontal lobe epilepsy and temporal lobe epilepsy patients. Furthermore, we discussed some of the work which has been published in the field of functional connectivity and epilepsy. In the following chapter, we will begin our data analysis, where we attempt to generate a fingerprint model to describe emerging functional connectivity patterns occurring in FLE and TLE using our SPARK methodology.

Chapter 4 – Whole brain profile of hub alteration patterns in focal epilepsy when compared to healthy controls

4.1 – Introduction

In this work, we intend to apply three previously proposed methods associated with the SPARK methodology, hub disruption index (HDI), hub emergence index (HEI), and the hierarchical segregation index (HSI) (Achard et al., 2012; Lee et al., 2018; Lee & Wang, n.d.; Wang, 2022) to generate a whole brain profile of hub alteration patterns occurring in focal epilepsy. Our overall objective is to investigate whether specific spatial profiles of connector hub reorganization can be associated with biomarkers of frontal lobe epilepsy and temporal lobe epilepsy to develop a fingerprint model to using HDI, HEI and HSI which show patterns of altered functional connectivity. Then, eventually, we will aim at developing a post-surgical prediction model to determine if a patient will present with either a surgical success or a surgical failure depending on the hubness reorganization patterns found with SPARK.

For this study, we hypothesize that on a group level, there will be hub disruption, hub emergence and hierarchical segregation patterns which are specific to either frontal lobe epilepsy patients or temporal lobe epilepsy patients. We wish to investigate connector hub reorganization not only in the presumed focus, but also for the first time in several other anatomical regions in the two populations of patients. Long term, upon the availability of post-surgical data, and an increased number of subjects, we hypothesize that connector hub reorganization in epilepsy will allow for the prediction of postsurgical outcome from non-invasive neuroimaging techniques: i) For an epileptic focus (EF) located in a region identified as a non-hub region in healthy subjects, we hypothesize that hub disruption will tend to isolate the epileptic network (EN) from the rest of the brain, resulting in local EN. Resection of a local EN would likely be associated with a good surgical outcome. ii) For an EF located in a region classified as a connector hub in healthy subjects, hub disruption and emergence will result in a widespread EN involving distant brain regions. Such epilepsy will be difficult to treat with focal resection.

4.2 – Proposed Methodology

This study was completed in close collaboration of Dr. Boris Bernhardt, Jessica Royer, Dr. Raul Rodriguez-Cruces, and Dr. Birgit Frauscher, who collected the data and performed most of the fMRI preprocessing using the MICApipe fMRI toolbox developed by the group of Dr. Bernhardt (Cruces et al., 2022). The healthy controls used in this project are also a part of an open source MRI dataset (Royer, Rodríguez-Cruces, et al., 2022). Furthermore, Yimeng Wang performed the additional fMRI preprocessing on the data, and collaborated on the identification of noisy atoms as a part of her MSc thesis (Wang, 2022). Finally, Dr. Kangjoo Lee provided input related to the SPARK metrics being used in this study. In this analysis, we propose to apply the SPARK methodology introduced in **Section 2.2.4** on this dataset and perform hub disruption (Achard et al., 2006; Lee et al., 2018), and hub segregation (Lee & Wang, n.d.) analyses on a group of TLE and FLE patients when compared to a group of healthy controls, while we try to develop a fingerprint model which show patterns of altered functional connectivity in the connector hub regions for TLE and FLE.

4.2.1 – Participant Selection

26 Healthy Controls (HC), 14 TLE patients (11 left-lateralized, 1 right-lateralized, and 2 bilateral), and 11 FLE patients (5 left-lateralized, 6 right-lateralized) were included in this study. Controls and patients were age and sex matched. All healthy subjects reported no history of neurological and/or psychiatric illness.

4.2.2 – Data Acquisition

The subjects were scanned at the McConnell Brain Imaging Centre of the Montreal Neurological Institute and Hospital. Using a 3T Siemens MRI system with a 64-channel head coil, all participants undertook two T1-weighted structural scans, diffusion weighted imaging (DWI) scans, and rs-fMRI. The rs-fMRI data were acquired using multiband acceleration 2D-BOLD imaging, for a total duration of 7 minutes, with 3mm isotropic voxels. There was a TR = 600ms, and TE = 30ms. All subjects were instructed to keep their eyes open while looking at a fixed cross, and refrain from falling asleep. The details regarding the scanning parameters can be found in (Royer, Rodríguez-Cruces, et al., 2022) (Wang, 2022).

4.2.3 – fMRI data preprocessing

The first part of the fMRI preprocessing was done using the MICApipe pipeline developed in the lab of Dr. Bernhardt (Cruces et al., 2022). In this phase of the preprocessing, the first 5 TRs were removed. Motion correction and distortion correction within the scans was applied using the '3dvolreg' function from AFNI (Cox, 1996). The function 'fsl_motion_outliers' from FSL was applied, identifying the timeframes exhibiting excessive motion and saving them as confounds (Woolrich et al., 2009). A high-pass filter of >0.1Hz was applied to remove unwanted frequencies. ICA-FIX from FSL was applied to remove nuisance variable signals (instead of removing signal from the white matter and cerebral spinal fluid) (Griffanti et al., 2014; Salimi-Khorshidi et al., 2014).

The second part of the fMRI preprocessing was completed to ensure data compatibility with SPARK, and was performed by Yimeng Wang during her Master's degree. Segmentation of the brain mask was obtained, and brain extraction took place by applying the 'recon-all' function by FreeSurfer (Reuter et al., 2012) on T1-weighted anatomical data and applying the BET toolbox on the fMRI data (Smith, 2002). Next, all fMRI data (3mm isotopic voxels) were first co-registered to the corresponding T1-weighted anatomical MRI (0.8mm isotopic voxels), and then co-registered and resampled at a 2mm resolution on the asymmetric nonlinear MNI152 template (Fonov et al., 2011) using FLIRT from FSL with 12 parameters affine transformation (Greve & Fischl, 2009; Jenkinson et al., 2002; Jenkinson & Smith, 2001). The 2mm MNI-space was finally down-sampled to 4mm resolution. Spatial smoothing with a full width at half maximum (FWHM) of 6mm was applied. The motion outlier confounds estimated from MICApipe were regressed out from the fMRI data through 'despiking' using FSL (Wang, 2022).

4.2.4 – Brain Masking and atlases

The SPARK methodology was applied to a grey matter mask, which was generated by Dr. Kangjoo Lee and Yimeng Wang for their upcoming publication (Lee & Wang, n.d.). The mask was generated by selecting only the grey matter voxels from a modified version of the AAL template (Tzourio-Mazoyer et al., 2002). The modified AAL template was generated by the Neuroimaging Analysis Toolkit NIAK (Bellec et al., 2010) using non-linear coregistration to the MNI ICBM 152 template. The AAL template was then resampled to a voxel resolution of $4 \times 4 \times 4\ mm^3$ (Wang, 2022).

For the proposed hub disruption and hierarchical segregation regional analysis, we considered two types of brain parcellations to exploit the different distribution of *k*-hubness values within differently sized regions: an anatomical parcellation and a functional network parcellation. The anatomical parcellation used the refined AAL template. Originally, the template comprised of 116 regions of interest (ROIs) that were then grouped into 19 ROIs with the help of neurologist Dr. Chifaou Abdallah. The resulting the 19 anatomical region ROIs were the following: (1) mesial motor and premotor cortex, (2) lateral motor cortex, (3) mesial frontal lobe, (4) lateral frontal lobe, (5) middle frontal lobe, (6) inferior frontal lobe, (7) olfactory cortex and rectus, (8) mesial temporal lobe, (9) temporal poles, (10) temporal gyri, (11) basal temporal lobe, (12) mesial parietal lobe and posterior cingulum, (13) lateral parietal lobe, (14) insula, (15) cingulum, (16) mesial occipital lobe, (17) lateral occipital lobe, (18) subcortical nuclei, and (19) cerebellum. We generated our functional network parcellation by using a modified version of the MIST_20 atlas (Urchs et al., 2017). The MIST_20 atlas was first resampled to a $4 \times 4 \times 4\ mm^3$ voxel resolution using 'mincresample' from the minc-toolkit (http://bic-mni.github.io/). The MIST_20 atlas has 7 parent functional network regions, which are divided into 20 children ((1) cerebellum – 2 children, (2) mesolimbic – 3 children, (3) somatomotor – 2 children, (4) visual – 2 children, (5) default mode – 4 children, (6) fronto-parietal and visual downstream – 3 children, (7) ventral attention, salience network, basal ganglia and thalamus – 4 children). The 20 children were regrouped to study the following 11 ROIs: (1) cerebellum, (2) mesolimbic, (3) somatomotor, (4) medial visual, (5) lateral visual, (6) default mode network, (7) ventral & dorsal visual stream, (8) frontoparietal network, (9) ventral attention, (10) auditory, (11) basal ganglia. The purpose of the regrouping was to fuse the four children of the default mode network and keep the children of the visual network separated. This would not be possible if the MIST_12 atlas would have been used. We decided to combine the children of the default mode network and separate the children of the visual network to keep the networks consistent with the most common spatial maps found by SPARK.

4.2.5 – Estimation of Hubs of the brain network using SPARK

For each selected subject, we used 7 minute runs of resting state fMRI data. Each preprocessed fMRI run had the SPARK methodology (Lee et al., 2016, 2018, 2022; Lee & Wang, n.d.; Razavipour et al., 2023; Wang, 2022) applied to estimate the organization of connector hubs for each individual at a whole brain level. SPARK uses a sparse-dictionary learning algorithm within a sparse Generalized Linear Model (GLM), which decomposes the fMRI signal of each voxel as a

linear sparse decomposition in *N* temporal time courses, learned iteratively from the data. Each of these dictionary time courses, entitled atoms, corresponds to a spatial map therefore defining *N* resting state networks. This is subject-specific dictionary learning. SPARK was implemented on as follows:

Step 1 – Sparse dictionary learning and spatial clustering: The core of the SPARK methodology consists in applying the vK-SVD algorithm, which is a variant of the K-SVD algorithm (Aharon et al., 2006), allowing for a voxel-level analysis. This algorithm was applied to each spatio-temporal fMRI dataset Y. The output of the vK-SVD iterative algorithm is dictionary learned from the data (as a list of characteristic atom time courses), as well as a sparse coding matrix assessing how the BOLD time course in each voxel could be decomposed, using the few (sparse) atom time courses. Each row in the sparse coding matrix is considered as a spatial map, characterizing an underlying RSN. For each voxel, *k*-hubness can be estimated as the number of non-zero sparse coefficients describing the specific time course of the voxel of interest, therefore providing a hubness map at the voxel level.

Step 2 - Bootstrap resampling of rs-fMRI data: To ensure SPARK would provide reliable estimates of *k*-hubness, the vK-SVD algorithm was applied to several bootstrap resampled datasets Y^b of the original data Y, following the methodology proposed in (Bellec et al., 2010). To do so, a circular bootstrap resampling of the preprocessed fMRI data was applied to generate $b = 1, \ldots 100$ resampled datasets Y^b, with equal dimensions to ensure individual level reproducibility of the sparse GLM decomposition. The length of each block was randomly chosen between 20 to 55 continuous sample time samples (Bellec et al., 2010). For each resampled dataset (Y^b), the same sparse GLM applied on the original dataset was applied. It is expected that each Y^b has a similar number of atoms. To find a spatially reproducible set of resting state networks across the B = 100 resampled datasets, we finally applied nearest neighbor spatial clustering to the collection of all B $\times$ *N* spatial maps to identify *N* stable and reliable clusters. The spatial maps were then spatially averaged within each cluster, therefore only retaining the most reproducible results at the individual level (*N* final spatial maps).

Step 3 – Removal of background noise: Any element which was inconsistent with a low signal amplitude in the averaged maps were considered as gaussian noise and removed by thresholding ($p<0.05$).

Step 4 – Removal of physiological noise: The spatial maps were visually inspected by myself and Yimeng Wang in order to exclude any maps which were contaminated with either physiological noise or motion (Griffanti et al., 2014; Lee et al., 2019). Furthermore, any spatial map which consisted of 30 voxels or less was also removed from the final sparse matrix (**Figure 4-1**).

Step 5 – Generation of the final k-hubness map: After this last thresholding of noisy non reproducible results over the averaged sparse coding matrix, we can now estimate a sparse matrix which is free of physiological noise, motion, background noise and small clusters. If we were to count the number of non-zero elements of each column will give us the discrete number of RSNs

associated with each voxel, which is the *k*-hubness value for said voxel. We can then generate the resulting *k*-map, which will show the location of all the connector hubs in the individual's brain.

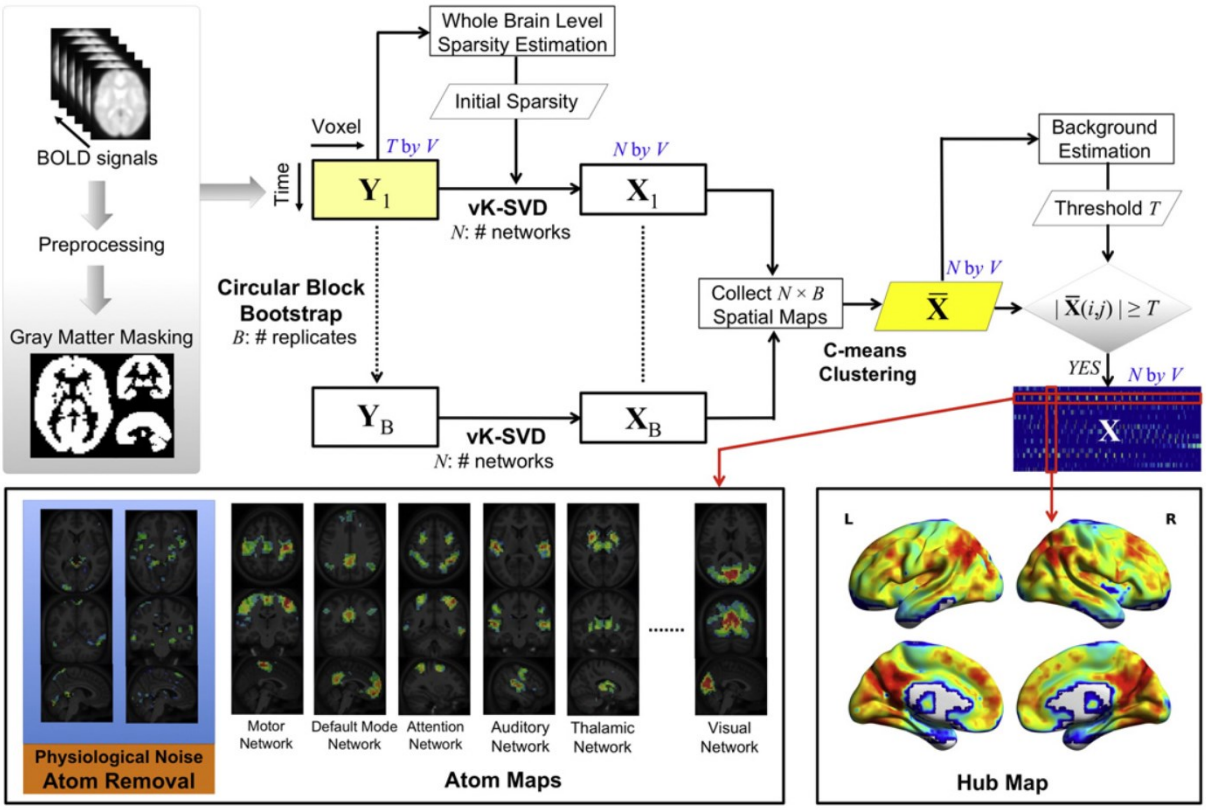

Figure 4-1 Summary of SPARK workflow. *Source: Lee et al., 2016*

4.2.6 – Incorrect removal of noisy atoms

While processing data, we found out that there was a small error in the code which was used to remove the atoms which were visually marked as noisy. This issue led to a mislabeling of the atoms, and therefore removal of the incorrect atoms. Due to this issue, atoms which were marked as noise could have remained in the analysis, and atoms which were marked as RSNs were accidentally being removed. When dealing with small and discrete *k* values (i.e: *k = 1,2,3,4….),* we first wanted to study the impact the issue had on our dataset before correcting it. Therefore, along with my colleague Édouard Delaire, we classified the number of mislabeled atoms, the difference in the percentage of *k*-hubness which occurred at a group level for each population. Finally, to visualize the regions impacted by the error, we calculated the difference in the average *k*-hubness maps for all three populations:

$$< kmap_{new} > - < kmap_{old} >$$

Where $kmap_{new}$ are the *k*-hubness maps after fixing the error, and $kmap_{old}$ are the *k*-hubness maps which included the error.

4.2.7 – Probability maps of *k*-hubness distribution and the impact of zeros

It is worth mentioning that voxels which did not exhibit reliable reproducible results over all bootstrap samples, which were thresholded at step 3 in **Section 4.2.5**, were therefore exhibiting *k*-hubness values of zero, mainly because no reliable findings could be exploited from those voxels. Before performing our analysis, we wanted to first characterize the spatial distribution of hubness within the brain. To do so, we generated maps, estimating for each voxel the probability of finding a specific *k*-hubness value across each population (HC, TLE, FLE) for k = 0, 1, 2, 3, 4, to understand where the hubs would be found in the brain. The purpose of this was to see if there were any ROIs we should focus on. Therefore, we generated maps which calculated the probability of finding a particular *k*-value across each population (HC, TLE, FLE). We may define the probability as:

$$Prob(k) = \frac{number\ of\ subjects\ in\ the\ population\ with\ (k)}{total\ number\ of\ subjects\ in\ the\ population}$$

where *k* is the *k*-hubness value of interest, with discrete values of 0, 1, 2, 3, 4.

4.2.8 – Hub Disruption in TLE and FLE

The hub disruption index (HDI) was first proposed by (Achard et al., 2012) and was applied to the SPARK framework and further validated by (Lee et al., 2018, 2022).

In this study, we wish to study HDI at the group level by comparing the distribution of *k*-hubness values of each participant to the distribution of the *k*-hubness values of the healthy control group. To achieve this, the following linear regression model was applied to the data:

$$d^P = a\frac{\mu_k^C}{\sigma_k^C} + b$$

$$d^P = \frac{\mu_k^P - \mu_k^C}{\sigma_k^C}$$

In this model, μ_k^C represents the mean *k*-hubness values across the healthy controls estimated for a particular voxel in a defined ROI, μ_k^P represents the mean *k*-hubness values across a patient group (in this case of this study, FLE or TLE) for a voxel in a defined ROI, and σ_k^C is the standard deviation of the *k*-hubness values across the healthy controls for a voxel in a defined ROI. The variable *a* represents the slope of the regression line, which is the HDI value; and the variable *b* represents the y-intercept of the regression line, which is the HEI value. As this is a linear regression model, d^P represents y-axis values and μ_k^C/σ_k^C represents x-axis values, a scatterplot with *N* datapoint will be generated (with N being the number of voxels in the ROI).

If the HDI value (i.e.: the slope) is negative, it means that a voxel which was considered a hub in the healthy population becomes a non-hub in the patient group, representing an overall hub

disruption within the ROI. If the HDI value is positive, it means that a voxel which was a hub in controls is becoming even more connected in the patient population. This means more connections are formed with distant brain regions, leading to 'hyperconnectivity'. For HEI, if we have a positive value (i.e.: a positive y-intercept), it means that a voxel which was considered a non-hub in the healthy population is becoming a hub in patients. HEI cannot be negative as a voxel cannot be associated with a negative number of networks (Lee et al., 2018, 2022).

To determine if the HDI and HEI values obtained were significant, for each defined ROI in both the anatomical and functional network segmentations, we performed a permutation test. Null data was created from mixing each individual subject group with the healthy subjects (i.e.: randomized FLE-HC data and TLE-HC data). We then created equally sized groups of our original cohorts using the randomized datasets. HDI and HEI were then calculated 1000 times and the empirical p-value was calculated from the null data (p<0.05). This validation scheme was inspired by (Lee et al., 2022).

4.2.9 – Hierarchical Segregation in TLE and FLE

To determine if a ROI is functionally segregated or divided into sub-networks, (Lee & Wang, n.d.) proposed the metric of the Hierarchical Segregation Index (HSI). In this context, HSI_i is defined for each voxel i as the ratio of regional k-hubness for the ROI of which the voxel belongs to ($k_{i\in R}^R$) and the corresponding voxel-level k-hubness (k_i^V):

$$HSI_i = \frac{k_{i\in R}^R}{k_i^V}$$

The regional k-hubness ($k_{i\in R}^R$) is estimated by counting the number of resting state networks involved in a specific ROI. First, the voxels which are associated with the ROI are identified using our predefined regions, and subsequently are extracted from the sparse coefficient matrix, generating a sub-matrix where each voxel is a member of the ROI. We then calculate the percentage voxels that each network occupies in the ROI by:

$$\%vol_j^R = \frac{n_j^R}{n^R} \times 100\%$$

where $\%vol_j^R$ is the percentage of voxels occupied by the network in the ROI, n_j^R is the count of the number of voxels belonging to the ROI involved with each network j, and n^R is the total number of voxels in the ROI. Finally, when estimating regional-k, we only want to consider the major networks involved in the ROI. We therefore set a threshold where $\%vol_j^R > 6\%$, following (Wang, 2022).

For a given voxel, having a high HSI value implies that the number of RSNs involved in the defined ROI is greater than the number of RSNs associated with the voxel, suggesting within-region inhomogeneity of the ROI, meaning that there are sub-networks involved within ROI, indicating functional network segregation. If we were to have a low HSI, it implies that the voxel

is involved in a similar number of RSNs as the total number of RSNs found in the ROI. Having a low HSI implies within-region homogeneity, or integration between subnetworks within the ROI. Having a voxel with a low HSI volume represents a voxel which is well integrated and is highly valuable within the ROI.

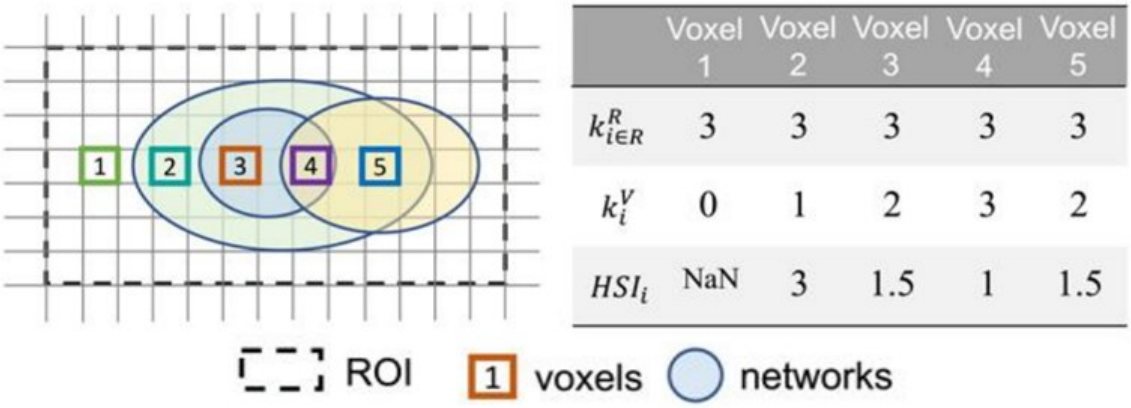

	Voxel 1	Voxel 2	Voxel 3	Voxel 4	Voxel 5
$k^R_{i\in R}$	3	3	3	3	3
k^V_i	0	1	2	3	2
HSI_i	NaN	3	1.5	1	1.5

Figure 4-2 The method of the hierarchical segregation index (HSI). HSI is computed for each voxel as the ratio of the regional *k*-hubness value and the voxel level *k*-hubness value. In this simplistic example, the regional-*k* ($\boldsymbol{k^R_{i\in R}}$) value is equal to three, as there are three networks in the ROI. The voxel-level *k*-hubness ($\boldsymbol{k^V_i}$) for this voxel is 3, due to the three networks belonging to the voxel. Therefore, HSI for this voxel will be low (i.e.: there is more integration or there is less segregation in the region). *Adapted figure from (Lee & Wang, n.d)*

4.2.10 – Voxel-wise between group comparisons for population *k*-maps, and HSI maps

To compare the resulting voxel level results for our group average *k*-maps and group average HSI maps between populations, we performed a voxel-wise two sample non-parametric permutation test where we tested for inter-population variability. We considered *n* individual hubness maps across subject groups A and B (i.e: HC and TLE), and calculated the group average *k*-hubness values $\langle h\rangle_A$ and $\langle h\rangle_B$ by average the *k*-hubness values for each voxel *i* across all subjects *n*. This generated a test-statistic *T* as the observed difference for each voxel.

$$T = \frac{meanA - meanB}{\frac{(nA-1)\times varA^2 + (nB-1)\times varB^2}{nA+nB-2} \times \sqrt{\frac{1}{nA}+\frac{1}{nB}}}$$

where $meanA$ is the mean of our first population, $meanB$ is the mean of our second population, nA is the number of subjects in the first population, nB is the number of subjects in the second population, $varA$ is the variance of the first populations and $varB$ is the variance of the second population.

To determine if our results were statistically significant, null data was generated using 10,000 permutations. For each permutation, the *n* hubness maps were pooled and randomly mixed to generate two randomized states *A'* and *B'*, each consisting of either *nA* or *nB* randomly selected maps. The T_{null} statistic was calculated using the aforementioned statistic. A *p*-value was estimated

from each T statistic for each voxel and was adjusted using the false discovery rate (FDR) correction (Benjamini & Hochberg, 1995). The resulting maps were thresholded at $p_{FDR} < 0.05$.

4.3 – Results

4.3.1 – Impact on the incorrect removal of noisy atoms

The problem with the mislabeling occurred after the manual denoising of the atoms took place. An example of the manual denoising process can be seen in **Figure 4-1- Atom Maps** and is a step where we manually remove atoms which exhibit physiological, respiratory or motion signals. Once noisy atom maps have been identified visually, they should be discarded from further analysis and the sparse matrix needs to be updated to estimate the final *k*-map, not impacted by physiological noise (i.e.: cardiac, respiration, motion).

At the time of writing this thesis, we were under the assumption as a team that the error had impacted all previous work involving SPARK, which was either published, or under review for publication. We decided to do an in-depth analysis on the impact of the error to determine whether it was necessary to further investigate the impact on our previous datasets. As a team, we were worried that there was a possibility that we would need to publish revision articles and redo all previous analyses. Thankfully, we concluded that the error only affected this dataset onwards, which has little impact on the previously completed work in the lab. We decided to include this analysis in the thesis to demonstrate the significant impact the error would have had on our subsequent analyses in this document, and future work done in the lab as well.

In fact, the software was generating two final sparse matrices: the first one entitled ('thrfinal') still contained the atoms with < 30 voxels, and the second entitled ('thrfinalX') from which atoms with less than 30 voxels were already removed. Unfortunately, we found out that the *thrfinal* was being loaded, and therefore atoms which needed to be manually discarded were being removed before removing atoms featuring less than 30 voxels. This confusion led to a mislabeling between the atoms. In **Table 4-1** an example of such mislabeling of the atoms is provided. In this example, there were 18 atoms which were available for manual classification and denoising. Through the manual denoising process, we had determined that atoms 2, 4, 10, and 13 were noisy atoms and needed to be removed from the sparse matrix. What happened was the *thrfinal* matrix was being loaded, and we removed the atoms with the indices 2, 4, 10, 13, even though there was one extra atom in the matrix (which was atom 3). This led to a mislabeling of the noisy and non-noisy atoms, meaning some of the atoms which were labeled as noise (4, 10, 13) were then labeled as non-noise, and atoms which were labeled as non-noise (5, 11, 14) ended up being labeled as noise and were removed from the sparse matrix. This resulted in physiological and motion noise being kept, whereas RSNs of interest were removed.

Total Number of displayed atoms	Number of atoms < 30 voxels	Atoms manually classified as noise	Atoms misclassified as noise
18	1	2, 4, 10, 13	2, 5, 11, 14

Table 4-1 Example of misclassification of atoms due to error in the code after manual denoising.

We wanted to further quantify impact of such misclassification. The number of misclassified atoms for each subject which can be found in **Figure 4-3** and are presented as follows: (1) the number of atoms which were classified as a RSN and remained a true RSN despite mislabelling (i.e: a true positive), (2) the number of atoms which were classified as noise and remained noise despite mislabeling (i.e: a true negative), (3) the number of atoms which were originally classified as RSN and became noise (i.e: a false negative), and (4) the number of atoms which were classified as noise and became considered as RSN (i.e: a false positive). From **Figure 4-3**, we found that around 50% of our subjects were impacted by the error, and had the wrong atoms being discarded from further analysis. This is a significant impact since we are working with small, discrete numbers for the *k*-hubness values (i.e: k = 1,2,3,4,5…), therefore an accidental removal of networks can drastically change the regions of connector hubs which would lead to false *k*-maps and impact all further analyses.

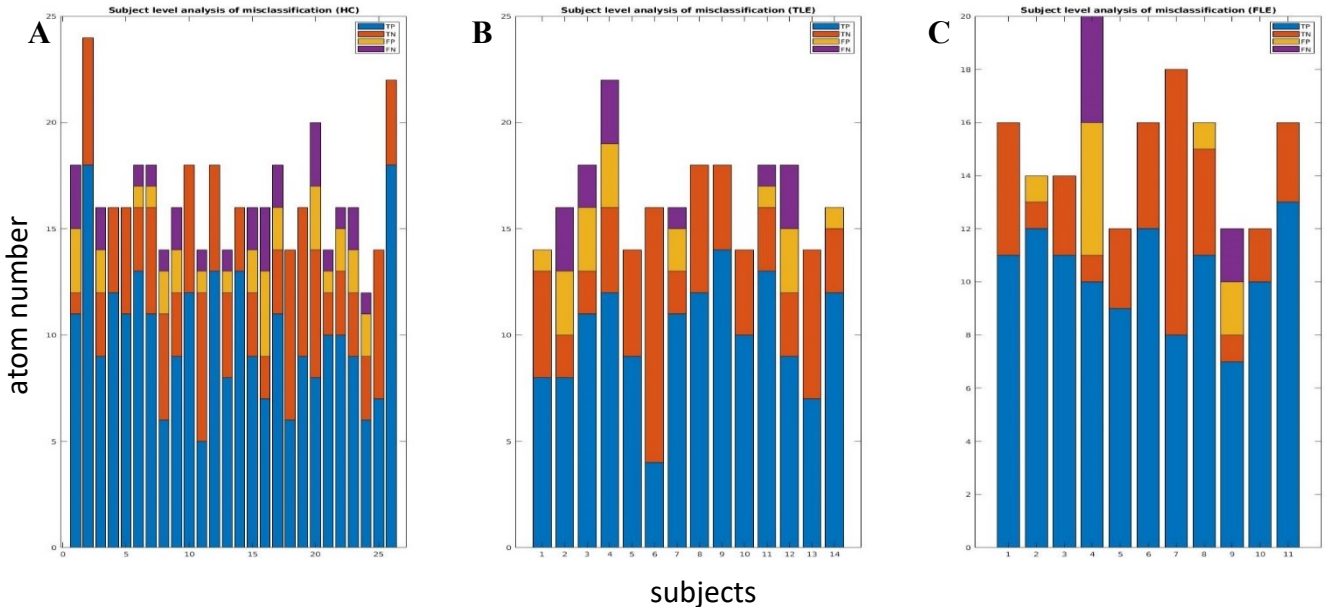

Figure 4-3 The impact of the misclassification of atoms for every subject. For each graph, blue is the number of atoms which were classified as a RSN and remained a RSN (i.e: a true positive), orange is the number of atoms which were classified as noise and remained noise (i.e: a true negative), yellow is the number of atoms which were classified as noise and became a RSN (i.e: a false positive) and purple is the number of atoms which were classified as a RSN and became noise (i.e: a false negative). Each subject is represented along the x-axis, while the number of atoms is along the y-axis. **(A)** Shows the analysis for Healthy Controls, **(B)** shows the analysis for Temporal Lobe Epilepsy and **(C)** shows the analysis for FLE patients.

To continue, we performed an analysis to study the impact of such misclassification of noisy atoms by studying the overall changes *k*-hubness values. This analysis was important for us to perform

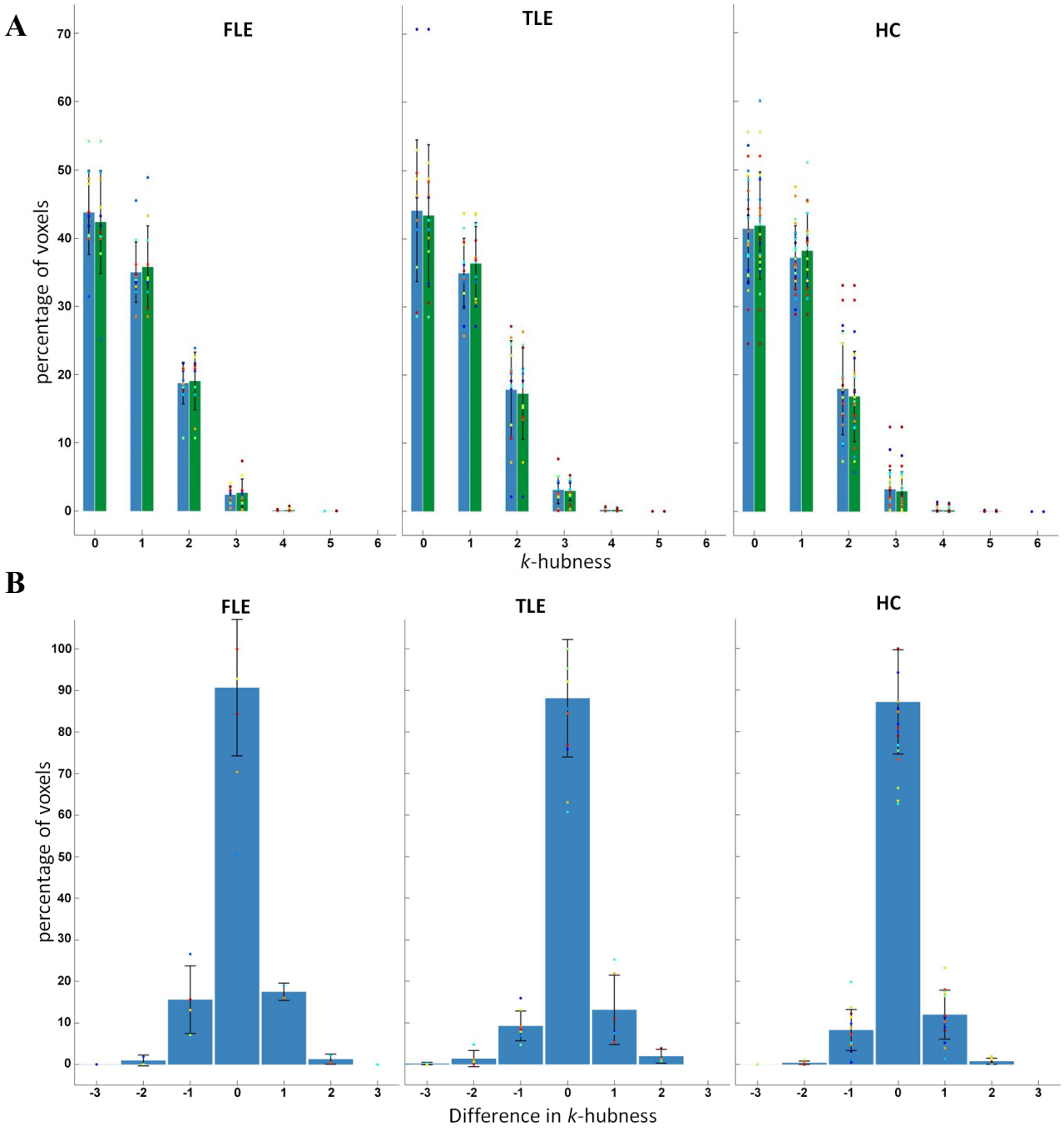

Figure 4-4 Difference in k-hubness after correcting the error due to manual denoising. Each colored dot represents one patient. The colored dots do not coincide between the two figures. **(A)** The percentage of k-hubness values for each voxel for every subject for the k-hubness maps with the error (blue) and the k-hubness maps without the error (green). **(B)** The percentage of voxels which had a difference of k-hubness values of either -3, -2, -1, 0, 1, 2, 3 between the k-hubness maps with the error and without the error for FLE, TLE, and HC.

since we are dealing with such small discrete values. Simply the change from a *k*-hubness value from one to two unveils a connector hub which was originally not there. In **Figure 4-4**Error! Reference source not found. we are displaying the overall change in *k*-hubness values as a percentage of all affected voxels for all participants. In **Figure 4-4A**, we can see the trend that the percentage of voxels which had a *k*-hubness of zero decreases in FLE and TLE cases, indicating that full RSNs have been restored after correcting the misclassification. Finally, in **Figure 4-4B**, we are able to see that the majority of voxels exhibited no change in the difference of *k*-hubness values, but there were some voxels which were associated with a change of *k*-hubness of -2, indicating that the region was influenced by noisy atoms.

Finally, to visualize the regions which were the most affected by such an error, we generated spatial maps which showed the difference between the average *k*-hubness maps across the three population groups. In **Figure 4-5**, blue regions represent areas where $kmap_{new} < kmap_{old}$, resulting in a negative difference in average *k*-hubness. These results suggest that these regions in $kmap_{old}$ were mainly impacted by the presence of noisy atoms, which were then removed and therefore decreased the *k*-hubness values in $kmap_{new}$. Regions which are yellow represented areas where $kmap_{new} > kmap_{old}$, indicating that full resting state networks have been reinstated into the analysis after correction of the mislabelling. The spatial maps indicate that many of these changes happened along the cortical surface, where most RSNs are found.

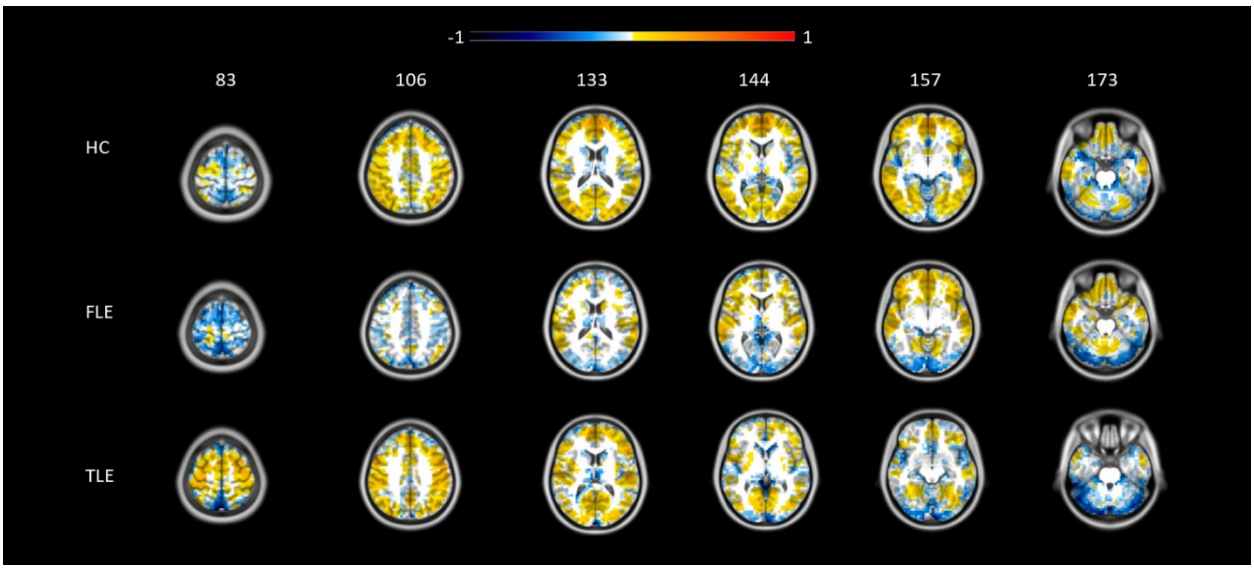

Figure 4-5 Impact of the mislabeling of noisy atoms during manual denoising. The difference between the group average voxel level ($\boldsymbol{k^V}$) k-hubness maps $< \boldsymbol{kmap_{new}} > - < \boldsymbol{kmap_{old}} >$.

4.3.2 – Probability maps of *k*-hubness distribution and the impact of zeros

After applying fMRI preprocessing and SPARK to estimate *k*-hubness values at an individual level, we generated probability maps to assess inter-subject reproducibility between resulting *k*-maps. To do so, for each discrete *k* value ($k = 0, 1, 2, 3, >4$), we estimated as the probability of finding such a *k* value at the voxel level along our studied population.

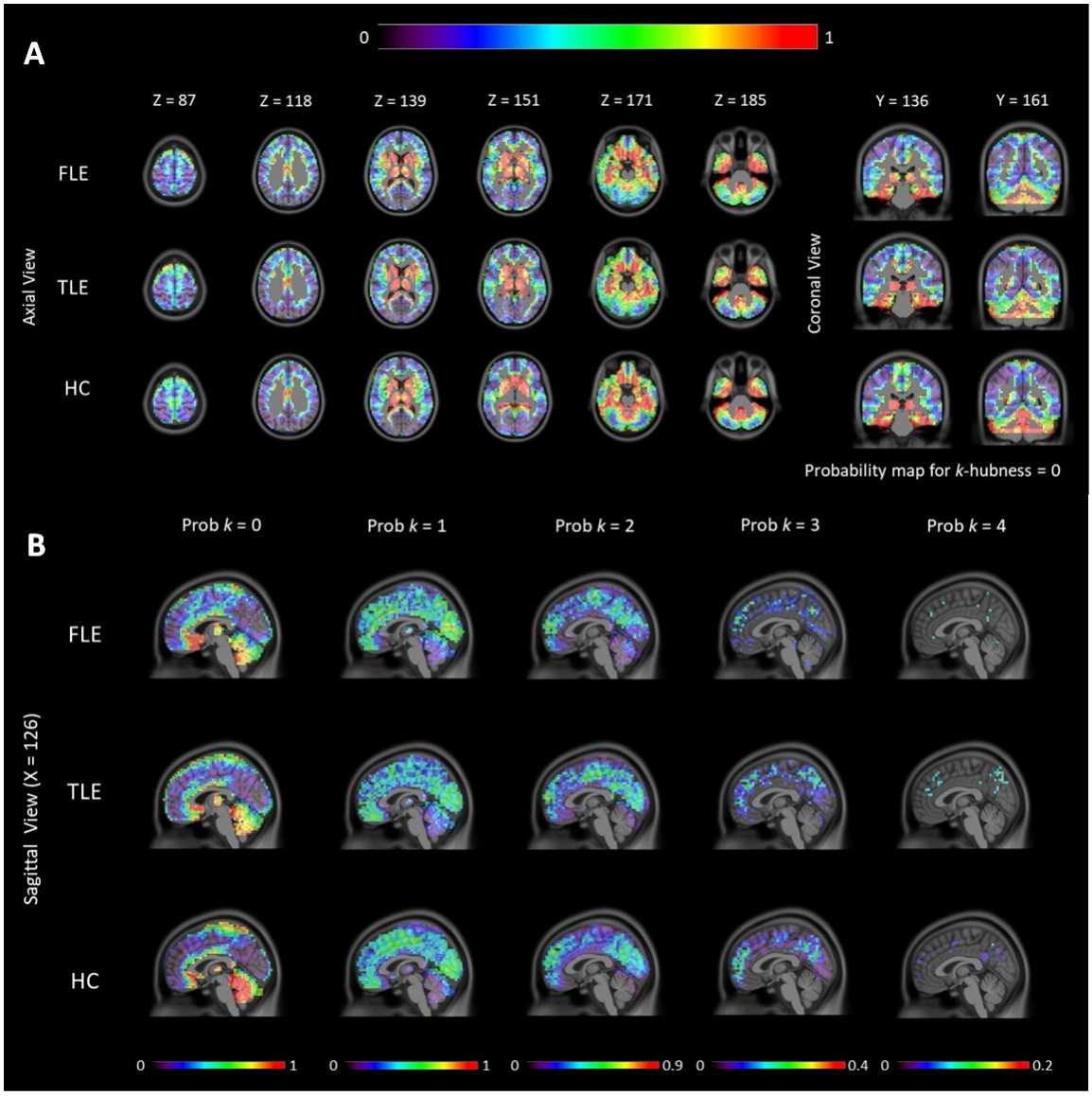

Figure 4-6 Functional hubness probability maps for FLE, TLE and HC subjects. The maps show the probability of finding a particular value of *k* at any voxel *i*. **(A)** Probability map for $k = 0$ in the axial and coronal plane for FLE, TLE and HC. **(B)** Probability maps for $k = 0, 1, 2, 3, 4$ for FLE, TLE and HC in the sagittal plane.

In **Figure 4-6**, we are displaying these probabilistic *k*-hubness maps, while emphasizing the probability map for $k = 0$ in **Figure 4-6A**, reporting voxels that were found less reliable at the subject level over the different bootstrap resamples. We found that the probability of observing $k = 0$ was very high and above 80% for the subcortical nuclei regions, and the temporal lobes after

denoising across all three populations Within the SPARK framework, whenever a voxel was attributed a $k = 0$ value, it does not mean that there was no resting state network associated with the voxel. The presence of zeros may rather indicate lack of stability and reliability over all bootstrap vK-SVD analyses or by large the influence of noisy components (such as physiological noise, cardiac, respiration, and motion artifact) which were removed during the manual denoising process. The physiological noise fluctuations were more likely of larger amplitude than the slow fluctuations of the resting state networks. It might also be the case that low sparse coefficients associated with those voxels were removed after the thresholding which takes place during the background noise thresholding (*step 3* in **Section 4.2.5**), therefore suggesting voxels exhibiting poor reproducibility over bootstrap samples. Importantly, we found that mesio-temporal regions as well as subcortical regions, which are quite important when studying TLE and FLE data were exhibiting a large proportion of $k = 0$ values. We also noticed that the cerebellar region also exhibited a high probability of $k = 0$ in healthy controls, whereas this was less the case for patients with epilepsy, suggesting hub reorganizations. These findings are important and could potentially impact future analyses which will take place in these regions since there might be an unreliable baseline which we are comparing to.

When assessing the *k*-hubness probability maps for our $k = 1, 2, 3, 4$ values, our findings reproduce other work by our group (Razavipour et al., 2023), showing regions involving the largest hubness values ($k = 3, 4$) were the posterior cingulate and the anterior mesial frontal lobe, as well as bilateral fontal and parietal regions. Regions exhibiting non-hubness values ($k = 1$) were mainly composed of central bilateral regions, and the cerebellum, whereas the visual cortex is characterized by hubness values of $k = 1$ and $k = 2$.

4.3.3 – Assessment of Hub Disruption and Hub Emergence Profiles in TLE and FLE

Whereas in our groups first study, (Lee et al., 2018), HDI and HEI were only evaluated within mesio-temporal regions and default mode networks in TLE patients, in this present analysis, our goal was to expand such analysis and explore a complete spatial distribution of HDI values within the whole brain in both TLE and FLE patients when compared to healthy controls. Therefore, we proposed two parcellations of the brain: (1) an anatomical segmentation consisting of 19 regions of interest covering the entire brain and (2) a functional resting state network segmentation consisting of 11 networks of interest. We believed that performing these two analyses were important to carefully assess whether hub disruption would be influenced by larger networks composed of multiple anatomical regions throughout the brain. We also believe that the functional segmentation will be less influenced by the presence of voxels with $k = 0$ values, leading to a more reliable HDI value when compared to the anatomical segmentation. This section will have the anatomical analysis presented first, and the functional analysis second.

In previous studies using this metric by our group (Lee et al., 2018; Wang, 2022), the hub disruption and emergence indices were extracted and used as a final conclusion to characterize the change in hubness in specific regions of interest. In this work, to assess whether the difference we found in HDI and HEI were indeed driven by differences between the two populations of interest

(i.e.: TLE versus controls and FLE versus controls), rather than by anatomical distribution of hub values in both populations, we performed a further validation by generating a null hypothesis distribution of HDI and HEI values. This was obtained by performing random permutations between the two groups of interest (i.e.: TLE versus controls and FLE versus controls) before estimating HDI and HEI values under such a null hypothesis, following the method proposed in (Lee et al., 2022). To generate the null data, we randomly assigned *k*-maps to each group (epilepsy or control), of equal size to the original groups and calculated HDI 1000 times. We then performed a unilateral uncorrected permutation test $p < 0.05$ to determine regions of significance, i.e: when HDI and HEI values measured on our patient population were significantly deviating from our null hypothesis empirical distribution.

Anatomical Segmentation Analysis

In **Figure 4-7**, we are presenting the anatomical segmentation with the 19 regions of interest for which we calculated HDI and HEI metrics.

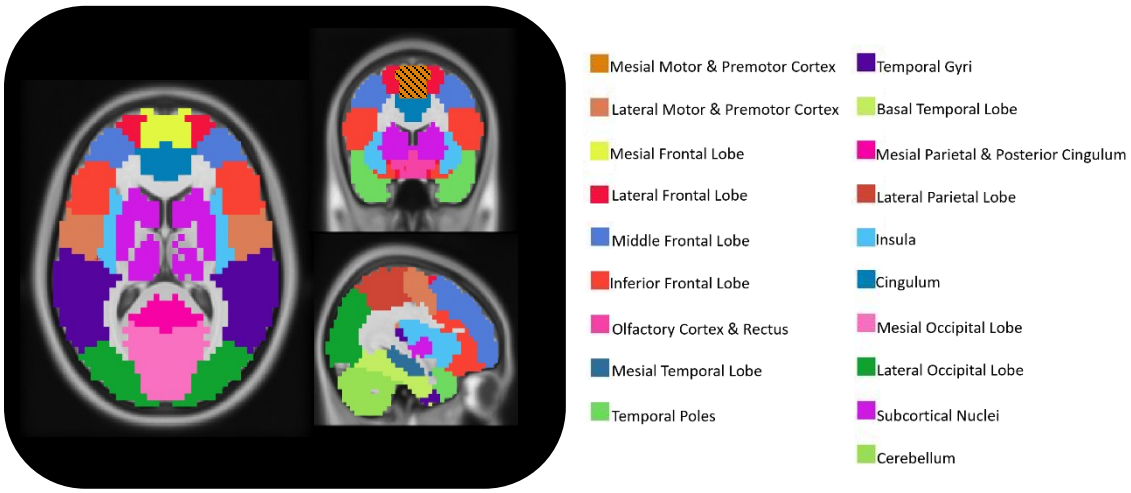

Figure 4-7 Anatomical brain segmentation. The anatomical segmentation has 19 regions of interest for which we will be calculating HDI and HEI.

In the plot found in Error! Reference source not found., we have a sample of the linear regression line plot from which we extract our HDI (slope) and HEI (intercept) values. In this figure, we are studying the cerebellum ROI. In red, we have the TLE group and in blue we have the FLE group. In the figure, we have included the HDI and HEI values for both TLE and FLE. We have also included the R2 metric which describes the fit of the regression line, showing the strength of the correlation between our patients and controls. The shaded region behind the regression line represents a 95% confidence interval, which is a visual representation of the error on the fit of the line. In the calculation for HDI and HEI, we are evaluating hub reorganization in our patient population when compared to our healthy controls. On the plot, each point represents a voxel in the ROI. For every voxel in the ROI, the x-value is equal to the mean *k*-hubness values across

healthy controls (μ_k^C), divided by the standard deviation of the k-hubness values across healthy controls (σ_k^C). The y-value of each datapoint is equal to the mean k-hubness values across the patient population (μ_k^P) of interest subtracted by the mean k-hubness values across the healthy population (μ_k^C), which is then all divided by the standard deviation of healthy patients (σ_k^C) in each voxel. The plots for the calculation of HDI and HEI in all the 19 anatomically defined regions can be found in **Figure 4-9**.

If we were to perform an analysis of HDI and HEI for healthy controls, the resulting regression line would have both a slope and intercept of zero by design. For this explanation, we shall define our 'baseline healthy controls' as Group A and our 'patient healthy controls' as Group B. Theoretically, the average k-hubness values across Group A and Group B should be similar to one another, as they are two groups of patients taken from the same population. In turn, this would make the difference calculation on the y-axis between the two populations equal to nearly zero, if not zero. This would lead to minimal to no variation along the y-axis. The only variation which

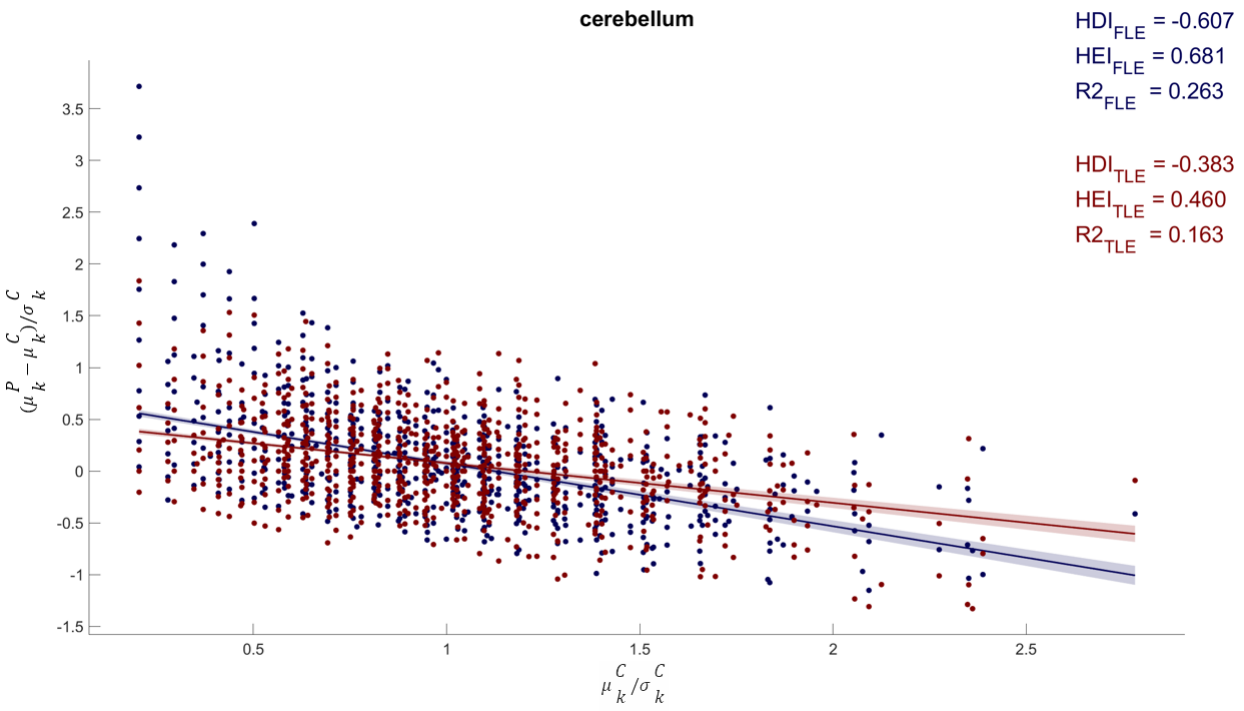

Figure 4-8 The linear regression plot for the cerebellum ROI in the anatomical segmentation. The FLE regression plot is demonstrated in blue and the TLE regression plot is demonstrated in red. Each point on the plot represents one voxel in the cerebellum ROI. The x-axis is the mean of the k-hubness values of the control group (μ_k^C) divided by the standard deviation of the control group (σ_k^C). The y-axis is the difference in the mean k-hubness between the patient population (μ_k^P) and the control group (μ_k^C), divided by the standard deviation (σ_k^C). These calculations were performed for each voxel in the ROI across all subjects. In this example, $HDI_{FLE} = -0.607$ and $HDI_{TLE} = -0.383$. A negative HDI value suggests that a connector hub found in our control population is becoming less connected, or a non-hub in our patient population. Furthermore, $HEI_{FLE} = 0.681$ and $HEI_{TLE} = 0.460$. A positive HEI suggests that a non-hub in controls is becoming a hub in patients. The $R2_{FLE} = 0.263$ and $R2_{TLE} = 0.163$, are indicating there a decent correlation between the two variables. The shaded region behind the regression line represents a 95% confidence interval, visualizing the error on the fit of the line.

would occur would be along the x-axis, where we would be calculating the average *k*-hubness values for Group A. The resulting regression line would be a horizontal line at y = 0.

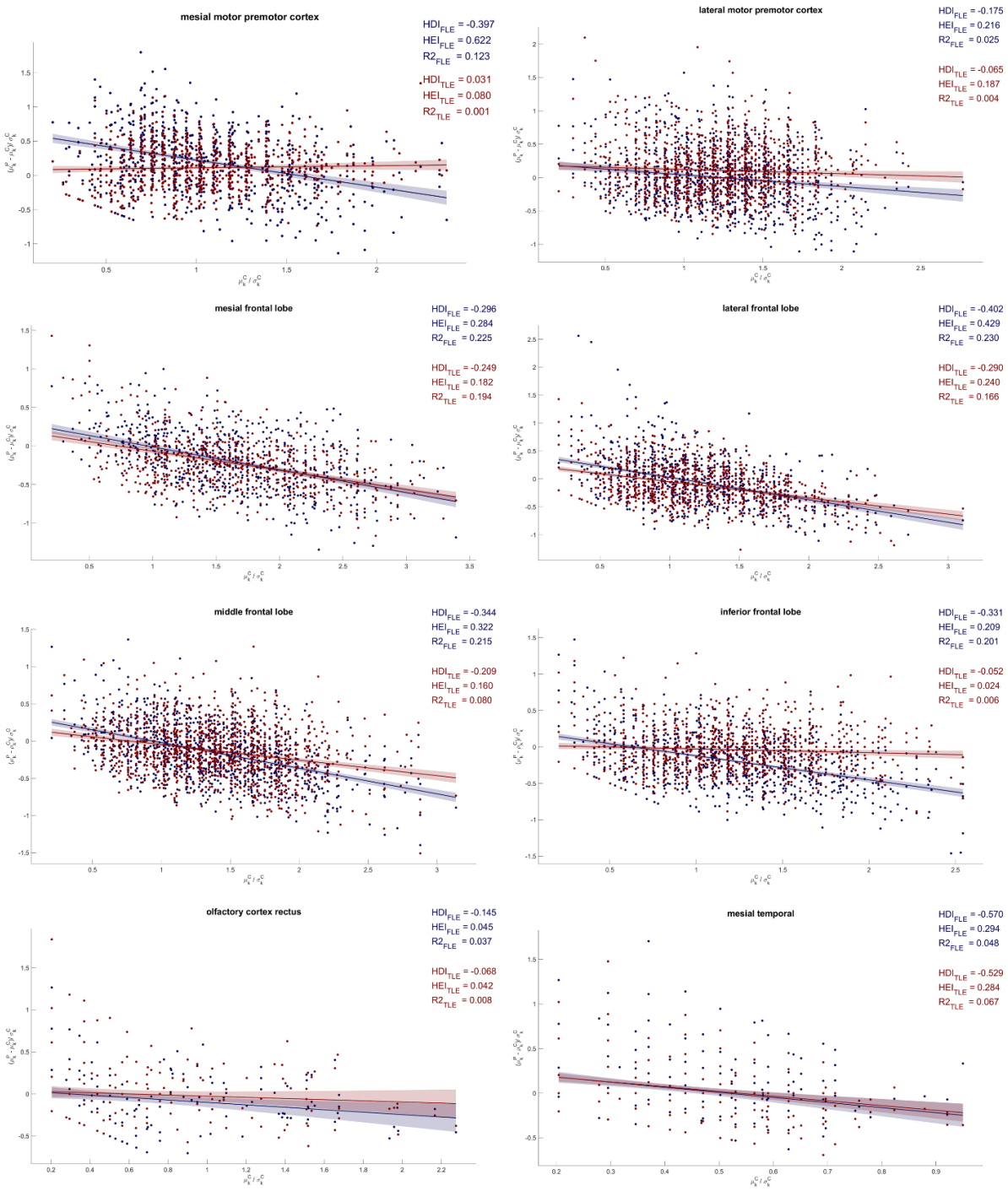

Figure 4-9 Hub disruption and hub emergence plots for all 19 anatomically defined regions. Frontal lobe epilepsy patients are shown in blue and temporal lobe epilepsy patients are in red. The HDI is the slope of the linear regression line and HEI is the y-intercept of the regression line. The x-axis is $\boldsymbol{\mu_k^C/\sigma_k^C}$, where $\boldsymbol{\mu_k^C}$is the mean *k*-hubness across all subjects in a voxel in healthy controls, $\boldsymbol{\sigma_k^C}$ is the standard deviation of the *k*-hubness values in a voxel across all controls and $\boldsymbol{\mu_k^P}$ is the average *k*-hubness for a voxel across patients.

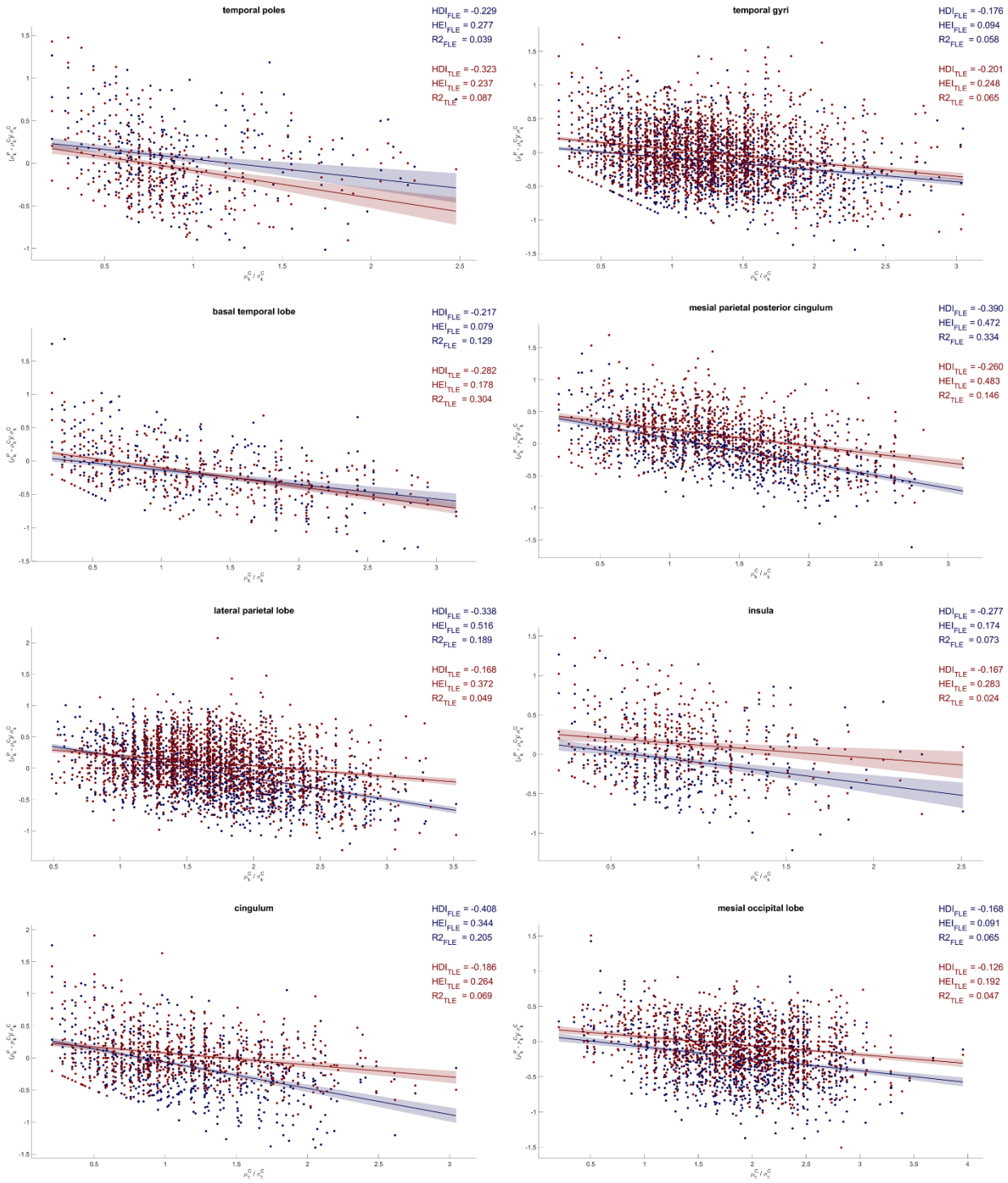

Figure 4-9 Hub disruption and hub emergence plots for all 19 anatomically defined regions (continued). Frontal lobe epilepsy patients are shown in blue and temporal lobe epilepsy patients are in red. The HDI is the slope of the linear regression line and HEI is the y-intercept of the regression line. The x-axis is $\boldsymbol{\mu_k^C/\sigma_k^C}$, where $\boldsymbol{\mu_k^C}$is the mean *k*-hubness across all subjects in a voxel in healthy controls, $\boldsymbol{\sigma_k^C}$ is the standard deviation of the *k*-hubness values in a voxel across all controls and $\boldsymbol{\mu_k^P}$ is the average *k*-hubness for a voxel across patients.

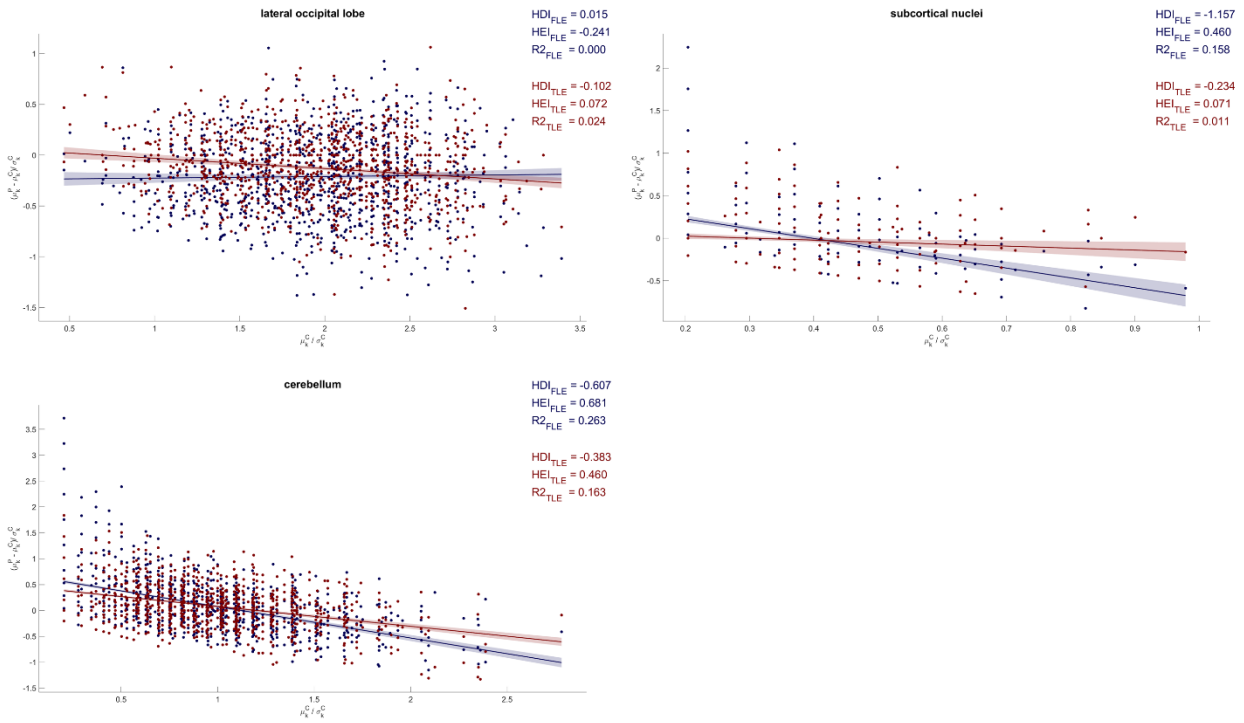

Figure 4-9 Hub disruption and hub emergence plots for all 19 anatomically defined regions (continued). Frontal lobe epilepsy patients are shown in blue and temporal lobe epilepsy patients are in red. The HDI is the slope of the linear regression line and HEI is the y-intercept of the regression line. The x-axis is $\boldsymbol{\mu_k^C/\sigma_k^C}$, where $\boldsymbol{\mu_k^C}$is the mean *k*-hubness across all subjects in a voxel in healthy controls, $\boldsymbol{\sigma_k^C}$ is the standard deviation of the *k*-hubness values in a voxel across all controls and $\boldsymbol{\mu_k^P}$ is the average *k*-hubness for a voxel across patients.

In **Figure 4-11**, we have our estimated HDI (**Figure 4-11A**) and HEI values (**Figure 4-11B**) plotted in dark blue for FLE and dark red for TLE patients against the null distribution for each group, which is light blue for FLE and light red for TLE. For HDI, after performing the permutation tests, we found that only the mesial motor and premotor cortex (p = 0.03, *HDI* = 0.031) were showing a significant increase in HDI value when compared to the null distribution for TLE. For FLE, the lateral frontal lobe (p = 0.04, *HDI* = -0.402), mesial parietal and posterior cingulum (p = 0.03, *HDI* = -0.390), lateral parietal lobe (p = 0.03, *HDI* = -0.338), cingulum (p = 0.02, *HDI* = -0.408) and cerebellum (p = 0.02, *HDI* = -0.607) were all exhibiting a significant decrease in HDI values when compared to the null distribution. For HEI, we found that for TLE, only the mesial parietal and posterior cingulum region (p = 0.02, *HEI* = 0.483) displayed a significant increase in HEI from the null distribution. For FLE, we found that the mesial motor and premotor cortex (p = 0.04, *HEI* = 0.277), and the cerebellum (p = 0.02, *HEI* = 0.681) displayed a significant increase in HEI when compared to the null distribution. Surprisingly, the lateral occipital lobe (p = 0.008, *HEI* = -0.241) showed a significant decrease in HEI compared to the null distribution, resulting in a negative HEI value which does not follow the theory of the metric, since exhibiting less hubness in patients than a non hub region in controls is not possible, therefore raising suspicions regarding the accuracy of this region. Such a specific finding should be investigated in further detail.

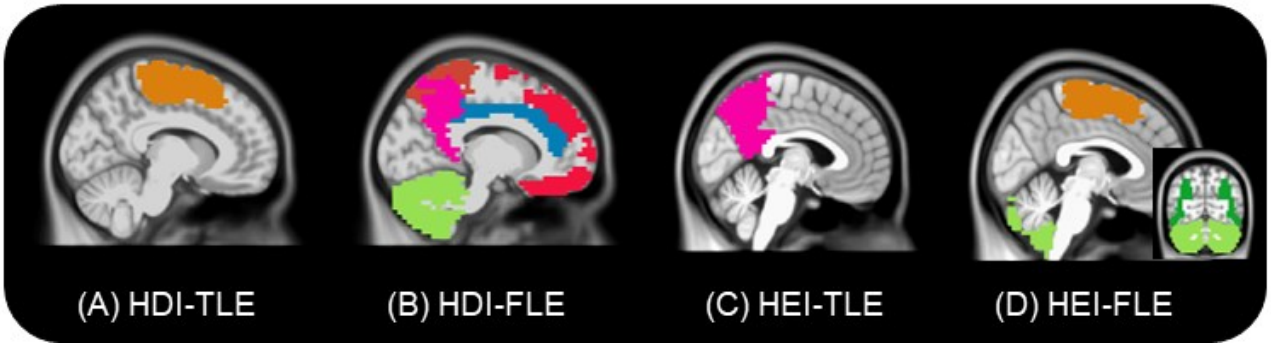

Figure 4-10 Anatomical regions which showed significant HDI and HEI values when compared to the null datasets. The colors are simply a way to differentiate the anatomical regions which were found to be significant and correspond with the colors found in **Figure 4-7**. (A) Significant increase in HDI for TLE was found in the mesial motor and premotor cortex. (B) Significant decrease in HDI for FLE was found in the lateral frontal lobe, mesial parietal and posterior cingulum, lateral parietal lobe, cingulum, and cerebellum. (C) Significant increase in HEI for TLE was found in the mesial parietal and posterior cingulum. (D) Significant increase in HEI for FLE was found in the mesial motor and premotor cortex and the cerebellum. There was a significant decrease in HEI for FLE found in the lateral occipital lobe.

In **Figure 4-10**,we are showing the anatomical regions which showed either significant hub disruption or hub emergence superimposed on the volume of the brain.

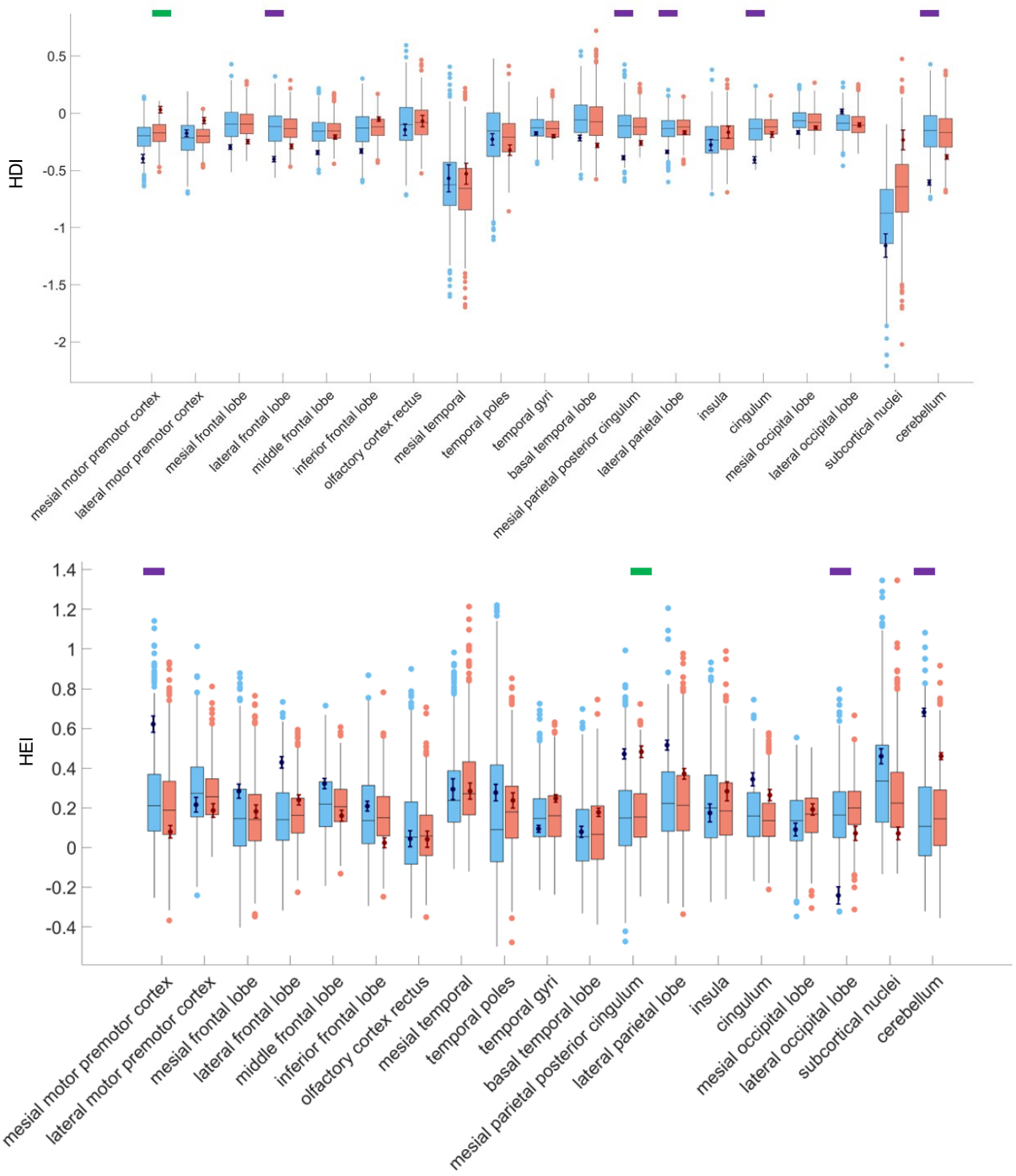

Figure 4-11 Hub disruption and emergence distribution for the anatomical segmentation. The null distribution for FLE is showed in light blue, the null distribution for TLE is shown in light red, the HDI values for FLE and TLE from **Figure 4-9** are in dark blue and dark red respectively. A unilateral uncorrected permutation test (1000 permutations, $p < 0.05$) was used to define regions of significance. Regions of significance are indicated with a purple bar for FLE and a green bar for TLE. (**top**) HDI analysis. **(bottom)** HEI analysis.

Functional Network Segmentation Analysis

In **Figure 4-12**, we are presenting the functional network segmentation with the 11 resting state networks for which we calculated HDI and HEI metrics. In **Figure 4-13**, we have the linear regression plots from which we extract our HDI (the slope) and HEI (the intercept) values. In these plots, TLE is found in red and FLE is found in blue. We have also included the R2 metric which describes the fit of the line, showing us the strength of the correlation between our patients and controls. For all of the plots in **Figure 4-13** except for the basal ganglia and auditory networks, the error on the fit of the line in **Figure 4-9** is pretty strong as the shaded regions represent a 95% confidence interval.

When studying HDI with the functional network segmentation, we found that for FLE, the cerebellar network (p = 0.02, HDI = -0.666), the default mode network (p = 0.04, HDI = -0.312) and the ventral dorsal visual stream (p = 0.03, HDI = -0.267) are all exhibiting a significant decrease in HDI values when compared to the null data distribution, suggesting overall hub disruption within those networks in FLE patients. When investigating TLE data, we found that the somatomotor network (p = 0.03, HDI = 0.075), the ventral attention network (p = 0.049, HDI = -0.013), and the auditory network (p = 0.003, HDI = -0.098) showed significant increases when compared to the null distributions, whereas the HDI value were still overall negative, except for the somatomotor network, suggesting values close to zero, i.e: hub disruption similar to healthy subjects as previously described. These results are surprising and are not in agreement with our previous investigations. When studying HEI with the functional network segmentations, we found that for FLE, only the cerebellum (p = 0.02, HEI = 0.751) exhibited a significant increase of HEI value when compared to the null dataset, suggesting emergence of new hubs when compared to healthy controls. When investigating TLE data, we found that the cerebellum (p = 0.04, HEI = 0.512) and the medial visual network (p = 0.04, HEI = 0.441) showed a significant increase of HEI values when compared to the null dataset, suggesting the emergence of new hubs within those regions.

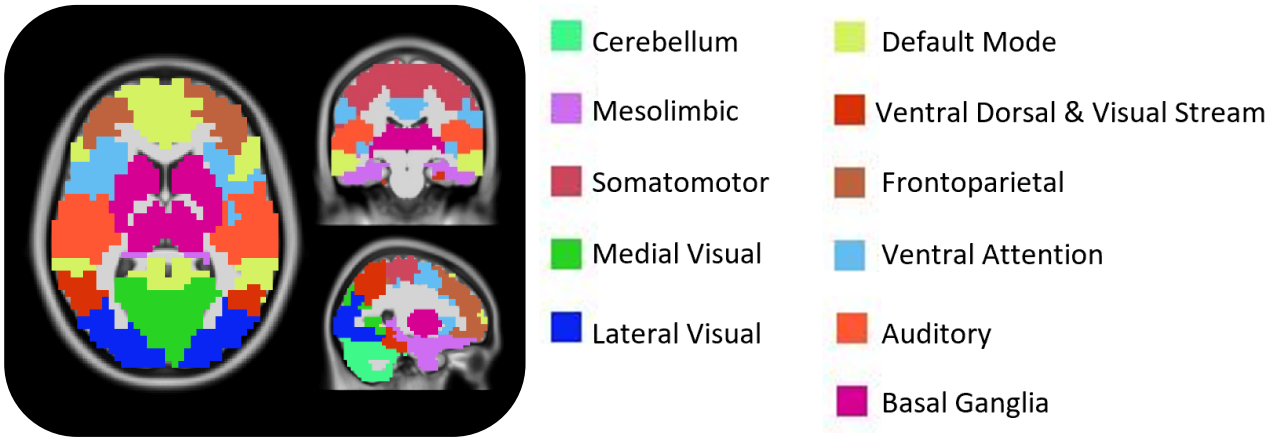

Figure 4-12 Functional brain segmentation. The functional segmentation has 11 regions of interest for which we will be calculating HDI and HEI.

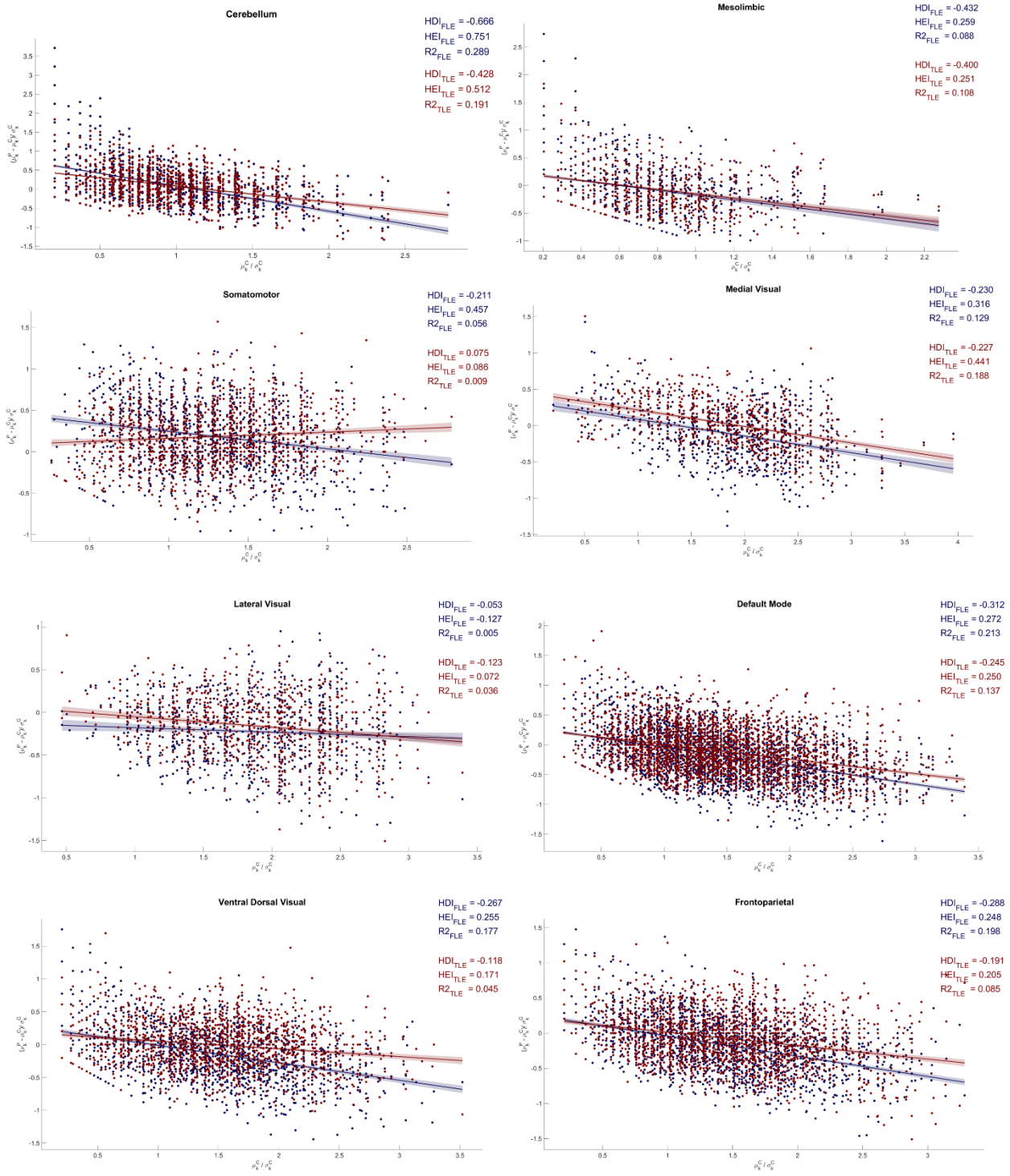

Figure 4-13 Hub disruption and hub emergence plots for all 11 functionally defined regions. Frontal lobe epilepsy patients are shown in blue and temporal lobe epilepsy patients are in red. The x-axis is $\boldsymbol{\mu_k^C/\sigma_k^C}$, where $\boldsymbol{\mu_k^C}$is the mean *k*-hubness across all subjects in a voxel in healthy controls, $\boldsymbol{\sigma_k^C}$ is the standard deviation of the *k*-hubness values in a voxel across all controls and $\boldsymbol{\mu_k^P}$ is the average *k*-hubness for a voxel across patients.

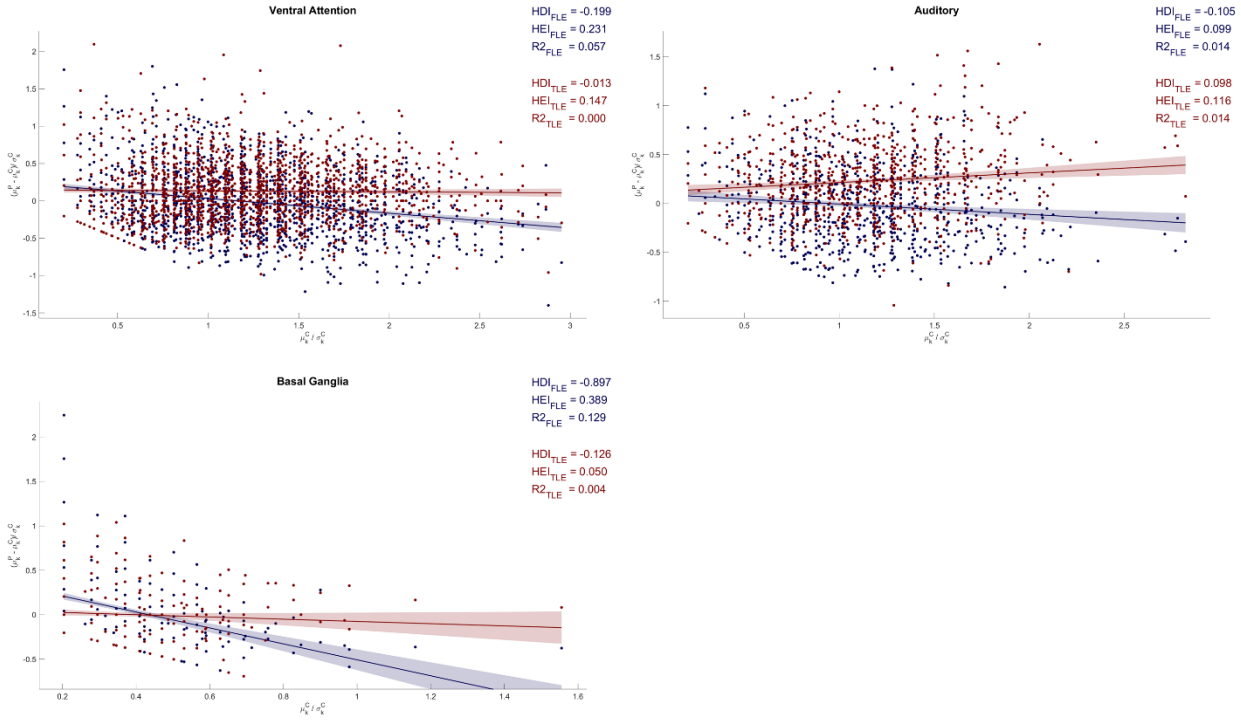

Figure 4-13 Hub disruption and hub emergence plots for all 11 functionally defined regions (continued). Frontal lobe epilepsy patients are shown in blue and temporal lobe epilepsy patients are in red. The x-axis is $\boldsymbol{\mu_k^C/\sigma_k^C}$, where $\boldsymbol{\mu_k^C}$is the mean *k*-hubness across all subjects in a voxel in healthy controls, $\boldsymbol{\sigma_k^C}$ is the standard deviation of the *k*-hubness values in a voxel across all controls and $\boldsymbol{\mu_k^P}$ is the average *k*-hubness for a voxel across patients.

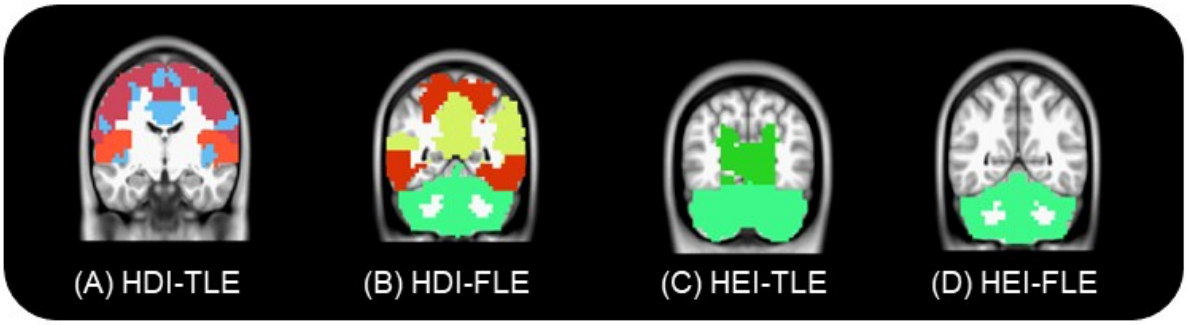

Figure 4-14 Functional network regions which showed significant HDI and HEI values when compared to the null datasets. The colors correspond to the functional network color code found in **Figure 4-12**. **(A)** Significant decreases in HDI for FLE was found in the cerebellum, default mode network, and the ventral dorsal and visual stream. **(B)** Significant increases in HDI for TLE were found in the somatomotor, ventral attention and auditory networks. **(C)** A significant increase of HEI was found in the cerebellum for FLE. **(D)** A significant increase in HEI was found in the cerebellum and medial visual network for TLE.

In **Figure 4-14**, we are showing the functional networks which showed significant HDI and HEI values in this analysis in FLE and TLE cases.

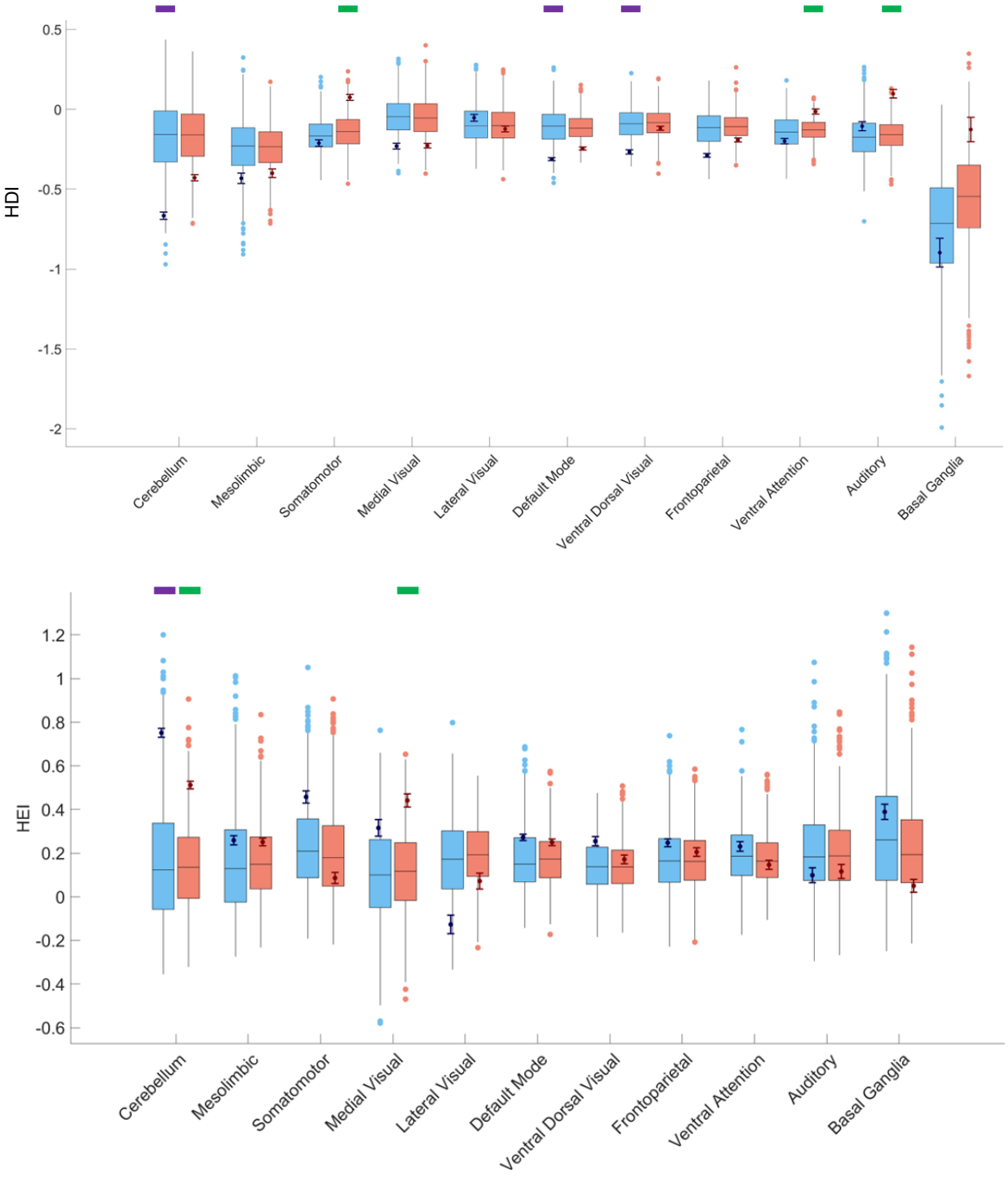

Figure 4-15 Hub disruption and hub emergence distributions for the functional segmentation. The null distribution for FLE is showed in light blue, the null distribution for TLE is shown in light red, the HEI values for FLE and TLE from **Figure 4-13** are in dark blue and dark red respectively. A unilateral uncorrected permutation test (1000 permutations, $p<0.05$) was used to define regions of significance. Regions of significance are indicated with a purple bar for FLE and a green bar for TLE **(A)** HDI analysis. **(B)** HEI analysis.

4.3.4 - Voxel Wise Group Comparisons

In **Figure 4-16A**, we are showing the group average *k*-hubness maps for each population, where we find higher hubness located in the posterior regions of the brain for each population. We performed two sample FDR corrected non-parametric permutation test at a voxel level between populations to determine if there were any significant differences in *k*-hubness occurring between populations. In **Figure 4-16**Error! Reference source not found.**B,** we found significant increases in hubness found between frontal lobe epilepsy patients and controls (FLE > HC) in the subcortical regions, and in the cerebellum (FLE > HC, TLE > HC). We believe that these results are strongly influenced by a poor fMRI signal, and the influence of *k*-hubness equaling zero in the region. This impact will be further discussed in **Section 4.4**.

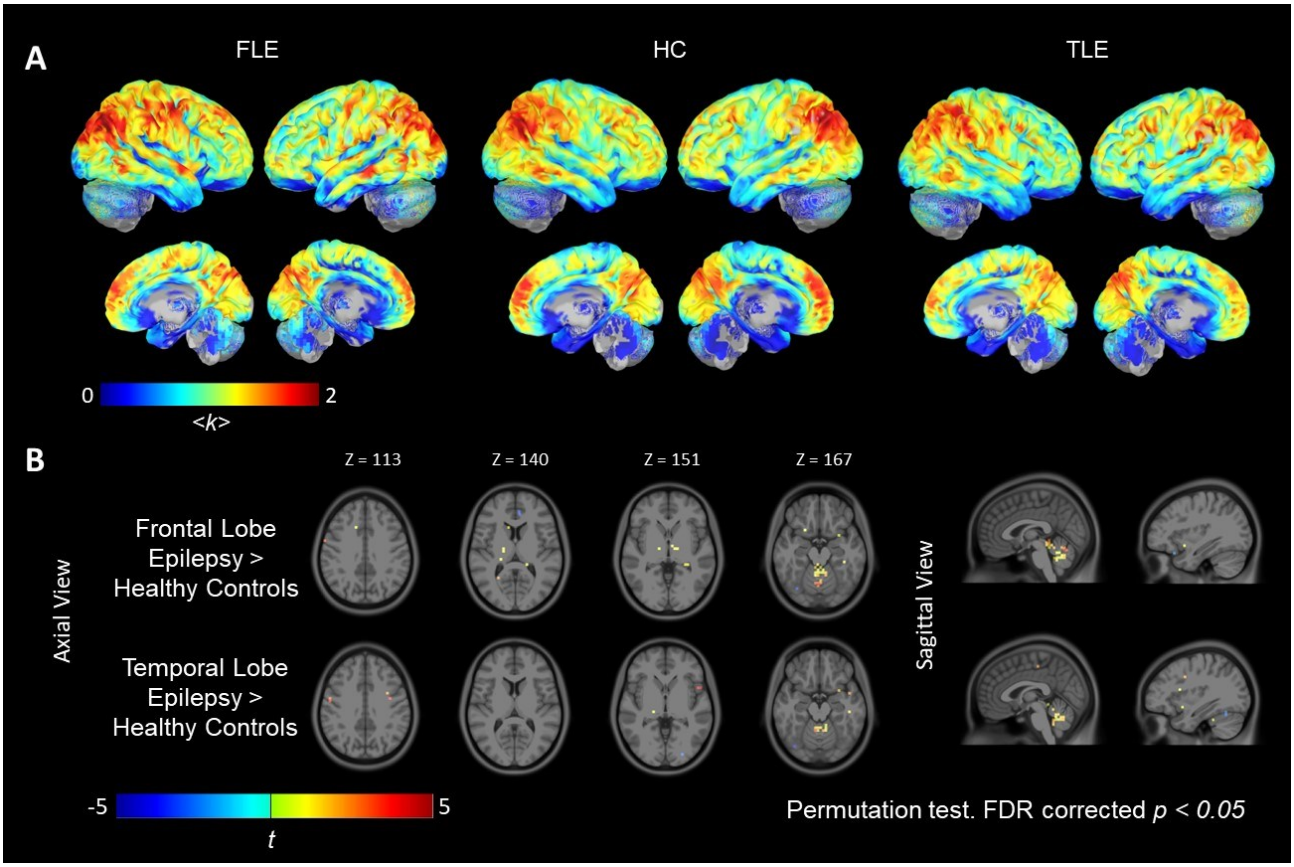

Figure 4-16 Group average k-hubness. (A) Voxel-wise group average k-hubness maps for the three subject groups, frontal lobe epilepsy, healthy controls, and temporal lobe epilepsy. **(B)** t-statistics map comparing voxel-level average k-hubness between subject groups: FLE > HC (top) and TLE > HC (bottom)**.** $p_{FDR} < 0.05$ using a two-sample permutation test with 10,000 permutations.

4.3.5 – Hierarchical Segregation of TLE and FLE

We performed a hierarchical segregation index analysis on the three subject groups using functional network segmentation. HSI was estimated as the ratio between regional level *k*-value over voxel level *k*-value. A large HSI value should therefore be interpreted as local segregation within the network (i.e.: more networks involved at the regional level which are less interconnected at the voxel level), whereas a small HSI would suggest more network integration within a specific region or network. Since the total number of atoms usually considered by SPARK is around 20, one should consider less regions to estimate regional-*k* values for this hierarchical measure. This is the reason why our group previously proposed and applied the HSI metric using a functional brain segmentation in nine networks when investigative reorganization of functional networks during sleep (Lee & Wang, n.d.). Our proposed analysis will investigate HSI once again at the functional network level, but we will follow the same functional regions we considered to estimate HDI and HEI values. For determining the regional *k*-hubness, a threshold must be set to quantify the number of major networks that are contributing to a specific region. This threshold was set at 6%, following the work from (Lee & Wang, n.d.). This threshold indicates that to be considered as major network within the region of interest, it must involve at least 6% of the voxels of this region.

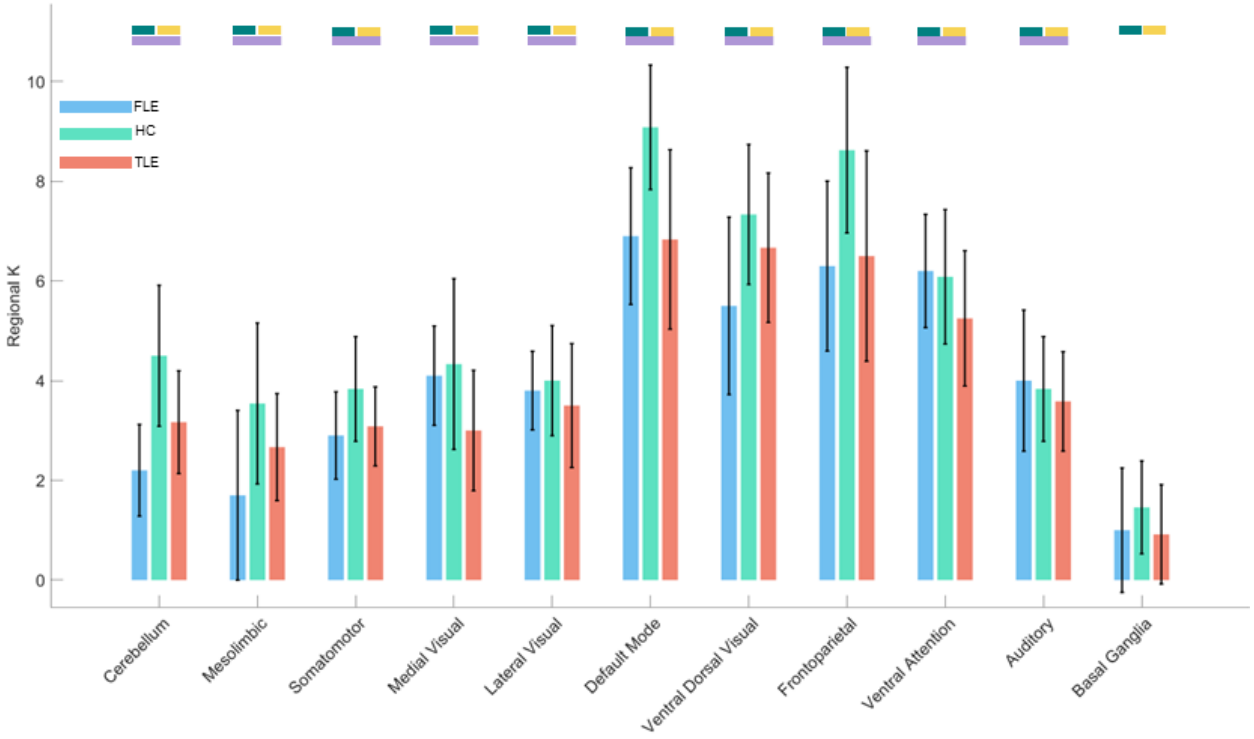

Figure 4-17 Group level regional *k* values for FLE, HC and TLE. The mean regional *k* value and standard deviation for each population and region. A Mann Whitney U Test, ($p< 0.05$, Bonferroni corrected for 33 tests) was applied to determine significant differences in regional *k* between populations. Populations which displayed significant differences are indicated with the bars on top of the plot: Teal bar is $p<0.002$ between FLE and HC, yellow bar is $p<0.002$ between TLE and HC, and purple bar is $p<0.002$ between TLE and FLE.

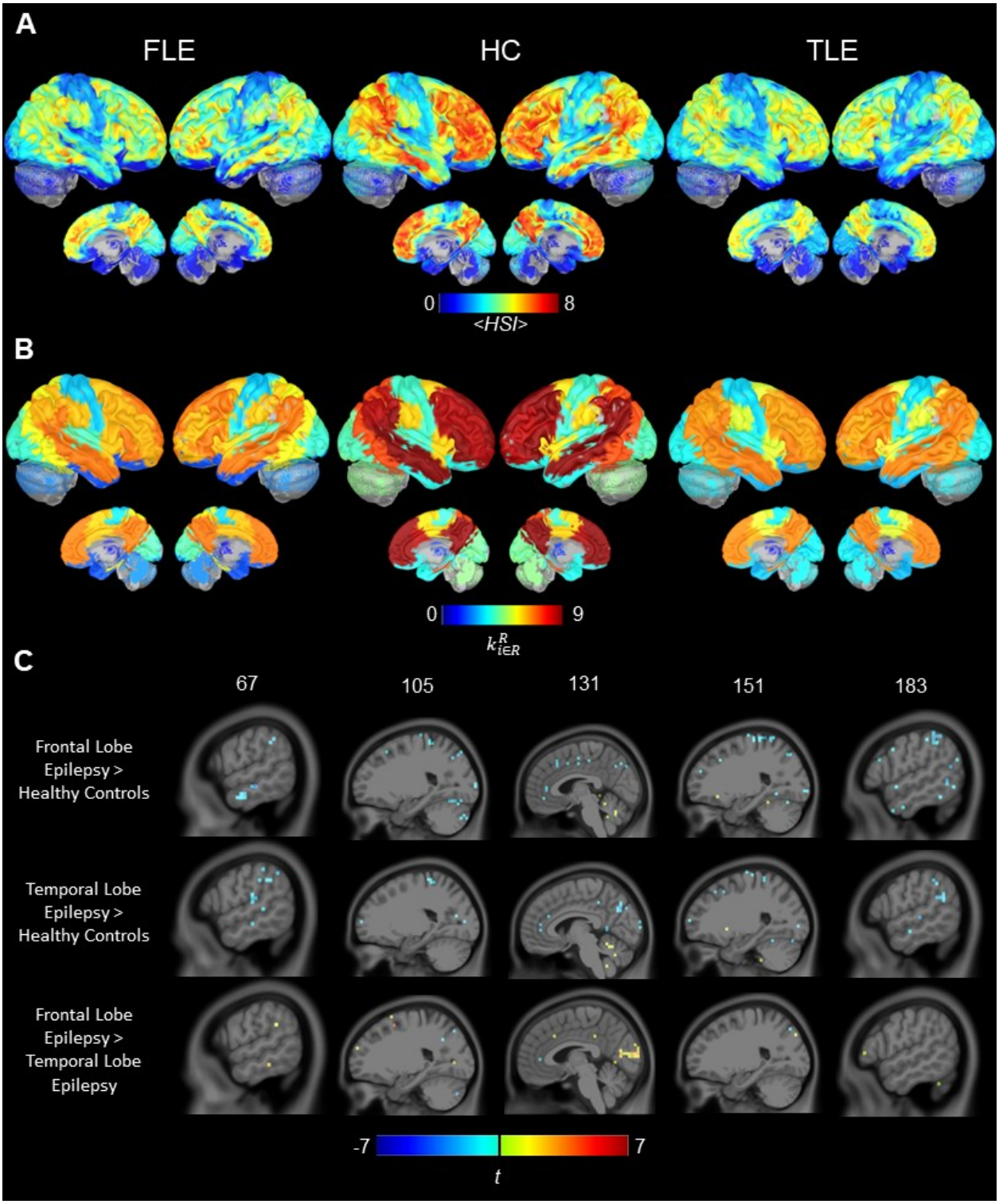

Figure 4-18 Group HSI and group regional k-hubness analysis performed with the functional segmentation. **(A)** Group average HSI plots across every voxel for frontal lobe epilepsy patients, healthy controls, and temporal lobe epilepsy patients. **(B)** Group average regional k-hubness for the 11 defined functional network regions. **(C)** t-statistics map comparing voxel-level HSI between subject groups: FLE > HC (top), TLE > HC (middle), FLE > TLE (bottom). $p_{FDR} < 0.05$ using a two-sample permutation test with 10,000 permutations.

In **Figure 4-18A**, we are presenting the group level HSI results, and are showing regions which demonstrated either a significant increase or decrease in HSI in epilepsy when compared to healthy controls in **Figure 4-18C** after performing a two-sample nonparametric permutation test with 10,000 permutations and corrected using FDR. We found that there was a significant decrease in HSI between frontal lobe epilepsy patients and healthy controls (FLE > HC) in the outer parts of the cerebellum, default mode network, frontoparietal network and the ventral attention network, suggesting that these networks are getting less segregated in FLE patients when compared to HC. When studying the changes of HSI between temporal lobe epilepsy and healthy controls (TLE > HC), we also found a significant decrease in HSI in the default mode network, the frontoparietal network and the auditory network, suggesting less segregation, i.e.: more network integration within these structures in TLE patients. Furthermore, we found a significant increase of HSI in the mesial cerebellum. Finally, when comparing the two epilepsy groups (FLE > TLE), we found mainly a significant increase in HSI in the medial visual network, suggesting more network segregation in FLE patients when compared to TLE patients.

Moreover, we also found significant differences occurring when investigating regional k between all three populations. The regional-*k* values are projected onto the cortical surface in **Figure 4-18B,** and the significant differences between the populations are shown in **Figure 4-17** after performing a Mann Whitney U Test, ($p< 0.05$) with Bonferroni correction for 33 tests, we found that only the basal ganglia network did not show a significant difference in regional *k* between FLE and TLE patients ($p = 0.3202$), but both FLE and TLE experienced a significant decrease in regional-*k* when compared to HC within the basal ganglia network. All comparisons except for the one between FLE and TLE in the basal ganglia network were significant at $p < 0.001$.

4.4 - Discussion and Conclusion

First, we found that the mislabeling of noisy atoms had a significant impact on the results, and we have corrected this error. Since we are working with small, discrete values of *k*-hubness (i.e: between *k*=1 to *k*=5), accidentally leaving in noisy atoms or removing network atoms would impact the resulting *k*-maps and all subsequent analyses. To study the impact throughout the whole brain, we calculated the difference in average *k*-hubness maps between the old average *k*-maps In particular, **Figure 4-5** shows us the spatial brain regions which were the most affected by the mislabeling error. In the figure, whenever the resulting map is blue, we are seeing areas where $kmap_{new} < kmap_{old}$, resulting in a negative difference in average *k*-hubness. These results suggest that these regions in $kmap_{old}$ were biased by noisy atoms which were accidentally kept in the *k*-map, and which were subsequently removed after correcting the mislabeling. The removal of these atoms therefore decreased the *k*-hubness values in $kmap_{new}$. In contrast, regions which are yellow represented areas where $kmap_{new} > kmap_{old}$, indicating that resting state networks were accidentally removed from the *k*-maps, and were reinstated when the mislabeling error was fixed. We found that the regions which were most impacted are shown in **Figure 4-5**, where we wish to highlight a few key, and important regions which may give us some insight into our

following results. Firstly, we can see that the frontal regions in slices 133, 144, and 157 all exhibited an increase in average *k*-hubness after the correction, shown by a deep orange color, meaning that we are reinstating networks in these regions. Secondly, we also observed an increase in *k*-hubness in the posterior cingulate cortex, as presented in slice 106. Furthermore, we can clearly see the impact of the sagittal sinus vein, particularly in slices 157 and 173, resulting in decreasing *k*-hubness after correcting the labeling. Leaving these results in would have creating false *k*-hubness values in critical regions for studying temporal lobe epilepsy, such as notably the mesial temporal structure regions that were highly impacted by the presence of cardiac physiological fluctuations. We also observed that the region of the basal ganglia, also had a large amount of mislabeling of noise, which could have had an impact on our results in that region. It is worth mentioning that our denoising scheme was probably too conservative, notably for mesio-temporal and subcortical structures. We find that noisy atoms involving those regions were often associated with a mixture of physiological fluctuations (i.e.: cardiac, respiration) and network patterns of interest that were not well separated. We are currently investigating new procedures to further denoise these structures in a more optimal manner. At the time of writing this thesis, we believed that there would have been an impact on all the previous work published by the lab using SPARK. Therefore, we wanted to perform this investigation to see the gravity of the impact, to determine if the error would have been significant enough to warrant an investigation into previous datasets. While we determined that the error had a impact on the results of this dataset, we thankfully able to conclude that it did not affect other work done in the lab. We deemed it necessary to include this analysis in the thesis as we believed there would have been a more widespread impact than there was in the end.

The analysis of *k*-hubness the probability maps reported in **Figure 4-6**. Particularly, in **Figure 4-6A**, we are studying the probability of a voxel having a *k*-hubness value of 0 across all subjects in each group. The results show that there were many regions where this probability was close to 100%, particularly in the regions of the basal ganglia, the mesial temporal lobe, and the medial cerebellum, therefore suggesting poorly reproducible results not passing our background noise thresholding or regions highly impacted by the manual removal of 'noisy' atoms. From the literature, we expect to see a decrease of functional connectivity in the basal ganglia network (Bettus et al., 2009), and the mesial temporal lobe (Vaughan et al., 2016), which theoretically through the SPARK framework would reduce the connector hubs down to a to a *k*-hubness value of k=1, meaning that a connector hub region would become a non-hub region, participating in only one RSN. However, our results in these regions are not showing such a pattern since they are mainly associated with $k = 0$ unstable results. This phenomenon may have occurred due to either of the following scenarios: (1) The SPARK method was not able to successfully characterize low amplitude signals within these regions, resulting in either an unstable or unreliable SPARK results that were filtered out from bootstrap analysis after background noise removal. This scenario is very likely for the region of the basal ganglia, as the algorithm randomly choses a starting seed within the brain to find correlating time courses with when learning the dictionary of time courses of key networks, in a purely iterative data driven manner. Out of the whole brain, the chance of

having signals resulting from the basal ganglia or mesiotemporal structures contributing to the dictionary is therefore small, especially knowing that deeper structures are usually associated with low Signal to Noise Ratio BOLD signals. (2) The SPARK method found atoms involving these regions, but they were highly contaminated with an amount of noise which required the atoms to be removed, especially remaining cardiac and respiration fluctuations, even if they were supposed to be removed by ICAFix during preprocessing. This scenario was most likely what resulted in the mesial temporal lobe and the medial cerebellum having many $k = 0$ voxels, since they are two regions which are very close to large blood vessels in the brain. Whatever the reason for the number of $k = 0$, the number of zeros present in these regions would have a direct influence on the plots presented in **Figure 4-9**, where there is a straight line which gives (x,y) pairs where they are of equal value. This 'line' of points only occurs when the mean *k*-hubness across all patients in a voxel is equal to zero, and we are therefore plotting the value of the mean *k*-hubness of the controls against itself. We believe that this so called "zero line" may have a small influence on pulling down the HDI and HEI values for every region in which occurs.

Regarding the number of zeros which were found, while not much can be done to fix scenario 2, it is critical that the SPARK methodology should be less biased by cortical large SNR regions during the dictionary learning phase. This work has already been assigned as the PhD project of a fellow member of the lab, proposing a new SPARK version where the dictionary would only be learnt from deep cortical and mesio-temporal regions. As the continuation of this thesis (during my PhD), we propose to carefully investigate why the analysis of this specific dataset resulted in so many $k = 0$ values (which was not the case in other SPARK analyses in the lab), reviewing carefully the different preprocessing steps (most notably ICAFix), which could have already removed some information of interest before we applied SPARK, as well as the investigate the impact of the number of bootstrap samples involved (B = 100 instead of 200 in our previous investigations).

For the main analysis of the thesis, we aimed to generate a whole brain profile of hub alterations in focal epilepsy when compared to healthy controls. Our overarching goal was to build a fingerprint model characterizing for the first time the reorganization of connector hubs within the whole brain for two patient populations, assessing what are the key regions exhibiting reorganization of connector hubs close to the presumed focus but also in distant regions. In the long term, following postsurgical workup of the patients, we expect to use these fingerprint models combining HDI and HEI as a tool to predict postsurgical outcome. We further adapted the work performed by our group on HDI and HEI in (Lee et al., 2018), by generating a null dataset of HDI and HEI values by randomizing the patient and healthy control cohorts, inspired by (Lee et al., 2022). We used the null dataset to perform a unilateral uncorrected permutation test with 1000 permutations to define regions exhibiting statistical significance for $p < 0.05$ when considering either the anatomical or the functional network segmentations when mapping for HDI and HEI values. It is important to note that the cerebellum and the basal ganglia were defined as nearly

identical regions within the two segmentation schemes, since they both constitute an anatomical brain region and a known resting state network.

The results for our anatomical segmentation are presented in **Figure 4-11**. We found that the mesial motor and premotor cortex was the only anatomically defined region exhibiting a significant change in HDI value for the TLE cohort. However, we surprisingly found a significant increase in HDI when compared to our null dataset. This was an interesting and unexpected finding, as we ended up with an $HDI = 0.031$, indicating that there is a slight positive HDI value, which would suggest that a hub in controls would become even more connected in the case of temporal lobe epilepsy patients. While the result was shown as significant through our statistical test, when looking at the plot for the mesial motor and premotor cortex in **Figure 4-9**, we can see that the fit of the regression line was $R2 = 0.001$, which is telling us that the regression is a very poor fit for the TLE patients. Therefore, this result should not be deemed reliable, as there was no true correlation found through the regression, suggesting rather not much change occuring in connector hub profiles when comparing healthy controls and TLE patients. When studying the results of HDI for the FLE cohort, we found a significant decrease in the lateral frontal lobe ($HDI = -0.402$), mesial parietal and posterior cingulum ($HDI = -0.390$), lateral parietal lobe ($HDI = -0.338$), cingulum ($HDI = -0.408$) and cerebellum ($HDI = -0.607$), suggesting hub disruption within those regions, i.e.: hubs in healthy population become non-hub regions in FLE patients. Each of these regions actually exhibited a strong negative trend in their individual plots in **Figure 4-9**, each associated with a relatively strong R2 values ranging from R2 = 0.189 for the lateral parietal lobe to R2 = 0.334 for the mesial parietal and posterior cingulum. We would therefore deem these results reliable, and we can confidently conclude that we have found significant hub disruption occurring in these regions, which imply that a hub in controls is becomes less connected in FLE patients. It is of great interest that regions a part of the fontal lobe were involved in such hub reorganization (i.e.: the lateral frontal lobe ROI) in FLE, but also more distant regions belonging to the default mode network (i.e.: the mesial parietal and posterior cingulum, the lateral parietal lobe and cingulum) and the cerebellum, suggesting extensive reorganization of brain networks architecture in the context of focal epilepsy. When studying HEI with this segmentation, we found a significant increase in HEI for TLE in the mesial parietal and posterior cingulum region ($HEI = 0.483$) when compared to the null dataset. The regional plots further confirm that we have a decent negative linear trend occurring in region (R2 = 0.146). A significant positive HEI value, i.e.: the appearance of a positive intercept in the linear fit, should be interpretated as the emergence of new hubs in patients, in regions considered as non-hubs in the healthy population, suggesting more connections being formed in the region, probably reflecting a compensatory mechanism in distant regions, associated with the hub disruption occurring elsewhere in the brain (such as suggesting new connections associated with the posterior cingulate region, a key region of the default mode network). When studying HEI in our FLE patients, we found that the mesial motor and premotor cortex ($HEI = 0.277$), and the cerebellum ($HEI = 0.681$) displayed a significant increase in HEI compared to the null distribution. Both regions show display a decent negative trend (R2 = 0.123 and R2=0.263 respectively), providing confidence in those results. Surprisingly, the lateral

occipital lobe ($HEI = -0.241$) showed a significant decrease in HEI when compared to the null distribution, resulting in a negative HEI value. Having a negative HEI value does not follow the theory associated with the metric, since a voxel cannot be associated with a negative number of networks. However, it is worth mentioning that the linear fit was poor for this region where $R2 = 0$. Therefore, we should not consider this finding significant as the linear model was unreliable.

The results with our functional network segmentation are found in **Figure 4-15**. We found when studying the changes in HDI in FLE that the cerebellar network ($HDI = -0.666$), the default mode network ($HDI = -0.312$) and the ventral dorsal visual stream ($HDI = -0.267$) all showed a significant decrease in HDI when compared to the null data. As previously mentioned, the cerebellum network nearly identical to the anatomically defined region, therefore we would expect the region to remain significant. These results are very interesting since they are suggesting hub disruption in several key regions. The default mode network has been previously found to exhibit a decrease in functional connectivity with mesio-temporal structure in temporal lobe epilepsy (Pittau et al., 2012), so finding a significant change in in the default mode network in frontal lobe epilepsy was of interest. The best fit line for the ventral dorsal visual stream and the default mode network are both decent (R2 = 0.177 and R2 = 0.213 respectively), with both plots showing a clear negative trend for FLE in **Figure 4-13**. When studying the TLE distribution, we found that the somatomotor network ($HDI = 0.075$), the ventral attention network ($HDI = -0.013$), and the auditory network ($HDI = -0.098$) all exhibited surprising significant increases when compared to the null distribution. However, exploring the linear fits in more detail (see **Figure 4-13)**, the R2 values for all three regions were all very close to zero, ranging from R2 = 0 for the ventral attention network to R2 = 0.01 for the auditory network, indicating no true correlation could be inferred. Therefore, we concluded that these TLE results are unreliable and should not be considered. Finally, when studying HEI with the functional segmentation, we found that for FLE, only the cerebellum ($HEI = 0.751$) exhibited a significant increase of HEI value when compared to the null dataset, in agreement with the results in the anatomical segmentation. When studying the TLE distribution, we found that the cerebellum ($HEI = 0.512$) and the medial visual network ($HEI = 0.441$) showed a significant increase of HEI values when compared to the null dataset. Both regional plots in **Figure 4-13** show decent R2 values (R2 = 0.191 for the cerebellum and R2 = 0.188 for the medial visual network) where we can determine that these are truly significant results for HEI.

Overall, we found interesting hub reorganization patterns for FLE patients, whereas not much was found for TLE patients. It is worth mentioning that our results are likely biased by the occurrence of too many $k = 0$ values, suggesting unstable SPRAK analyses, especially in mesio-temporal, subcortical and cerebellum regions. Therefore, our results should still be interpreted with caution. Several detailed further analyses should be considered to carefully investigate SPARK analysis on this dataset: (i) carefully investigating the impact of the preprocessing steps and notably ICAfix and the fact that we did not remove frame with motion (scrubbing as in our previous studies (Lee et al., 2016, 2018)) but here we rather regressed our the 'spiking' effect using motion outlier

confounds estimated from MICApipe using FSL. (ii) Investigating the impact of the number of bootstrap samples that occur (here B = 100 instead of B = 200 in our previous studies). (iii) Improving the separation between physiological noise fluctuations and signals of interest in those mesial structures by proposing a dictionary learning informed specifically by those structures.

In **Figure 4-16** we are reporting a voxel-level permutation test of all individual *k*-hubness maps to determine if there were significant differences between epilepsy patients and healthy controls. Our results indicate that there was a significant increase in average *k*-hubness in both the subcortical and cerebellum for FLE > HC, and in the cerebellum for TLE > HC. These results must be interpreted with caution since these regions were highly influenced by $k = 0$ in our probability maps in **Figure 4-6**. Therefore, we can conclude since we are comparing some non-zero values in epilepsy to the mostly zeros in our healthy cohort, we will obviously obtain a significant increase. However, finding these results in the cerebellum were more stable in epilepsy patients ($k = 1$) than in healthy controls ($k = 0$) is a finding of interest.

We then introduced the notion of regional *k* value by assessing the overall number of networks identified by SPARK within a specific predefined functional network (see **Figure 4-17**). When studying the differences in regional *k* across the three populations, we indeed found strong significant results for every comparison except within the basal ganglia network for FLE and TLE. These results are presented in **Figure 4-17,** and most tests we found highly significant ($p < 0.001$). When comparing regional-*k* for FLE and HC, we found a significant decrease in regional-*k* in the cerebellum, mesolimbic, somatomotor, medial visual, lateral visual, default mode, ventral dorsal visual stream, and the basal ganglia networks, indicating that there is an overall reduction of the number of networks involved within those regions. We also found a significant increase in regional-*k* in the ventral attention and auditory networks, indicating that the networks may have been rearranged due to the disease and are now involved in those regions. Moreover, we also found a significant decrease in regional-*k* between TLE and HC in all networks investigated. When comparing the two patient populations, we found a significant decrease in networks in FLE when compared to TLE in the cerebellum, mesolimbic, somatomotor, ventral dorsal visual stream, and frontoparietal networks. All other regions displayed a decrease in TLE. These results suggest that the resting state networks are less connected with each other in epilepsy, supporting the concept of hub disruption in **Figure 4-15.**

Additionally, in this project, we performed a hierarchical segregation index (HSI) analysis on our three groups using our proposed functional network segmentation. HSI was estimated as the ratio between regional level *k*-value over voxel level *k*-value. A large HSI value should therefore be interpreted as local segregation within the network (i.e.: more networks involved at the regional level which are less interconnected at the voxel level), whereas a small HSI would suggest more network integration within a specific region or network. This metric has been proposed as a SPARK generalization of functional clustering ratio metric of integration or segregation within hierarchical models of brain networks originally proposed by (Boly et al., 2012). The uniqueness of HSI as well as *k*-hubness mapping, provides us the ability to use study metrics at the voxel level,

whereas other metrics proposed in the literature only allow investigation at the regional level. Overall, our findings suggest there is a significant increase of HSI between FLE patients and HC medial cerebellum (more segregation), and a decrease of HSI in the default mode network, frontoparietal network, and the ventral attention network (more integration). When comparing TLE and HC, we found that regions within the default mode network, the frontoparietal network and the auditory network exhibited a significant decrease in HSI (more integration). We also found that when we compare the two epilepsy groups, there was a significant increase in HSI in the medial visual network, suggesting more segregation in FLE when compared to TLE.

Chapter 5 – Conclusion

In **Chapter 2**, we introduced the imaging modality of magnetic resonance imaging (MRI) which was used for this study. In this chapter, we introduced the physics of the modality, and introduced the blood-oxygen-level-dependent (BOLD) signal, which is used to obtain functional MRI (fMRI), which is used to study the activation patterns in the brain in either a task or resting-state condition. Furthermore, in this chapter, we introduced the popular measures of functional connectivity, and introduce the method developed in our lab, SParsity-based Analysis of Reliable k-hubness (SPARK). In **Chapter 3** we introduced the epilepsy disease and the patient cohorts we will be studying, frontal lobe epilepsy and temporal lobe epilepsy. In **Chapter 4**, we used our SPARK methodology (Lee et al., 2016) and the metrics of hub disruption index (HDI) and hub emergence index (Lee et al., 2018) to generate a fingerprint model characterizing for the first time the reorganization of connector hubs within the whole brain for two patient populations, assessing what are the key regions exhibiting reorganization of connector hubs either close to the presumed focus but also in distant regions. Furthermore, we also further investigated the functional connectivity in FLE and TLE when compared to healthy controls by comparing voxel-level *k*-hubness values, a regional *k*-hubness metric and the hierarchical segregation index (HSI) as a measure of network integration and segregation, recently proposed in (Lee & Wang, n.d.).

To generate our whole brain fingerprint, we calculated HDI and HEI for each region of interest while considering either an anatomical brain segmentation with 19 regions or a functional network segmentation with 11 networks. To determine if our calculated HDI and HEI values were deemed significant, we generated a null dataset by randomizing the *k*-maps of the healthy controls and the epilepsy group of interest. We wanted to determine if there was a better way in which to segment the brain for this analysis. We found that the functional network segmentation exhibited more significant regions for the TLE cohort, while the anatomical segmentation exhibited more significant regions for the FLE cohort. In addition, there were some regions which were identified as significant, in fact were unreliable due to their line of best fit due to their regional plots. As a final analysis, we also compared voxel-level HSI for each population, as well as group regional-*k* hubness to determine if any patterns arose between epilepsy groups and healthy controls. We found highly significant changes in regional-*k* when comparing each epilepsy group to healthy controls, indicating that hubs are becoming less connected in epilepsy.

There were some limitations which greatly impacted the work of this thesis. Most importantly, the presence of $k = 0$ has a large influence on many results. Further investigation is required as to why SPARK has problems in certain regions, and an update to the method is necessary if we would like to have SPARK known as a reliable functional connectivity tool. Finally, we believe that we can further optimize the generation of the null data for our HDI and HEI permutations. We believe that randomizing the healthy controls and epilepsy population might inherently create bias in the null-dataset, since we are inherently dragging down the null-dataset through the inclusion of patients since they theoretically all have lower *k*-hubness values by design. In the future, we wish to propose a bootstrap among the controls, where we calculate the average from a subgroup of the controls many times. We believe by taking the average of all the bootstraps, we will have a more

stable result for the healthy controls, and therefore a more reliable baseline to compare our epilepsy data with.

Finally, there are many future directions which can be taken in both the use of SPARK and the metrics used in this study. Firstly, regarding the SPARK methodology, we can start using the method as the first step to studying connector hubs in other modalities. We can use SPARK to locate the connector hubs in the brain, and then use other modalities such as diffusion weighting imaging (DWI), and positron emission tomography (PET) to study the anatomical and metabolic substrate associated with the connector hubs in patients when compared to healthy controls. Furthermore, SPARK can be used outside the scope of epilepsy, and be used to study hub reorganization of other neurological diseases or neurological disorders. Furthermore, as mentioned previously, we would eventually like to develop a surgical prediction model, by using the metrics of HDI, HEI, HSI, and regional-k to find possible biomarkers to predict if a patient will have a positive or negative outcome after surgery. Finally, SPARK and its metrics can be adapted to work in the individual subject space, which will allow the method to transform from a more research-based method to a clinical tool in the future.

References

Abarrategui, B., Mai, R., Sartori, I., Francione, S., Pelliccia, V., Cossu, M., & Tassi, L. (2021). Temporal lobe epilepsy: A never-ending story. *Epilepsy & Behavior*, *122*, 108122. https://doi.org/10.1016/j.yebeh.2021.108122

Achard, S., Delon-Martin, C., Vértes, P. E., Renard, F., Schenck, M., Schneider, F., Heinrich, C., Kremer, S., & Bullmore, E. T. (2012). Hubs of brain functional networks are radically reorganized in comatose patients. *Proceedings of the National Academy of Sciences*, *109*(50), 20608–20613. https://doi.org/10.1073/pnas.1208933109

Achard, S., Salvador, R., Whitcher, B., Suckling, J., & Bullmore, E. (2006). A Resilient, Low-Frequency, Small-World Human Brain Functional Network with Highly Connected Association Cortical Hubs. *The Journal of Neuroscience*, *26*(1), 63–72. https://doi.org/10.1523/JNEUROSCI.3874-05.2006

Aharon, M., Elad, M., & Bruckstein, A. (2006). $rm K$-SVD: An Algorithm for Designing Overcomplete Dictionaries for Sparse Representation. *IEEE Transactions on Signal Processing*, *54*(11), 4311–4322. https://doi.org/10.1109/TSP.2006.881199

Bassett, D. S., & Bullmore, E. T. (2017). Small-World Brain Networks Revisited. *The Neuroscientist*, *23*(5), 499–516. https://doi.org/10.1177/1073858416667720

Beckmann, C. F., DeLuca, M., Devlin, J. T., & Smith, S. M. (2005). Investigations into resting-state connectivity using independent component analysis. *Philosophical Transactions of the Royal Society B: Biological Sciences*, *360*(1457), 1001–1013. https://doi.org/10.1098/rstb.2005.1634

Behrens, T. E. J., Johansen-Berg, H., Woolrich, M. W., Smith, S. M., Wheeler-Kingshott, C. A. M., Boulby, P. A., Barker, G. J., Sillery, E. L., Sheehan, K., Ciccarelli, O., Thompson, A.

J., Brady, J. M., & Matthews, P. M. (2003). Non-invasive mapping of connections between human thalamus and cortex using diffusion imaging. *NATURE NEUROSCIENCE*, *6*(7).

Beleza, P., & Pinho, J. (2011). Frontal lobe epilepsy. *Journal of Clinical Neuroscience*, *18*(5), 593–600. https://doi.org/10.1016/j.jocn.2010.08.018

Bell, A. J., & Sejnowski, T. J. (1995). *An information-maximisation approach to blind separation and blind deconvolution*.

Bellec, P., Rosa-Neto, P., Lyttelton, O. C., Benali, H., & Evans, A. C. (2010). Multi-level bootstrap analysis of stable clusters in resting-state fMRI. *NeuroImage*, *51*(3), 1126–1139. https://doi.org/10.1016/j.neuroimage.2010.02.082

Benjamini, Y., & Hochberg, Y. (1995). Controlling the False Discovery Rate: A Practical and Powerful Approach to Multiple Testing. *Journal of the Royal Statistical Society: Series B (Methodological)*, *57*(1), 289–300. https://doi.org/10.1111/j.2517-6161.1995.tb02031.x

Bettus, G., Bartolomei, F., Confort-Gouny, S., Guedj, E., Chauvel, P., Cozzone, P. J., Ranjeva, J.-P., & Guye, M. (2010). Role of resting state functional connectivity MRI in presurgical investigation of mesial temporal lobe epilepsy. *Journal of Neurology, Neurosurgery & Psychiatry*, *81*(10), 1147–1154. https://doi.org/10.1136/jnnp.2009.191460

Bettus, G., Guedj, E., Joyeux, F., Confort-Gouny, S., Soulier, E., Laguitton, V., Cozzone, P. J., Chauvel, P., Ranjeva, J.-P., Bartolomei, F., & Guye, M. (2009). Decreased basal fMRI functional connectivity in epileptogenic networks and contralateral compensatory mechanisms. *Human Brain Mapping*, *30*(5), 1580–1591. https://doi.org/10.1002/hbm.20625

Binder, J. R., Frost, J. A., Hammeke, T. A., Bellgowan, P. S. F., Rao, S. M., & Cox, R. W. (1999). Conceptual Processing during the Conscious Resting State: A Functional MRI Study. *Journal of Cognitive Neuroscience*, *11*(1), 80–93. https://doi.org/10.1162/089892999563265

Biswal, B., Zerrin Yetkin, F., Haughton, V. M., & Hyde, J. S. (1995). Functional connectivity in the motor cortex of resting human brain using echo-planar mri. *Magnetic Resonance in Medicine*, *34*(4), 537–541. https://doi.org/10.1002/mrm.1910340409

Blume, W. T., Lüders, H. O., Mizrahi, E., Tassinari, C., Van Emde Boas, W., & Engel, J. (2002). Glossary of Descriptive Terminology for Ictal Semiology: Report of the ILAE Task Force on Classification and Terminology. *Epilepsia*, *42*(9), 1212–1218. https://doi.org/10.1046/j.1528-1157.2001.22001.x

Blumenfeld, H. (2014). What Is a Seizure Network? Long-Range Network Consequences of Focal Seizures. In H. E. Scharfman & P. S. Buckmaster (Eds.), *Issues in Clinical Epileptology: A View from the Bench* (Vol. 813, pp. 63–70). Springer Netherlands. https://doi.org/10.1007/978-94-017-8914-1_5

Boly, M., Perlbarg, V., Marrelec, G., Schabus, M., Laureys, S., Doyon, J., Pélégrini-Issac, M., Maquet, P., & Benali, H. (2012). Hierarchical clustering of brain activity during human nonrapid eye movement sleep. *Proceedings of the National Academy of Sciences*, *109*(15), 5856–5861. https://doi.org/10.1073/pnas.1111133109

Cole. (2010). Advances and pitfalls in the analysis and interpretation of resting-state FMRI data. *Frontiers in Systems Neuroscience*. https://doi.org/10.3389/fnsys.2010.00008

Cordes, D., Haughton, V. M., Arfanakis, K., Wendt, G. J., Turski, P. A., Moritz, C. H., & Meyerand, M. E. (2000). *Mapping Functionally Related Regions of Brain with Functional Connectivity MR Imaging*.

Cox, R. W. (1996). AFNI: Software for Analysis and Visualization of Functional Magnetic Resonance Neuroimages. *Computers and Biomedical Research*, *29*(3), 162–173. https://doi.org/10.1006/cbmr.1996.0014

Cruces, R. R., Royer, J., Herholz, P., Larivière, S., Vos de Wael, R., Paquola, C., Benkarim, O., Park, B., Degré-Pelletier, J., Nelson, M. C., DeKraker, J., Leppert, I. R., Tardif, C., Poline, J.-B., Concha, L., & Bernhardt, B. C. (2022). Micapipe: A pipeline for multimodal neuroimaging and connectome analysis. *NeuroImage*, *263*, 119612. https://doi.org/10.1016/j.neuroimage.2022.119612

Culhane-Shelburne, K., Chapieski, L., Hiscock, M., & Glaze, D. (2002). Executive functions in children with frontal and temporal lobe epilepsy. *Journal of the International Neuropsychological Society*, *8*(5), 623–632. https://doi.org/10.1017/S1355617702801308

Englot, D. J., Yang, L., Hamid, H., Danielson, N., Bai, X., Marfeo, A., Yu, L., Gordon, A., Purcaro, M. J., Motelow, J. E., Agarwal, R., Ellens, D. J., Golomb, J. D., Shamy, M. C. F., Zhang, H., Carlson, C., Doyle, W., Devinsky, O., Vives, K., … Blumenfeld, H. (2010). Impaired consciousness in temporal lobe seizures: Role of cortical slow activity. *Brain*, *133*(12), 3764–3777. https://doi.org/10.1093/brain/awq316

Filler, A. G. (2009). The History, Development and Impact of Computed Imaging in Neurological Diagnosis and Neurosurgery: CT, MRI, and DTI. *Nature Precedings*, *1*.

Fisher, R. S., Acevedo, C., Arzimanoglou, A., Bogacz, A., Cross, J. H., Elger, C. E., Engel, J., Forsgren, L., French, J. A., Glynn, M., Hesdorffer, D. C., Lee, B. I., Mathern, G. W.,

Moshé, S. L., Perucca, E., Scheffer, I. E., Tomson, T., Watanabe, M., & Wiebe, S. (2014). ILAE Official Report: A practical clinical definition of epilepsy. *Epilepsia*, *55*(4), 475–482. https://doi.org/10.1111/epi.12550

Fonov, V., Evans, A. C., Botteron, K., Almli, C. R., McKinstry, R. C., & Collins, D. L. (2011). Unbiased average age-appropriate atlases for pediatric studies. *NeuroImage*, *54*(1), 313–327. https://doi.org/10.1016/j.neuroimage.2010.07.033

Fox, M. D., & Raichle, M. E. (2007). Spontaneous fluctuations in brain activity observed with functional magnetic resonance imaging. *Nature Reviews Neuroscience*, *8*(9), 700–711. https://doi.org/10.1038/nrn2201

Greve, D. N., & Fischl, B. (2009). Accurate and robust brain image alignment using boundary-based registration. *NeuroImage*, *48*(1), 63–72. https://doi.org/10.1016/j.neuroimage.2009.06.060

Griffanti, L., Salimi-Khorshidi, G., Beckmann, C. F., Auerbach, E. J., Douaud, G., Sexton, C. E., Zsoldos, E., Ebmeier, K. P., Filippini, N., Mackay, C. E., Moeller, S., Xu, J., Yacoub, E., Baselli, G., Ugurbil, K., Miller, K. L., & Smith, S. M. (2014). ICA-based artefact removal and accelerated fMRI acquisition for improved resting state network imaging. *NeuroImage*, *95*, 232–247. https://doi.org/10.1016/j.neuroimage.2014.03.034

Grinenko, O., Li, J., Mosher, J. C., Wang, I. Z., Bulacio, J. C., Gonzalez-Martinez, J., Nair, D., Najm, I., Leahy, R. M., & Chauvel, P. (2018). A fingerprint of the epileptogenic zone in human epilepsies. *Brain*, *141*(1), 117–131. https://doi.org/10.1093/brain/awx306

Hampson, M., Peterson, B. S., Skudlarski, P., Gatenby, J. C., & Gore, J. C. (2002). Detection of functional connectivity using temporal correlations in MR images. *Human Brain Mapping*, *15*(4), 247–262. https://doi.org/10.1002/hbm.10022

He, X., Doucet, G. E., Sperling, M., Sharan, A., & Tracy, J. I. (2015). Reduced thalamocortical functional connectivity in temporal lobe epilepsy. *Epilepsia*, *56*(10), 1571–1579. https://doi.org/10.1111/epi.13085

Hillman, E. M. C. (2014). Coupling Mechanism and Significance of the BOLD Signal: A Status Report. *Annual Review of Neuroscience*, *37*(1), 161–181. https://doi.org/10.1146/annurev-neuro-071013-014111

Hoge, R. D., Atkinson, J., Gill, B., Crelier, G. R., Marrett, S., & Pike, G. B. (1999). Investigation of BOLD signal dependence on cerebral blood flow and oxygen consumption: The deoxyhemoglobin dilution model. *Magnetic Resonance in Medicine*, *42*(5), 849–863. https://doi.org/10.1002/(SICI)1522-2594(199911)42:5<849::AID-MRM4>3.0.CO;2-Z

Huettel, S. A., Song, A. W., & McCarthy, G. (2008). *Functional magnetic resonance imaging* (2nd ed). Sinauer Associates.

Jenkinson, M., Bannister, P., Brady, M., & Smith, S. (2002). Improved Optimization for the Robust and Accurate Linear Registration and Motion Correction of Brain Images. *NeuroImage*, *17*(2), 825–841. https://doi.org/10.1006/nimg.2002.1132

Jenkinson, M., & Smith, S. (2001). A global optimisation method for robust affine registration of brain images. *Medical Image Analysis*, *5*(2), 143–156. https://doi.org/10.1016/S1361-8415(01)00036-6

Kalilani, L., Sun, X., Pelgrims, B., Noack-Rink, M., & Villaneuva, V. (2018). The epidemiology of drug-resistant epilepsy: A systematic review and meta-analysis. *Epilepsia*, *59*, 2179–2193. https://doi.org/10.1111/epi.14596

Kannurpatti, S. S., Rypma, B., & Biswal, B. B. (2012). Prediction of Task-Related BOLD fMRI with Amplitude Signatures of Resting-State fMRI. *Frontiers in Systems Neuroscience*, *6*. https://doi.org/10.3389/fnsys.2012.00007

Kim, D.-J., & Min, B.-K. (2020). Rich-club in the brain's macrostructure: Insights from graph theoretical analysis. *Computational and Structural Biotechnology Journal*, *18*, 1761–1773. https://doi.org/10.1016/j.csbj.2020.06.039

Kramer, M. A., & Cash, S. S. (2012). Epilepsy as a Disorder of Cortical Network Organization. *The Neuroscientist*, *18*(4), 360–372. https://doi.org/10.1177/1073858411422754

Krucoff, M. O., Chan, A. Y., Harward, S. C., Rahimpour, S., Rolston, J. D., Muh, C., & Englot, D. J. (2017). Rates and predictors of success and failure in repeat epilepsy surgery: A meta-analysis and systematic review. *Epilepsia*, *58*(12), 2133–2142. https://doi.org/doi: 10.1111/epi.13920

Lee, K. (2011). A Data-Driven Sparse GLM for fMRI Analysis Using Sparse Dictionary Learning With MDL Criterion. *IEEE Transactions on Medical Imaging*, *30*(5), 1076–1089. https://doi.org/10.1109/TMI.2010.2097275

Lee, K., Horien, C., O'Connor, D., Garand-Sheridan, B., Tokoglu, F., Scheinost, D., Lake, E. M. R., & Constable, R. T. (2022). Arousal impacts distributed hubs modulating the integration of brain functional connectivity. *NeuroImage*, *258*, 119364. https://doi.org/10.1016/j.neuroimage.2022.119364

Lee, K., Khoo, H. M., Fourcade, C., Gotman, J., & Grova, C. (2019). Automatic classification and removal of structured physiological noise for resting state functional connectivity MRI analysis. *Magnetic Resonance Imaging*, *58*, 97–107. https://doi.org/10.1016/j.mri.2019.01.019

Lee, K., Khoo, H. M., Lina, J.-M., Dubeau, F., Gotman, J., & Grova, C. (2018). Disruption, emergence and lateralization of brain network hubs in mesial temporal lobe epilepsy. *NeuroImage: Clinical*, *20*, 71–84. https://doi.org/10.1016/j.nicl.2018.06.029

Lee, K., Lina, J.-M., Gotman, J., & Grova, C. (2016). SPARK: Sparsity-based analysis of reliable k-hubness and overlapping network structure in brain functional connectivity. *NeuroImage*, *134*, 434–449. https://doi.org/10.1016/j.neuroimage.2016.03.049

Lee, K., & Wang, Y. (n.d.). Hierarchical segregation of functional brain networks at NREM sleep and attention function. *In Preparation*.

Levitt, M. H. (2008). *Spin Dynamics Basics of Nuclear Magnetic Resonance* (Second edition). John Wiley & Sons, Ltd.

Liao, C., Wang, K., Cao, X., Li, Y., Wu, D., Ye, H., Ding, Q., He, H., & Zhong, J. (2018). Detection of Lesions in Mesial Temporal Lobe Epilepsy by Using MR Fingerprinting. *Radiology*, *288*(3), 804–812. https://doi.org/10.1148/radiol.2018172131

Logothetis, N. K. (2008). What we can do and what we cannot do with fMRI. *Nature*, *453*(7197), 869–878. https://doi.org/10.1038/nature06976

Logothetis, N. K., & Wandell, B. A. (2004). Interpreting the BOLD Signal. *Annual Review of Physiology*, *66*(1), 735–769. https://doi.org/10.1146/annurev.physiol.66.082602.092845

Löscher, W., Potschka, H., Sisodiya, S. M., & Vezzani, A. (2020). Drug Resistance in Epilepsy: Clinical Impact, Potential Mechanisms, and New Innovative Treatment Options. *Pharmacological Reviews*, *72*(3), 606–638. https://doi.org/10.1124/pr.120.019539

Lowe, M. J., Mock, B. J., & Sorenson, J. A. (1998). Functional Connectivity in Single and Multislice Echoplanar Imaging Using Resting-State Fluctuations. *NeuroImage*, *7*(2), 119–132. https://doi.org/10.1006/nimg.1997.0315

Ma, L., Wang, B., Chen, X., & Xiong, J. (2007). Detecting functional connectivity in the resting brain: A comparison between ICA and CCA. *Magnetic Resonance Imaging*, *25*(1), 47–56. https://doi.org/10.1016/j.mri.2006.09.032

Maier, A., Steidl, S., Christlein, V., & Hornegger, J. (Eds.). (2018). *Medical Imaging Systems: An Introductory Guide* (Vol. 11111). Springer International Publishing. https://doi.org/10.1007/978-3-319-96520-8

Manson, E. N., Inkoom, S., & Mumuni, A. N. (2022). Impact of Magnetic Field Inhomogeneity on the Quality of Magnetic Resonance Images and Compensation Techniques: A Review. *Reports in Medical Imaging*, *Volume 15*, 43–56. https://doi.org/10.2147/RMI.S369491

Mazoyer, B., Zago, L., Mellet, E., Bricogne, S., Etard, O., Houdé, O., Crivello, F., Joliot, M., Petit, L., & Tzourio-Mazoyer, N. (2001). Cortical networks for working memory and executive functions sustain the conscious resting state in man. *Brain Research Bulletin*, *54*(3), 287–298. https://doi.org/10.1016/S0361-9230(00)00437-8

Mckeown, M. J., Makeig, S., Brown, G. G., Jung, T.-P., Kindermann, S. S., Bell, A. J., & Sejnowski, T. J. (1998). Analysis of fMRI data by blind separation into independent spatial components. *Human Brain Mapping*, *6*(3), 160–188. https://doi.org/10.1002/(SICI)1097-0193(1998)6:3<160::AID-HBM5>3.0.CO;2-1

McKeown, M. J., & Sejnowski, T. J. (1998). Independent component analysis of fMRI data: Examining the assumptions. *Human Brain Mapping*, *6*(5–6), 368–372. https://doi.org/10.1002/(SICI)1097-0193(1998)6:5/6<368::AID-HBM7>3.0.CO;2-E

Morgan, V. L., Johnson, G. W., Cai, L. Y., Landman, B. A., Schilling, K. G., Englot, D. J., Rogers, B. P., & Chang, C. (2021). MRI network progression in mesial temporal lobe

epilepsy related to healthy brain architecture. *Network Neuroscience*, *5*(2), 434–450. https://doi.org/10.1162/netn_a_00184

Morgan, V. L., Sainburg, L. E., Johnson, G. W., Janson, A., Levine, K. K., Rogers, B. P., Chang, C., & Englot, D. J. (2022). Presurgical temporal lobe epilepsy connectome fingerprint for seizure outcome prediction. *Brain Communications*, *4*(3), fcac128. https://doi.org/10.1093/braincomms/fcac128

Narasimhan, S., González, H. F. J., Johnson, G. W., Wills, K. E., Paulo, D. L., Morgan, V. L., & Englot, D. J. (2022). Functional connectivity between mesial temporal and default mode structures may help lateralize surgical temporal lobe epilepsy. *Journal of Neurosurgery*, *137*(6), 1571–1581. https://doi.org/10.3171/2022.1.JNS212031

Negishi, M., Martuzzi, R., Novotny, E. J., Spencer, D. D., & Constable, R. T. (2011). Functional MRI connectivity as a predictor of the surgical outcome of epilepsy: Connectivity Study of Surgical Outcome. *Epilepsia*, *52*(9), 1733–1740. https://doi.org/10.1111/j.1528-1167.2011.03191.x

Newman, M. E. J. (2006). Modularity and community structure in networks. *Proceedings of the National Academy of Sciences*, *103*(23), 8577–8582. https://doi.org/10.1073/pnas.0601602103

Ogawa, S., Lee, T. M., Kay, A. R., & Tank, D. W. (1990). Brain magnetic resonance imaging with contrast dependent on blood oxygenation. *Proceedings of the National Academy of Sciences*, *87*(24), 9868–9872. https://doi.org/10.1073/pnas.87.24.9868

Pittau, F., Grova, C., Moeller, F., Dubeau, F., & Gotman, J. (2012). Patterns of altered functional connectivity in mesial temporal lobe epilepsy: Functional Connectivity in MTLE. *Epilepsia*, *53*(6), 1013–1023. https://doi.org/10.1111/j.1528-1167.2012.03464.x

Power, J. D., Schlaggar, B. L., Lessov-Schlaggar, C. N., & Petersen, S. E. (2013). Evidence for Hubs in Human Functional Brain Networks. *Neuron*, *79*(4), 798–813. https://doi.org/10.1016/j.neuron.2013.07.035

Raichle, M. E., MacLeod, A. M., Snyder, A. Z., Powers, W. J., Gusnard, D. A., & Shulman, G. L. (2001). A default mode of brain function. *Proceedings of the National Academy of Sciences*, *98*(2), 676–682. https://doi.org/10.1073/pnas.98.2.676

Razavipour, S. F., Bin Ka'b Ali, O., Lee, K., Grimault, S., Blinder, S., Soucy, J.-P., Gauthier, C., & Grova, C. (2023). Multiresolution Metabolic Profile of Functional Hubness in the Resting Human Brain. *Manuscript Submitted to PNAS for Publication*.

Reuter, M., Schmansky, N. J., Rosas, H. D., & Fischl, B. (2012). Within-subject template estimation for unbiased longitudinal image analysis. *NeuroImage*, *61*(4), 1402–1418. https://doi.org/10.1016/j.neuroimage.2012.02.084

Rolls, E. T., Huang, C.-C., Lin, C.-P., Feng, J., & Joliot, M. (2020). Automated anatomical labelling atlas 3. *NeuroImage*, *206*, 116189. https://doi.org/10.1016/j.neuroimage.2019.116189

Royer, J., Bernhardt, B. C., Larivière, S., Gleichgerrcht, E., Vorderwülbecke, B. J., Vulliémoz, S., & Bonilha, L. (2022). Epilepsy and brain network hubs. *Epilepsia*, *63*(3), 537–550. https://doi.org/10.1111/epi.17171

Royer, J., Rodríguez-Cruces, R., Tavakol, S., Larivière, S., Herholz, P., Li, Q., Vos De Wael, R., Paquola, C., Benkarim, O., Park, B., Lowe, A. J., Margulies, D., Smallwood, J., Bernasconi, A., Bernasconi, N., Frauscher, B., & Bernhardt, B. C. (2022). An Open MRI Dataset For Multiscale Neuroscience. *Scientific Data*, *9*(1), 569. https://doi.org/10.1038/s41597-022-01682-y

Rubinov, M., & Sporns, O. (2010). Complex network measures of brain connectivity: Uses and interpretations. *NeuroImage*, *52*(3), 1059–1069. https://doi.org/10.1016/j.neuroimage.2009.10.003

Sala-Padro, J., Miró, J., Rodriguez-Fornells, A., Rifa-Ros, X., Plans, G., Santurino, M., Falip, M., & Càmara, E. (2021). Mapping connectivity fingerprints for presurgical evaluation of temporal lobe epilepsy. *BMC Neurology*, *21*(1), 442. https://doi.org/10.1186/s12883-021-02469-1

Salimi-Khorshidi, G., Douaud, G., Beckmann, C. F., Glasser, M. F., Griffanti, L., & Smith, S. M. (2014). Automatic denoising of functional MRI data: Combining independent component analysis and hierarchical fusion of classifiers. *NeuroImage*, *90*, 449–468. https://doi.org/10.1016/j.neuroimage.2013.11.046

Seitzman, B. A., Snyder, A. Z., Leuthardt, E. C., & Shimony, J. S. (2019). The State of Resting State Networks. *Topics in Magnetic Resonance Imaging*, *28*(4), 189–196. https://doi.org/10.1097/RMR.0000000000000214

Smith, S. M. (2002). Fast robust automated brain extraction. *Human Brain Mapping*, *17*(3), 143–155. https://doi.org/10.1002/hbm.10062

Smith, S. M., Fox, P. T., Miller, K. L., Glahn, D. C., Fox, P. M., Mackay, C. E., Filippini, N., Watkins, K. E., Toro, R., Laird, A. R., & Beckmann, C. F. (2009). Correspondence of the brain's functional architecture during activation and rest. *Proceedings of the National Academy of Sciences*, *106*(31), 13040–13045. https://doi.org/10.1073/pnas.0905267106

Soares, J. M., Magalhães, R., Moreira, P. S., Sousa, A., Ganz, E., Sampaio, A., Alves, V., Marques, P., & Sousa, N. (2016). A Hitchhiker's Guide to Functional Magnetic

Resonance Imaging. *Frontiers in Neuroscience*, *10*. https://doi.org/10.3389/fnins.2016.00515

Spencer, S., & Huh, L. (2008). Outcomes of epilepsy surgery in adults and children. *The Lancet Neurology*, *7*(6), 525–537. https://doi.org/10.1016/S1474-4422(08)70109-1

Sporns, O. (2018). Graph theory methods: Applications in brain networks. *Dialogues in Clinical Neuroscience*, *20*(2), 111–121. https://doi.org/10.31887/DCNS.2018.20.2/osporns

Tellez-Zenteno, J. F., Dhar, R., Hernandez-Ronquillo, L., & Wiebe, S. (2007). Long-term outcomes in epilepsy surgery: Antiepileptic drugs, mortality, cognitive and psychosocial aspects. *Brain*, *130*(2), 334–345. https://doi.org/10.1093/brain/awl316

Theodore, W. H., Spencer, S. S., Wiebe, S., Langfitt, J. T., Ali, A., Shafer, P. O., Berg, A. T., & Vickrey, B. G. (2006). Epilepsy in North America: A Report Prepared under the Auspices of the Global Campaign against Epilepsy, the International Bureau for Epilepsy, the International League Against Epilepsy, and the World Health Organization. *Epilepsia*, *47*(10), 1700–1722. https://doi.org/10.1111/j.1528-1167.2006.00633.x

Thomas Yeo, B. T., Krienen, F. M., Sepulcre, J., Sabuncu, M. R., Lashkari, D., Hollinshead, M., Roffman, J. L., Smoller, J. W., Zöllei, L., Polimeni, J. R., Fischl, B., Liu, H., & Buckner, R. L. (2011). The organization of the human cerebral cortex estimated by intrinsic functional connectivity. *Journal of Neurophysiology*, *106*(3), 1125–1165. https://doi.org/10.1152/jn.00338.2011

Tracy, J. I., & Doucet, G. E. (2015). Resting-state functional connectivity in epilepsy: Growing relevance for clinical decision making. *Current Opinion in Neurology*, *28*(2), 158–165. https://doi.org/10.1097/WCO.0000000000000178

Tzourio-Mazoyer, N., Landeau, B., Papathanassiou, D., Crivello, F., Etard, O., Delcroix, N., Mazoyer, B., & Joliot, M. (2002). Automated Anatomical Labeling of Activations in SPM Using a Macroscopic Anatomical Parcellation of the MNI MRI Single-Subject Brain. *NeuroImage*, *15*(1), 273–289. https://doi.org/10.1006/nimg.2001.0978

Urchs, S., Armoza, J., Moreau, C., Benhajali, Y., Jolène, S.-A., Orban, P., & Bellec, P. (2017). MIST: A multi-resolution parcellation of functional brain networks [version 2; peer review: 4 approved]. *MNI Open Research*, 1:3.

Van Den Heuvel, M. P., & Hulshoff Pol, H. E. (2010). Exploring the brain network: A review on resting-state fMRI functional connectivity. *European Neuropsychopharmacology*, *20*(8), 519–534. https://doi.org/10.1016/j.euroneuro.2010.03.008

Van Den Heuvel, M. P., & Sporns, O. (2011). Rich-Club Organization of the Human Connectome. *The Journal of Neuroscience*, *31*(44), 15775–15786. https://doi.org/10.1523/JNEUROSCI.3539-11.2011

Vaughan, D. N., Rayner, G., Tailby, C., & Jackson, G. D. (2016). MRI-negative temporal lobe epilepsy: A network disorder of neocortical connectivity. *Neurology*, *87*(18), 1934–1942. https://doi.org/10.1212/WNL.0000000000003289

Výtvarová, E., Mareček, R., Fousek, J., Strýček, O., & Rektor, I. (2017). Large-scale cortico-subcortical functional networks in focal epilepsies: The role of the basal ganglia. *NeuroImage: Clinical*, *14*, 28–36. https://doi.org/10.1016/j.nicl.2016.12.014

Waites, A. B., Briellmann, R. S., Saling, M. M., Abbott, D. F., & Jackson, G. D. (2006). Functional connectivity networks are disrupted in left temporal lobe epilepsy. *Annals of Neurology*, *59*(2), 335–343. https://doi.org/10.1002/ana.20733

Wang, Y. (2022). *Reorganization of functional hubs in sleep and in epilepsy*. Concordia University.

Watts, D. J., & Strogatz, S. H. (1998). *Collective dynamics of 'small-world' networks*. *393*.

Wills, K. E., González, H. F. J., Johnson, G. W., Haas, K. F., Morgan, V. L., Narasimhan, S., & Englot, D. J. (2021). People with mesial temporal lobe epilepsy have altered thalamo-occipital brain networks. *Epilepsy & Behavior*, *115*, 107645. https://doi.org/10.1016/j.yebeh.2020.107645

Woodward, K. E., Gaxiola-Valdez, I., Goodyear, B. G., & Federico, P. (2014). Frontal Lobe Epilepsy Alters Functional Connections Within the Brain's Motor Network: A Resting-State fMRI Study. *Brain Connectivity*, *4*(2), 91–99. https://doi.org/10.1089/brain.2013.0178

Woolfe, M., Prime, D., Gillinder, L., Rowlands, D., O'keefe, S., & Dionisio, S. (2019). Automatic detection of the epileptogenic zone: An application of the fingerprint of epilepsy. *Journal of Neuroscience Methods*, *325*, 108347. https://doi.org/10.1016/j.jneumeth.2019.108347

Woolrich, M. W., Jbabdi, S., Patenaude, B., Chappell, M., Makni, S., Behrens, T., Beckmann, C., Jenkinson, M., & Smith, S. M. (2009). Bayesian analysis of neuroimaging data in FSL. *NeuroImage*, *45*(1), S173–S186. https://doi.org/10.1016/j.neuroimage.2008.10.055

Zhang, D., & Raichle, M. E. (2010). Disease and the brain's dark energy. *Nature Reviews Neurology*, *6*(1), 15–28. https://doi.org/10.1038/nrneurol.2009.198

Zhang, D., Snyder, A. Z., Fox, M. D., Sansbury, M. W., Shimony, J. S., & Raichle, M. E. (2008). Intrinsic Functional Relations Between Human Cerebral Cortex and Thalamus. *Journal of Neurophysiology*, *100*(4), 1740–1748. https://doi.org/10.1152/jn.90463.2008

Zhang, X., Tokoglu, F., Negishi, M., Arora, J., Winstanley, S., Spencer, D. D., & Constable, R. T. (2011). Social network theory applied to resting-state fMRI connectivity data in the identification of epilepsy networks with iterative feature selection. *Journal of Neuroscience Methods*, *199*(1), 129–139. https://doi.org/10.1016/j.jneumeth.2011.04.020

Zhao, X., Glahn, D., Tan, L. H., Li, N., Xiong, J., & Gao, J.-H. (2004). Comparison of TCA and ICA techniques in fMRI data processing. *Journal of Magnetic Resonance Imaging*, *19*(4), 397–402. https://doi.org/10.1002/jmri.20023

.